

**GEOMECHANICAL CHARACTERIZATION OF THE MONTNEY SHALE
NORTHWEST ALBERTA AND NORTHEAST BRITISH COLUMBIA, CANADA**

By Heather Davey

A thesis submitted to the Faculty and the Board of Trustees of the Colorado School of Mines in partial fulfillment of the requirements for the Degree of Master of Science (Geology).

Golden, Colorado

Date: _____,

Signed: _____,

Heather Davey

Signed: _____,

Dr. Thomas L. Davis

Thesis Advisor

Signed: _____,

Dr. John B. Curtis

Thesis Co-advisor

Golden, Colorado

Date: _____,

Signed: _____,

Dr. John D. Humphrey

Professor and Head

Department of Geology and Geological Engineering

ABSTRACT

Unconventional reservoirs require hydraulic stimulation to be commercially productive. Recently, distinctions have been made between reservoir quality vs. completion quality (Cipolla et al. 2012), emphasizing the importance of both elements for production. There are many sources of variability in reservoir quality; in this thesis I examine several fundamental reservoir properties in detail and combine them in a new way: the Rock Quality Index (RQI). Through the definition of a geomechanical model and corresponding mechanical stratigraphy, those factors having a substantial effect on reservoir quality became apparent. Two fundamental categories; compositional variation and fabric variation, are used to characterize overall reservoir variation. Burial, compaction, hydrocarbon generation, diagenesis, and tectonics all affect the mechanical character and in-situ stress state of the reservoir. The Rock Quality Index (RQI) is an effort to understand how composition and fabric relate to stress anisotropy, fracturing, and rock properties, and ultimately aid in defining the best zones for exploitation. Therefore, this Rock Quality Index (RQI) is vital for the defining the second element of unconventional reservoir success; completion quality. Without a reservoir framework to drive the completion design, high completion quality will be harder to achieve.

The original mechanical stratigraphy definition is in turn used as a framework for relating Rock Quality Index (RQI) variations to the factors which caused them. The comparison between Rock Quality Index (RQI) and mechanical stratigraphy shows that zones traditionally thought of as desirable for hydraulic completion (brittle) are also zones of high internal heterogeneity. Formation heterogeneity may be detrimental to hydraulic fracture growth.

Using several other data types (multicomponent time-lapse seismic, microseismic, and reservoir engineering tests) in conjunction with the Rock Quality Index (RQI), it is observed that there is a strong formation influence on the progression of hydraulic fractures. The locations of interfaces between changes in rock properties and/or stress state are locations where the hydraulic fracture character will also change. It was found that energy is dissipated in heterogeneous/brittle zones, while hydraulic growth occurs in homogenous zones. However, at the intersection of a homogenous zone with a brittle zone, both hydraulic fracture growth and energy dissipation is possible. Here relatively higher production is observed. Stress shadowing amplifies the effects of energy dissipation in brittle zones.

Understanding the geological factors that have the greatest influence on stimulation has proven to be a useful method of predicting productivity and efficiency in shale reservoirs. The results of this geomechanical study are calibrated with diagnostic fracture injection tests, microseismic, spinner gas data, and time-lapse multicomponent seismic to corroborate the predictions of reservoir performance in the Montney Shale.

TABLE OF CONTENTS

ABSTRACT	iii
LIST OF FIGURES	vii
LIST OF MAPS & TABLES	xiv
ACKNOWLEDGEMENTS.....	xv
GLOSSARY OF TERMS	xvi
CHAPTER 1- GEOLOGICAL BACKGROUND.....	1
1.1 Structural Framework.....	2
1.2 Available Data	3
1.3- Previous Research by Talisman Energy Inc.....	6
1.3.1 Farrell Creek.....	7
1.3.2 Pouce Coupe.....	7
CHAPTER 2- SEQUENCE STRATIGRAPHY	8
CHAPTER 3- COMPONENTS OF MECHANICAL STRATIGRAPHY	12
3.1 Compositional Variation- Petrographic Factors.....	13
3.1.1 Thermal Maturity.....	15
3.2 Fabric Variation- Depositional Factors	16
3.2.1 Laminations	17
3.2.2 Microfractures.....	17
3.2.3 Large-scale Fractures	18
3.3 Integration of Rock Variability	19
CHAPTER 4- ROCK PROPERTIES & STRESS PROFILES	20
4.1 Implications of Stress for the Geomechanical Model	21
4.2 Log-derived Rock Properties	23
4.3 Core-derived Rock Properties	23
4.4 Calibration Points.....	25
4.5 Empirical Equations for Study Wells	27
4.6 Pore Pressure	28
4.7 Results	29

4.7.1 Pouce Coupe.....	29
4.7.2 Farrell Creek.....	30
CHAPTER 5- MONTNEY MECHANICAL STRATIGRAPHY	31
5.1 Rock Quality Index	33
CHAPTER 6- MICROSEISMIC	43
6.1 Microseismic Background Theory	43
6.2 Montney Microseismic	46
6.3 Datasets	47
6.4 Bulk Analysis.....	47
6.5 High-graded Analysis.....	47
6.6 B-value Analysis	53
6.7 Seismic Moment	56
6.8 Perforation Placement.....	56
6.9 Implications of Analysis.....	57
CHAPTER 7- NATURAL FRACTURES.....	60
7.1 Relationships between Rock Quality Index and Natural Fracture Failure	60
7.2 Quantitative Fracture Failure	62
7.3 The Importance of Natural Fractures- Analogous Case Study.....	64
7.4 Mohr Coulomb Analysis.....	65
7.5 Euler Angle Rotation	65
7.6 Hydraulic Stimulation.....	66
CHAPTER 8- UPSCALING TO SEISMIC	76
CHAPTER 9- INTEGRATION OF RESULTS.....	86
CHAPTER 10- CONCLUSIONS	94
10.1 Recommendations for Future Work	95
REFERENCES	97
SELECTED BIBLIOGRAPHY.....	103

LIST OF FIGURES

Figure 1.1 – Overall depositional model for the Montney Formation. Mass-wasting events on the ramp slope generate turbidity currents and result in downslope turbidite deposition. Moving basinward facies become finer grained and more organic-rich (courtesy of Lindsay Dunn, Talisman Energy Inc.).	2
Figure 1.2- The stratigraphic framework at Farrell Creek and Pouce Coupe. Maximum regressive surfaces are defined by red lines while maximum flooding surfaces are defined by green lines (courtesy of Lindsay Dunn, Talisman Energy Inc.).	3
Figure 2.1- Gamma Ray Logs showing the commonalities of North American Gas Shales (Rodriguez et. al 2000). A basal transgressive systems tract (organic-rich/phosphate-rich fining upward) shaley interval is capped by an organic-rich, high gamma ray shale, followed by a highstand systems tract (clay/quartz-rich coarsening upward) interval (Slatt et al 2011).	9
Figure 2.2 - Geometrical relationships between the highstand systems tract, transgressive systems tract, lowstand systems tract, and maximum flooding surface (MFS- Posamentier et al. 2011).	11
Figure 3.1- Shale heterogeneity divided into two main categories of composition and texture. Changes in the abundance of clay volume, kerogen volume, and mineralogy will affect the rock properties of the formation, as will the abundance of laminations, other sedimentary structures, and natural fractures.	14
Figure 3.2- The variability in reservoir fabric which will occur with various inclusion shapes and orientations (Bandyopadhyay 2009).	16
Figure 3.3- The different types of fracturing which can occur in an unconventional reservoir, from the largest scale (through-going fractures) to the finest scale (lamina bound fractures- modified from Zahm & Hennings 2009).	18
Figure 3.4- Relative ages and petrophysical parameters of North American gas shales; oldest to youngest Utica, Marcellus, Muskwa, Barnett, and Montney.	19
Figure 4.1- Normal, strike-slip, and reverse stress regimes, varying with relative magnitudes of the three principal stresses σ_{HMax} , σ_{hmin} , and σ_v .	20

Figure 4.2- Shale heterogeneity factors as components of production factors. In a successful hydraulic stimulation, both brittle rock and failing natural fractures are desired to create a complex fracture network and provide the greatest reservoir reach.....22

Figure 4.3- The use of a geomechanical model to define the mechanical stratigraphy of the reservoir, and ultimately relate this stratigraphy to hypothesized fracture failure and brittle zones.22

Figure 4.4 –Stress cycling of core sample, and effect on Young’s Modulus. Different methods of measuring Young’s Modulus values are shown by E1-E5 on the plot (Barree et al 2009).24

Figure 4.5- Limited amounts of engineering data will result in limited knowledge of fracture parameters, while the availability of DFIT’s and flow tests allow for more accurate characterization (Mayerhofer 2012).....25

Figure 4.6- Principal stress components acting on the reservoir; overburden stress, minimum horizontal stress, and maximum horizontal stress (Mishra 2011).26

Figure 4.7- The mini-frac test is performed by injecting enough fluid to breakdown the formation (breakdown pressure). Constant-rate injection then occurs, until the treatment is shut-in (ISIP- instantaneous shut-in pressure) and following this closure pressure is determined.27

Figure 4.8- Pouce Coupe Stress Profile, with predicted pore pressure shown by the blue curve and predicted σ_{hmin} shown by the red curve. Calibration points for pore pressure and σ_{hmin} are pink diamonds and red diamonds respectively.29

Figure 4.9- Farrell Creek Stress Profile, with predicted pore pressure shown by the blue curve and predicted σ_{hmin} shown by the red curve. Calibration points for pore pressure and σ_{hmin} are orange triangles and red diamonds respectively.30

Figure 5.1- Farrell Creek mechanical stratigraphy definition. Yellow facies are relatively ductile, red facies are relatively brittle, and blue facies are relatively laminated/brittle. The pre-defined MNTN E and F1 horizon and maximum flooding surfaces (MFS2, MFS3) are also shown.32

Figure 5.2- Pouce Coupe mechanical stratigraphy definition. Yellow facies are relatively ductile, red facies are relatively brittle, and blue facies are relatively laminated/brittle.33

Figure 5.3- Parameters for defining the Rock Quality Index (RQI). Rock fabric and rock composition-based brittleness terms are added together, and then minimum horizontal stress is subtracted to generate the Rock Quality Index (RQI).36

Figure 5.4 - Log representation of Rock Quality Index (RQI), with normalized total brittleness on the far left and normalized stress differential in the center.....37

Figure 5.5 - The change in hydraulic fracture character with stress regime shift; from vertical transverse fracture (left) to horizontal pancake fracture (right). On the left, least stress is σ_{hmin} and therefore the hydraulic fracture propagating from the wellbore (blue plane) is vertical. On the right, least stress is now σ_v and the propagating hydraulic fracture is horizontal.39

Figure 5.6- Modified Rock Quality Index (RQI) equation. The original stress term (σ_{hmin}) has been modified to the normalized stress differential ($\sigma_v - \sigma_{hmin}$), to amplify changes in stress.39

Figure 5.7 - Comparison of results of full (left) and pseudo (right) Rock Quality Index (RQI) analysis for well C-85-I.....41

Figure 5.8 - C-85-I Modified Rock Quality Index (RQI- left log), plotted with the gamma ray curve (center, on a scale from 0-400 API), and the mechanical stratigraphy.....42

Figure 6.1 - B-Values (left), on a scale of 0-4, superimposed with microseismicity (right), indicating different fracture activation mechanisms in different areas of the hydraulic treatment (Maxwell 2011). Higher b-values are associated with the propagation of a hydraulic fracture while lower b-values are associated with natural fracture re-activation.....46

Figure 6.2- Mechanical stratigraphy defined for Farrell Creek, the Montney Shale, BC48

Figure 6.3- Total event counts for all well pads are shown by the grey bars, on a scale of 0-450 events. Mechanical stratigraphy previously defined is shown by the background colors.50

Figure 6.4 - High-graded event dataset. High-graded event counts for all well pads are shown by the grey bars, on a scale of 0-20 events. Mechanical stratigraphy previously defined is shown by the background colors.51

Figure 6.5 - Correlation of high-graded events to mechanical stratigraphy. In the Yellow 5A and Yellow 5 facies high event counts remain, which correlated with the lowermost homogenous zone in the Rock Quality Index (RQI) log.52

Figure 6.6- B-values correlated to mechanical stratigraphy. Higher b-values, corresponding to the propagation of a hydraulic fracture and lower material heterogeneity, are seen in the Yellow 5 and Yellow 5A facies, strengthening the argument that growth of a hydraulic fracture is most prolific here. A much lower b-value is seen starting at the Blue 5 facies, indicating a stress change and different fracturing mechanism.....54

Figure 6.7- B-values correlating to mechanical stratigraphy and Rock Quality Index (RQI).55

Figure 6.8- Hydraulic fracture propagation in lower stress zone (red arrows); natural fracture re-activation and shear in higher stress zone (blue arrows). The point of interaction between these two fracturing mechanisms, at the Blue 5 facies, appears to be an area of prolific production...56

Figure 6.9- Moment magnitude of largest 25 events per zone.....58

Figure 6.10 - Stage placement indicated by black box, event distribution indicated by grey bars, overlying mechanical stratigraphy as previously defined. In this case, stage placement in a brittle facies results in little hydraulic growth outside this facies.....58

Figure 6.11- Stage placement indicated by black box, event distribution indicated by grey bars, overlying mechanical stratigraphy as previously defined. In this case, stage placement in a more ductile but homogenous facies results in more distributed hydraulic fracture energy in all facies.59

Figure 7.1- Layered rock formation “loaded” with the stress of a propagating hydraulic stimulation (red plane).....61

Figure 7.2- Changes in layer properties with loading (modified from Teufel et al 1984). The induced change in horizontal stress is compressional in a low shear modulus layers while in high shear modulus layers the horizontal stress is compressional.....62

Figure 7.3 - Dominant natural fracture orientations, sub-parallel to minimum horizontal stress (red outline) and sub-parallel to maximum horizontal stress (yellow outline). Orientation of maximum horizontal stress (N40E) shown by red arrow.....63

Figure 7.4- Process of Euler angle rotation about the principal axes.66

Figure 7.5- Representation of stress rotation. The principal stress σ_{hmin} will be slightly altered depending on the orientation of a natural fracture face. The magnitude of this stress aligned with the fracture plane itself must be defined.....66

Figure 7.6 - Mohr-Coulomb failure theory. Effective normal stress is along the x-axis, as represented by equation 7.3- 7.4. With an increase in the pore pressure term in this equation, a reduction in effective stress occurs and the stress state shifts to the left, from the original reservoir state (red circle) to the elevated pressure state (blue circle). At this point, any fracture lying on the portion of the semi-circle which surpasses the shear failure envelope will be critically-stressed.67

Figure 7.7- Pressure progression of a hydraulic fracture treatment (Jones & Britt 2009).68

Figure 7.8- C-65-I Fracture failure progression. The original reservoir stress state on natural fractures is shown by the dark blue diamonds. Elevated pressures are shown by the yellow diamonds (breakdown pressure), orange diamonds (average treating pressure), red diamonds (maximum treating pressure), and light blue diamonds (net pressure).69

Figure 7.9 - B-H94-I Fracture failure progression. Elevated pressures are shown by the yellow diamonds (breakdown pressure), orange diamonds (average treating pressure), red diamonds (maximum treating pressure), and light blue diamonds (net pressure).70

Figure 7.10 - D-A82-I Fracture failure progression. Elevated pressures are shown by the yellow diamonds (breakdown pressure), orange diamonds (average treating pressure), red diamonds (maximum treating pressure), and light blue diamonds (net pressure).71

Figure 7.11- General orientation of fractures which are critically stressed in the Montney lie within the zone outlined in red.72

Figure 7.12- Orthogonal natural fracture (black lines) and hydraulic fracture (red arrow) interaction.72

Figure 7.13 - DFIT Fracture height recession example. G (time) is plotted on the x-axis, pressure is plotted on the y-axis.75

Figure 8.1 - Map view of wells and timeline for multicomponent seismic survey. The baseline survey was shot before stimulation; Monitor 1 and 2 are shot following stimulation of the 02-07 well and the 07-07 well respectively.78

Figure 8.2 - SWVA/SWSA in Monitor 1 & 2 of the time lapse survey (Steinhoff 2012). Anisotropy is displayed on a scale from -8-8% anisotropy, and the PS1 orientation is shown by the dark

grey lines. Spinner gas flow rates for each perforation are shown in percent flow for that wellbore.82

Figure 8.3 - Baseline SWVA correlated with Rock Quality Index (RQI). Initially high Rock Quality Index (RQI) corresponds to areas of elevated baseline anisotropy, indicating a correlation between initially brittle rock and a greater degree of natural fracturing on the seismic scale.83

Figure 8.4 - Monitor 1- Baseline anisotropy correlated with Rock Quality Index (RQI). As hypothesized in earlier analysis, hydraulic energy will preferentially propagate to more homogenous areas of the reservoir. Monitor 1 comparison shows induced anisotropy correlating to more homogenous areas of the Rock Quality Index (RQI) curve, as expected.....84

Figure 8.5 - Monitor 2- Baseline anisotropy correlated with Rock Quality Index (RQI).....84

Figure 8.6 - Determination of homogenous zones, performed by overlaying a line of zero-variation Rock Quality Index and observing where the curve deviated from this straight line.....85

Figure 8.7 - Microseismic results correlated to Rock Quality Index (RQI). More prolific microseismic is observed in the first three stages and energy dissipation at the third stage results in a more planar geometry and fewer events in stage 4 and 5.85

Figure 9.1 - Rock Quality Index (RQI), mechanical stratigraphy, and microseismic event abundance. In the Yellow 5A and Yellow 5 facies high event counts are observed, correlating with the lowermost homogenous zone in the Rock Quality Index (RQI) log.87

Figure 9.3 -Rock Quality Index (RQI), mechanical stratigraphy, and spinner-derived gas flow. .89

Figure 9.4 - Fracture abundance, plotted as a function of dip, correlated to the mechanical stratigraphy and Rock Quality Index (RQI). In the Yellow 8 facies distance from the propagating hydraulic fracture is large; however the presence of abundant steeply-dipping natural fractures appears to compensate for the lesser pressure effects.90

Figure 9.5 - SWVA signature in Monitor 2 with proposed homogenous zone, brittle zone, and fracture barrier outlined in purple.91

Figure 9.6 - Microseismic events correlated with spinner gas data and the Rock Quality Index (RQI). Both prolific microseismic and relatively high gas flow are observed at the intersection between a homogenous Rock Quality Index (RQI) zone and a brittle zone.92

Figure 9.7 - Energy dissipation due to stress shadowing and fracture activation in both
horizontal (top) and vertical (bottom) well cases.....93

LIST OF MAPS & TABLES

Map 1.1 – Study Area Map	1
Map 1.2 – Pouce Coupe data locations	5
Map 1.3 – Farrell Creek data locations.....	6
Table 1.1 – Farrell Creek available data.....	4
Table 1.2 - Pouce Coupe available data.....	4
Table 1.3 - Color legend for Tables 1 and 2	5
Table 1.4 - Abbreviation legend for Table 1 and 2.....	5
Table 5.1 - Log and Data requirements for geomechanical characterization	40
Table 5.2 -Abbreviation list for Table 5.....	41
Table 6.1 - Mechanical stratigraphy depth and thicknesses.	49
Table 6.2 - Data used for microseismic event analysis.....	49
Table 6.3 - Percentage of total events SNR >5 & distance <500m from the monitoring array....	52
Table 8.1 - Timeline of completions and production in the area of the seismic survey.....	78

ACKNOWLEDGEMENTS

I would like to acknowledge first and foremost my partner in this project and favorite geophysicist, Chris Steinhoff. Chris's unrelenting questioning of all my results and how they related to his work were invaluable in making this project what it was. I would like to acknowledge other peers and mentors whose help was essential in the success of this project; Tom Davis, my advisor, was an incredible source of support and wisdom throughout the last 18 months. Kurt Wikel, Tom Bratton, Jared Atkinson, and Eric Andersen were all sources of outstanding advice and without exception, available at all hours and for any length of time for my questions. At Talisman Energy, Frank Walles, Lindsay Dunn, and the Montney Delivery Unit were all essential in the shaping of my research. The good friends I have made here at CSM will be friends I will never forget, and must be acknowledged for the laughter they provided and support they gave: Lillian Comegys, Kelsey Shiltz, Guillaume Barnier, Imad Ashtan, Isabel White, Sean O'Brien, and Holly Robinson, thank you for your smiling faces.

A big thank you to my Thesis Committee: Tom Davis, Jennifer Miskimins, John Curtis, John Warne, and Eric Andersen for their help and advice throughout the process of writing and research.

Last but not least, thank you to my family for always letting me spread my wings in whatever direction I wanted. You have never been anything but supportive and loving through everything. This thesis is for you.

GLOSSARY OF TERMS

SEQUENCE STRATIGRAPHY

Condensed Section (CS) - Deposited during maximum transgression of the shoreline. The condensed section commonly forms the upper layer of the transgressive systems tract (TST), often characterized by high gamma ray signatures. The condensed section consists of hemipelagic and pelagic sediments deposited firstly in more distal slope and basin settings, then as the shoreline backsteps these facies move further up the slope and shelf. Sedimentation rates are lesser due to distance from the continental margin; therefore skeletal remains of pelagic fauna form the dominant facies (Loutit et al 1988).

Highstand Systems Tract (HST) - Bound by the maximum flooding surface (below) and an unconformity (above- Embry et al 2007).

Lowstand Systems Tract (LST) - bound by the sequence boundary (time surface) below and “transgressive surface” above. Includes all the sediments deposited during base level fall (Embry et al 2007).

Maximum Flooding Surface (MFS) - A surface of deposition at the time the shoreline is at its maximum landward position (Posamentier & Allen 1999). The MFS separates the transgressive and highstand systems tract. Marine shelf and basinal sediments associated with this surface are consist of slow deposition of pelagic & hemipelagic sediments and are usually thin and fine grained. These fine sediments make up the condensed section (Mitchum 1977).

Progradational Facies - an overall “shallowing-upward” trend in the facies, due to a progressive advancement of the shoreline seaward (Embry et al 2007).

Transgressive Systems Tract (TST) - bounded by the transgressive surface below and the maximum flooding surface above (Embry et al 2007).

Transgressive surface of erosion (TSE) - marine flooding surface, marking the change from a regressive trend below to a transgressive trend above. Includes all the sediments deposited during transgression (Embry et al 2007).

SEDIMENT DEPOSITION

Anoxic conditions - a depositional environment restricted from oxygen, due to a stratified stagnant water column. Anoxic conditions results in enhanced preservation of organic-rich sediments such as deepwater shale.

Argillaceous - rocks with a high clay content, and with a sufficient percentage of organic material to be considered a source rock for hydrocarbon generation (Schlumberger 2012).

Claystone - a non-fissile indurated rock with greater than 2/3 fraction clay-sized particles.

Termed clay-shale if the unit is fissile (Folk 1980).

Clay-sized particles - 0.06-2 microns (0.00006-0.0020 millimeters) (Folk 1980).

Hyperpycnal flow - depositional method produced by high-density fluvial discharge events resulting in relatively slow moving and long-lived turbulent sediment gravity flows, which may extend offshore for considerable distances (O'Connell 2011).

Mudrock - general term referring to terrigenous rocks containing greater than 50% silt and/or clay (Folk 1980).

Mudstone - a non-fissile indurated rock with sub-equal portions of silt and clay. Termed mud-shale if the unit is fissile (Folk 1980).

Pelagic Sediments - fine grained deep sea sediment composed of largely biogenic ooze that is often rich in foraminifera with 60% pelagic and neritic grains.

Siltstone - a non-fissile indurated rock with greater than 2/3 fraction silt-sized particles. Termed silt-shale if the unit is fissile (Folk 1980).

Silt-sized particles - 3.9-31 microns (0.0039-0.031 millimeters) for very fine- medium silt, 31-62.5 microns (0.031-0.0625 millimeters) for coarse silt (Folk 1980).

STRESS/ROCK PROPERTIES

Core Triaxial Test- Determines the unconsolidated, undrained, compressive strength of cylindrical specimens of cohesive soils in an undisturbed condition, using a strain-controlled application of the axial compression-test load where the specimen is subjected to a confining fluid pressure in a triaxial chamber (TXDOT 1999). This test provides data for determining strength properties and stress-strain relationships (TXDOT 1999)

Pore-pressure/Stress Coupling- $\Delta\sigma_3=2/3\Delta PP$. Data suggests minimum horizontal stress increases anywhere from 60-80% the rate of the increase in pore pressure. Therefore, contrary to uncoupled modeling predictions, decreased differential stress ($\sigma_v-\sigma_{hmin}$) will occur with increased pore pressure (Hillis 2000).

Fabric-based brittleness index - Brittleness Index $B_7=OCR^b \rightarrow OCR=(\sigma_{v(max)}/\sigma_v)$, $b=0.89$

Over-consolidation Ratio (OCR) - The ratio of past effective stress to present effective stress ($\sigma_{v(max)}/\sigma_v$ - Holt et al 2011).

Maximum past effective stress ($\sigma_{v(max)}$) - $((\sigma_{v(max)} \text{ (Mpa)}) = 8.6C_0 \text{ (Mpa)}^{0.55}$

Unconfined Rock Strength (C_0) - C_0 (Mpa) = $0.77 V_p(\text{km/s})^{2.93}$ (empirical relationship established by Hosrud, where V_p is the P-wave velocity in km/s - Holt et al 2011)

Square of the Travel-Time Ratio - $R = \text{DTS}^2 / \text{DTC}^2$

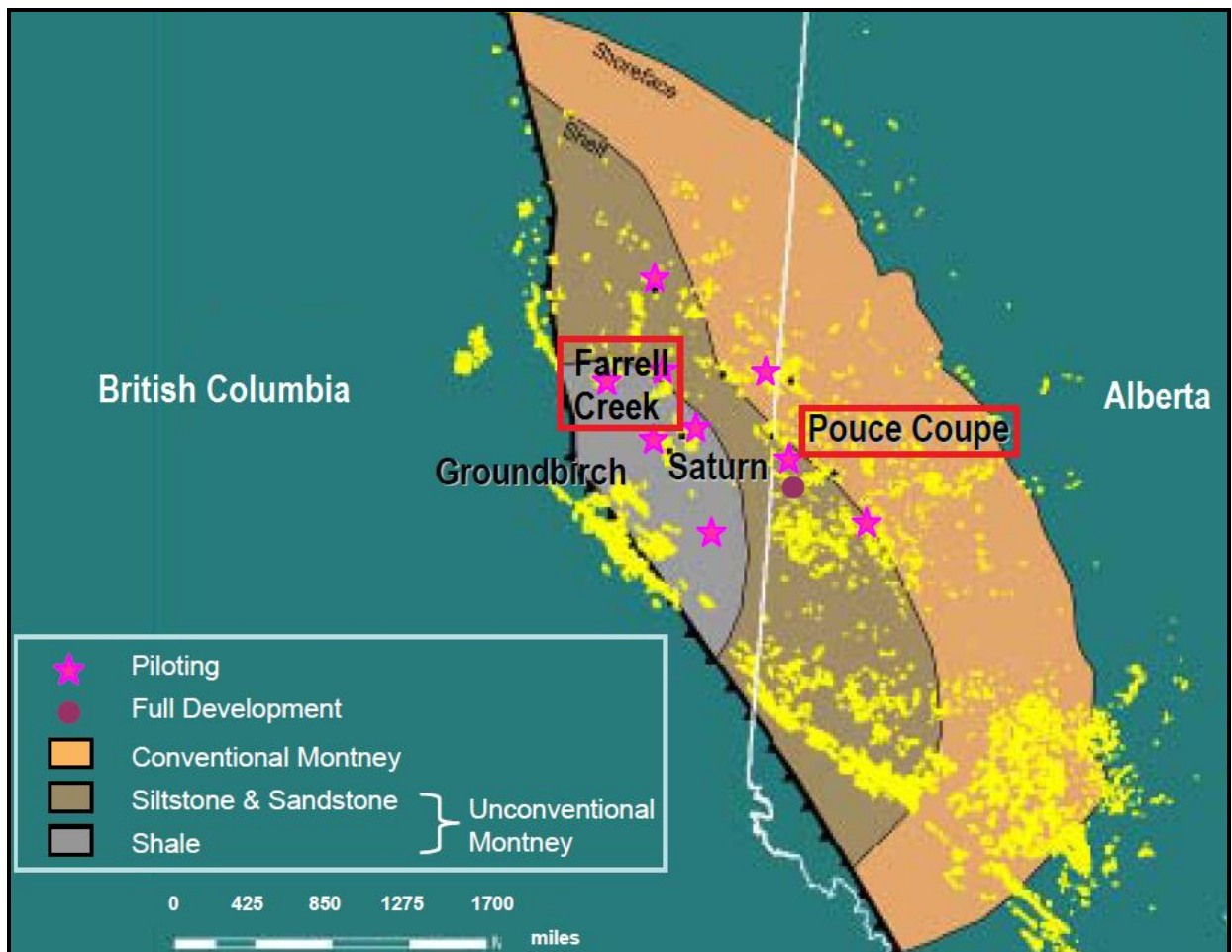
Term Abbreviations

ECS	Elemental capture spectroscopy
XRF	X-Ray Fluorescence
XRD	X-Ray Diffraction
LIBS	Laser-induced breakdown spectroscopy
SEM	Scanning Electron Microscopy
UCS	Unconfined Compressive Strength
C_0	Compressive Strength
σ_{hmin}	Minimum horizontal stress
σ_{HMax}	Maximum horizontal stress
σ_V	Overburden Stress
PHIE	Effective permeability
DTS	Shear wave travel time (us/m)
DTP	Compressional Wave travel time
V_p	Compressional wave velocity
V_{clay}	Clay Volume
RHOZ	Bulk density (kg/m ³)
PP	Pore Pressure
PR	Poisson's Ratio

CHAPTER 1

GEOLOGICAL BACKGROUND

The Lower Triassic Montney is the only documented turbidite siltstone reservoir in the Western Canada Sedimentary Basin (Moslow 2000). This reservoir has been developed since 1993 and has produced over 1.5 TCF of gas, and additional liquids (Moslow 2000). Facies grade from conventional sandstones in the East through shelf siltstones and sandstones to shale facies in the West (Map 1.1). In this study, the facies of interest are organic-rich argillaceous siltstones and shales.



Map 1.1 - Area map, with the two study areas outlined in red. Talisman pilot and development locations are outlined with pink stars and circles respectively (courtesy of Talisman Energy Inc.).

Deposition occurred in a ramp setting, and a ramp-“edge” or slope break defines the updip depositional limit of the turbidite facies (Moslow 2000). Figure 1.1 shows the generalized

depositional model for the entire Montney, defining the break in slope and sedimentary depositional processes at play. Two producing fields form the basis for my study. The Pouce Coupe Field produces from facies deposited on the slope while the Farrell Creek Field produces from more distal facies formed in a basinal setting (Figure 1.2). As shown in Figure 1.2, these two fields occur in very different stratigraphic positions. “Event beds”, a term used to describe pseudo-turbidite facies, are common in Pouce Coupe and distinctly absent in Farrell Creek. Facies exploited at Pouce Coupe are tight gas silts and sands, producing both gas and liquid hydrocarbons, due to thermal maturity in the peak oil to early gas generation window. Farrell Creek is actively being developed for its unconventional shale assets and produces entirely dry gas hydrocarbons.

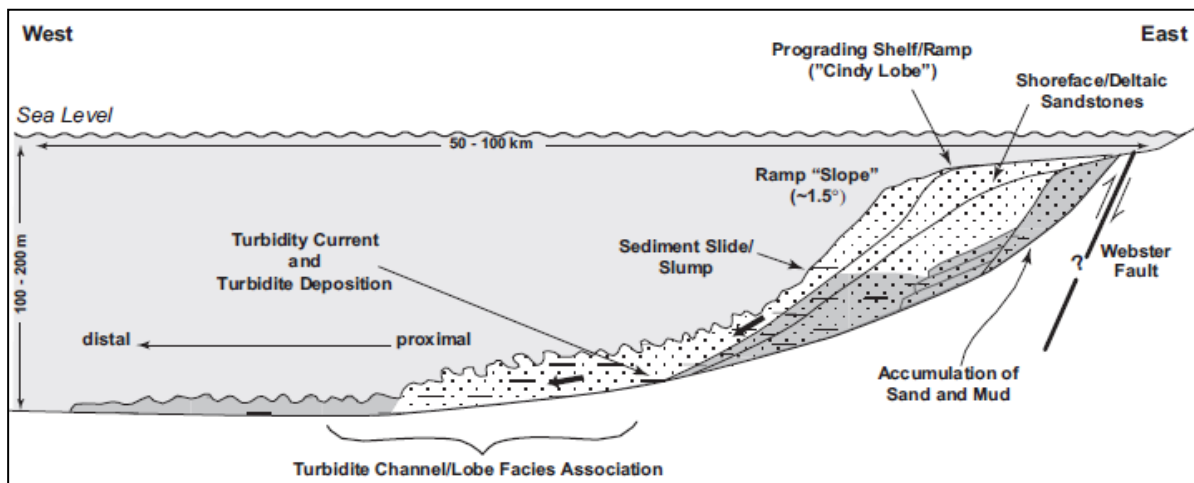


Figure 1.1 – Overall depositional model for the Montney Formation. Mass-wasting events on the ramp slope generate turbidity currents and result in downslope turbidite deposition. Moving basinward facies become finer grained and more organic-rich (courtesy of Lindsay Dunn, Talisman Energy Inc.).

1.1 Structural Framework

Structural influence plays an important role in the distribution of facies in the Montney. The Devonian-Mississippian Antler Orogeny created a regional strike-slip component that likely contributed to subsidence of the Peace River Arch, creating the Peace River Embayment on the Dawson Creek graben complex (Moslow 2000). Subsidence continued throughout the Montney depositional period. Throughout the Triassic, re-activation of extensional faults occurred contemporaneously with the formation of the Dawson Creek graben complex (Moslow 2000). Lows in the basin due to the graben complex allowed for sediment to be transported further into the basin (Moslow 2000). Therefore, Montney deposition is influenced both by syn and post-

depositional faulting. In addition, underlying Devonian carbonate reefs cause northeast-southwest trending structural highs and lows due to differential compaction.

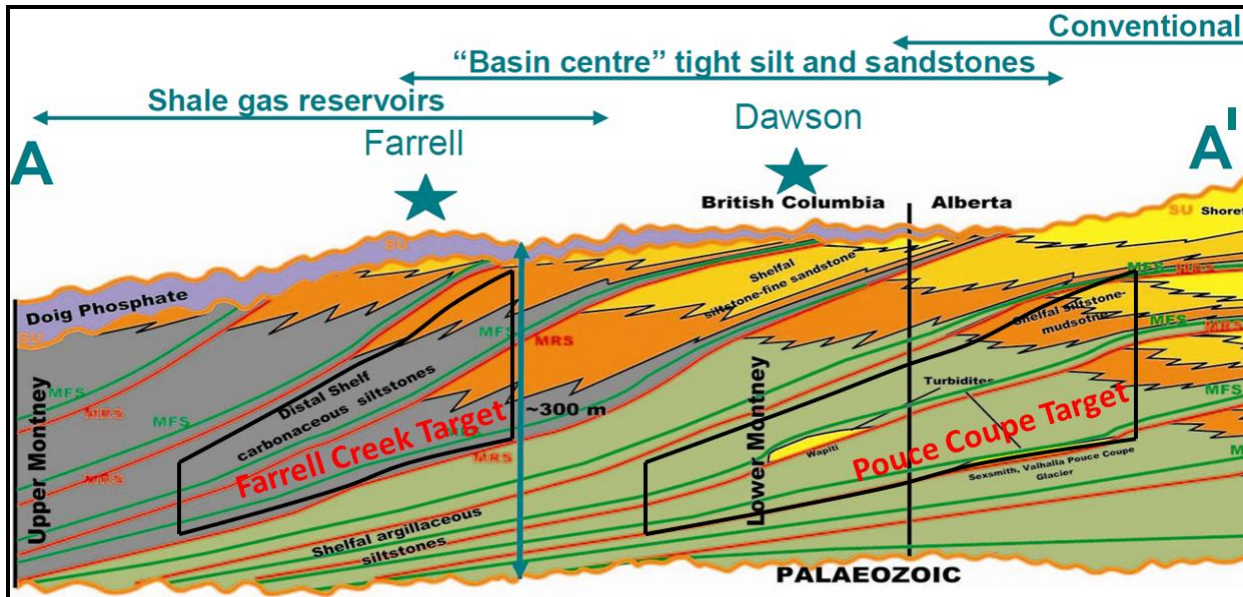


Figure 1.2- The stratigraphic framework at Farrell Creek and Pouce Coupe. Maximum regressive surfaces are defined by red lines while maximum flooding surfaces are defined by green lines (courtesy of Lindsay Dunn, Talisman Energy Inc.).

1.2 Available Data

The Farrell Creek and Pouce Coupe databases are shown in Tables 1.1 and 1.2, as well as in Maps 1.2 and 1.3. Colors refer to the components of the geomechanical analysis these wells were used for. Color legends shown in Tables 1.3 and 1.4.

Table 1.1- Farrell Creek database (see Table 1.3 and 1.4 for color legend).

WELL	LOGS	CORE	GEOPHYS.	ENGINEERING						
C-85-I/94-B-1	Full suite, image log	TRP, Rock-Eval	N/A	DFIT, S&T						
16-17-83-25W6	Full suite, Image log	TRP, Rock-Eval	N/A	N/A						
B-15-I/94-B-1	Full suite, Image log	N/A	N/A	DFIT						
C-B85-I/94-B-1	GR	N/A	MS (3-9)*	N/A						
C-C85-I/94-B-1	GR	N/A	MS (3-12)	N/A						
C-D85-I/94-B-1	GR	N/A	MS (7-14)	N/A						
C-F89-I/94-B-1	GR	N/A	MS (1-11)	N/A						
D-87-I/94-B-1	Full suite	N/A	MS (1-7)	N/A						
C-D89-I/94-B-1	GR	N/A	MS (3-12)	N/A						
C-E89-I/94-B-1	GR	N/A	MS (1-11)	N/A						
D-82-I/94-B-1	GR	N/A	N/A	DFIT						
A-A92-I/94-B-1	GR	N/A	N/A	DFIT						
C-B65-I/94-B-1	Image log	N/A	N/A	DFIT						
C-D65-I/94-B-1	GR	N/A	N/A	DFIT						

* Number refers to microseismic stages included in the analysis.

Table 1.2 - Pouce Coupe databases (see Tables 1.3 and 1.4 for color legend).

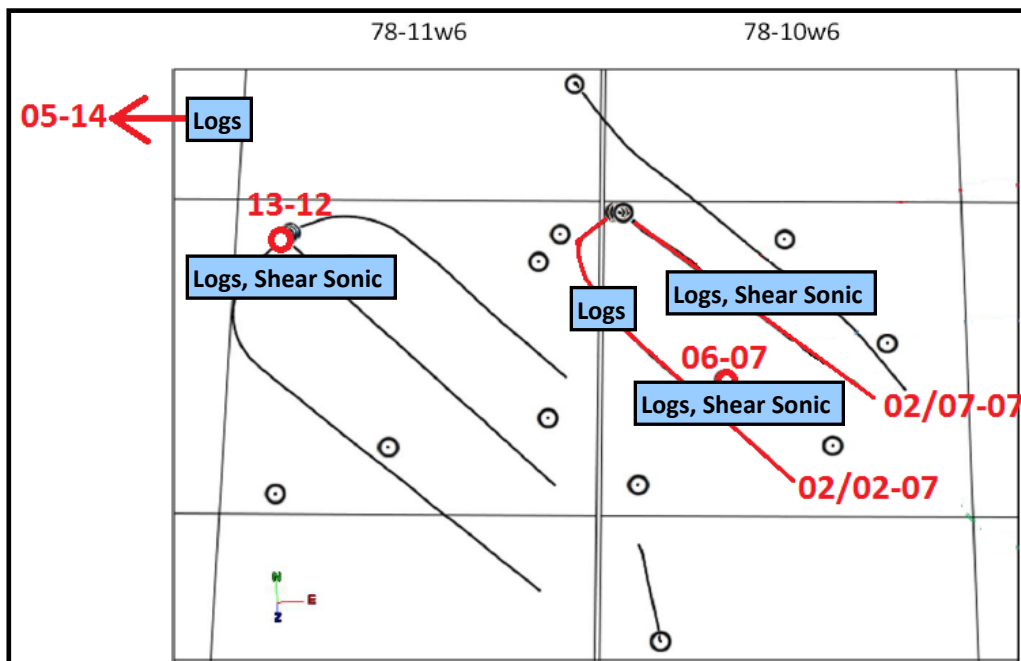
WELL	LOGS	CORE	GEOPHYS.	ENGINEERING						
0/7-7-78-10W6	Full suite	N/A	MS, 4D	S&T, FG						
2/7-7-78-10W6	Full suite, DTS	N/A	MS, 4D	S&T, ISIP, FG						
0/2-7-78-10W6	Full suite	N/A	MS, 4D	FG						
2/2-7-78-10W6	Strip log	N/A	MS, 4D	FG						
5-14-78-11W6	Full suite	N/A	N/A	N/A						
13-12-7811W6	Full suite, DTS spectral GR	Por& Perm	N/A	N/A						
5-26-80-13W6	Full suite	Por& Perm	N/A	N/A						
6-7-78-10W6	Full suite, DTS		N/A	FG						

Table 1.3- Color legend for data usage.

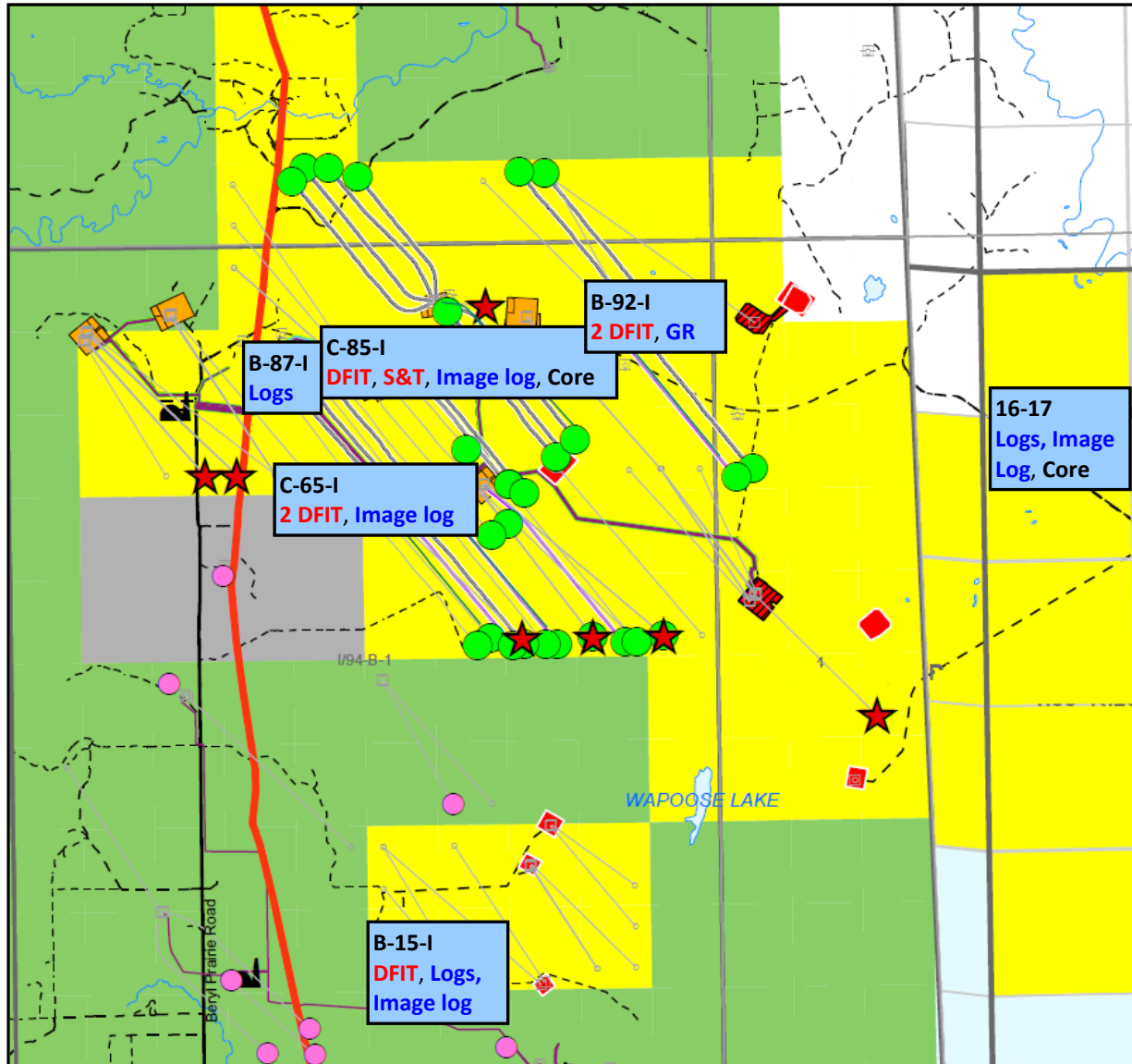
Stress Profile	
Rock properties/ RQI	
Production Correlation	
Fracture Identification and behavior (quality control)	
Microseismic Fracture network (quality control)	
Microseismic B-value and Magnitude	

Table 1.4 – Abbreviation legend for Table 1.1 and 1.2

Microseismic	MS
Rock Quality Index	RQI
Static and Dynamic Triaxial Rock Properties	TRP
Mohr-Coulomb Failure	MC
Spinner & Tracer log	S&T
Fracture gradient	FG
Porosity	Por.
Permeability	Perm.



Map 1.2- Pouce Coupe Data Locations. Wells outlined in red are those which were used for analysis, and accompanying text boxes refer to what data was available in that wellbore.



Map 1.3- Farrell Creek Data Locations. Text boxes refer to what data was used at each well location.

1.3- Previous Research by Talisman Energy Inc.

The Montney Shale is currently being developed and produced by numerous operators. Talisman Energy, in addition to designing and shooting the 4D time-lapse seismic survey in the Pouce Coupe area, is actively developing the Farrell Creek Field in Northeastern British Columbia. Three pilot wells; well 02/07-07-78-10W6 in Pouce Coupe, C-85-I/094-B-01 and 16-17-83-25W6 in Farrell Creek (see Tables 1.1 and 1.2) included abundant data and were primarily used to characterize the reservoir.

1.3.1 Farrell Creek

Stress gradient work and rock property analysis used in this report has been previously done on several wells in the Farrell Creek area. Kurt Wikel (currently of Petrobank Resources) generated stress profiles using wellbore breakout data and empirical correlations from logs while working at Talisman. These results were calibrated to pore pressure and stress data provided by completion and pressure gauge data in the field. Stress directions were determined through examination of drilling-induced fractures and breakouts in image logs. The magnitude of maximum horizontal stress (σ_{Hmax}) was inferred using available drilling and stress data as inputs into GMI SFIB software. Rock properties, namely Young's Modulus, Shear Modulus, and Poisson's Ratio, were determined using empirical correlations from logs, and calibrated to values provided by core triaxial testing. Core triaxial test results from Core Labs and TerraTek provided ground-truth values for the unconfined compressive strength of the formation.

Core facies characterization was completed by Lindsay Dunn, and additionally correlated to thermal maturity and vitrinite reflectance data which were analyzed by Lindsay Dunn, Dr. Muki, Basim Faraj, and the author. For a general overview of the Montney sedimentary framework and stratigraphic architecture, see the joint study by the University of Alberta and the Ichnology Research Group (IRG- see Selected Bibliography section).

1.3.2 Pouce Coupe

Stress profiles were generated in the same manner as in Farrell Creek, and calibrated with completion and pressure gauge data. Stress directions and magnitudes are more difficult to constrain here due to a lack of image logs, so inferences were made using the Farrell Creek dataset. Core facies characterization was completed by Dawn Jobe. This previous work was used to aid in the definition of mechanical stratigraphy for the two study areas, which will be expanded on in Chapters 3 and 5.

CHAPTER 2

SEQUENCE STRATIGRAPHY

Conventional play evaluation involves the identification of three critical elements; hydrocarbon charge, reservoir, and trap. Hydrocarbon charge includes the presence of a source rock, thermal maturity, and appropriate migration pathways. The reservoir must be sufficiently porous and permeable to house migrated hydrocarbons. Finally, both closure (trap volume) and seal (trap efficiency) are necessary for maintaining hydrocarbons in the reservoir (Toro 2011). Conventional sequence stratigraphic models have long been used in connection with depositional systems to predict the origin and extent of facies with appropriate hydrocarbon charge, reservoir, and seal. By using vertical stacking patterns and lateral associations within a sequence, facies can be placed within a framework relating them to the surrounding rock. Chronological evolution of a basin can also be established through time boundaries interpreted from seismic and paleo-biologic controls.

In unconventional shale reservoirs, sequence stratigraphy must be approached differently than it would be in a conventional shelf setting. Hydraulic fracturing of shale is necessary to create sufficient permeability for commercial production, so a method of relating stratigraphy to geomechanical and hydraulic properties is essential for successful reservoir development. In the study areas presented here, a portion of the total stratigraphic package is being examined, without the entire framework to correlate to. Facies prediction and association must still be employed despite the more subtle variations in these stratal packages. The depositional pattern in deepwater settings ultimately conforms to known stratigraphic controls and architectures (Passey et al 2010). In addition, it is hypothesized by Slatt et al 2011 that many deepwater shale reservoirs were deposited under similar environmental conditions, with similar transport mechanisms, and therefore a generalized model can be defined (see Figure 2.1). The common model is a basal transgressive surface of erosion (TSE), followed by a marine transgression depositing the fining-upward facies of the transgressive systems tract (TST). In some cases a high gamma ray condensed section caps the TST, and is followed by a downlapping progradational highstand systems tract (HST). A diagram of these terms is outlined in Figure 4. Other commonalities amongst shales include presence of pyrite, indicating reducing conditions in the depositional environment (noted in the Barnett, Haynesville, Marcellus, Woodford, and Horn River Shales, Slatt et al 2011).

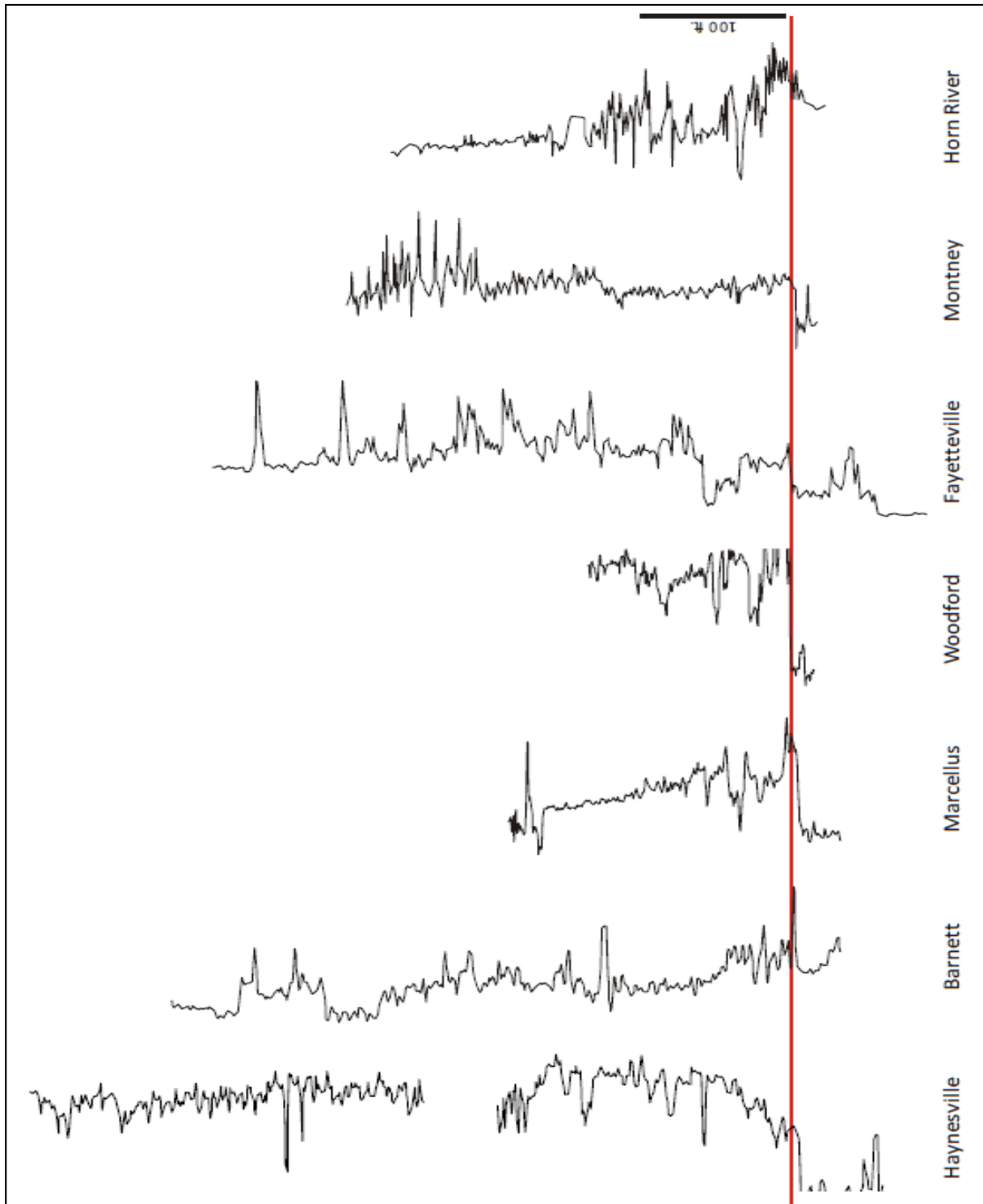


Figure 2.1- Gamma Ray Logs showing the commonalities of North American Gas Shales (Rodriguez et. al 2000). A basal transgressive systems tract (organic-rich/phosphate-rich fining upward) shaley interval is capped by an organic-rich, high gamma ray shale, followed by a highstand systems tract (clay/quartz-rich coarsening upward) interval (Slatt et al 2011).

While the similar depositional conditions and architectures of various shale reservoirs aids in the use of a sequence stratigraphic model, the starved sediment conditions of deepwater shales hinders the use of sequence stratigraphy in the traditional sense. Starved sediment conditions means the stratigraphic record does not have relative sea level defined by proximal basin-margin facies. Examination of the Bakken and Exshaw formations of Western Canada exemplifies this problem. The Bakken and Exshaw are distal deepwater hemipelagic mud formations; however a lack of contemporaneous offshore/shoreface mudstone or sandstone deposits means that the linkage between distal and proximal facies is missing (Bustin and Smith 2000).

Due to this disconnect the current strategy relies heavily on the gamma ray curve (Crews et al 2000). Additional parameters are required to correlate distinct stratal patterns. Of these parameters, the two that are related to this study are the use of geomechanical rock properties to create facies types, and using sequence stratigraphy to relate natural fracture type to the type of failure expected in the subsurface (Billingsley et al 2006). These methods will be discussed further in Chapters 4, 5, and 7.

The most productive portion of shale reservoirs are associated with the thermally mature strata of the transgressive systems tract/condensed section (TST/CS) (Hart 2011). The TST/CS is characterized by high TOC (Type I/II) and a high silica and/or carbonate component. In terms of rock properties, this makes the TST/CS shales relatively brittle and ideal candidates for fracture treatments. Additionally, TST/CS shales are considered to have less variability in lithology and thickness throughout the reservoir, making them more predictable for horizontal well development (Hart 2011).

While unconventional reservoirs such as the Montney are often referred to as “black shales”, clays can comprise less than 20% of the rock (Hart 2011). The most accurate description of the Montney “shale” is an organic-rich argillaceous mudrock (see Glossary of Terms). The Lower Montney consists of transgressive and highstand systems tracts, while the Upper Montney consists of a lowstand systems tract turbidite facies assemblage as well as transgressive and highstand systems tracts. In the East, the sequence boundary separating the Upper and Lower underlies a laterally discontinuous dolomitic coquina, and basinward toward the West this boundary underlies the turbidite coarser facies of the lowstand systems tract in the Upper Montney (Moslow 2000). Figure 2.2 shows the generalized systems tract model.

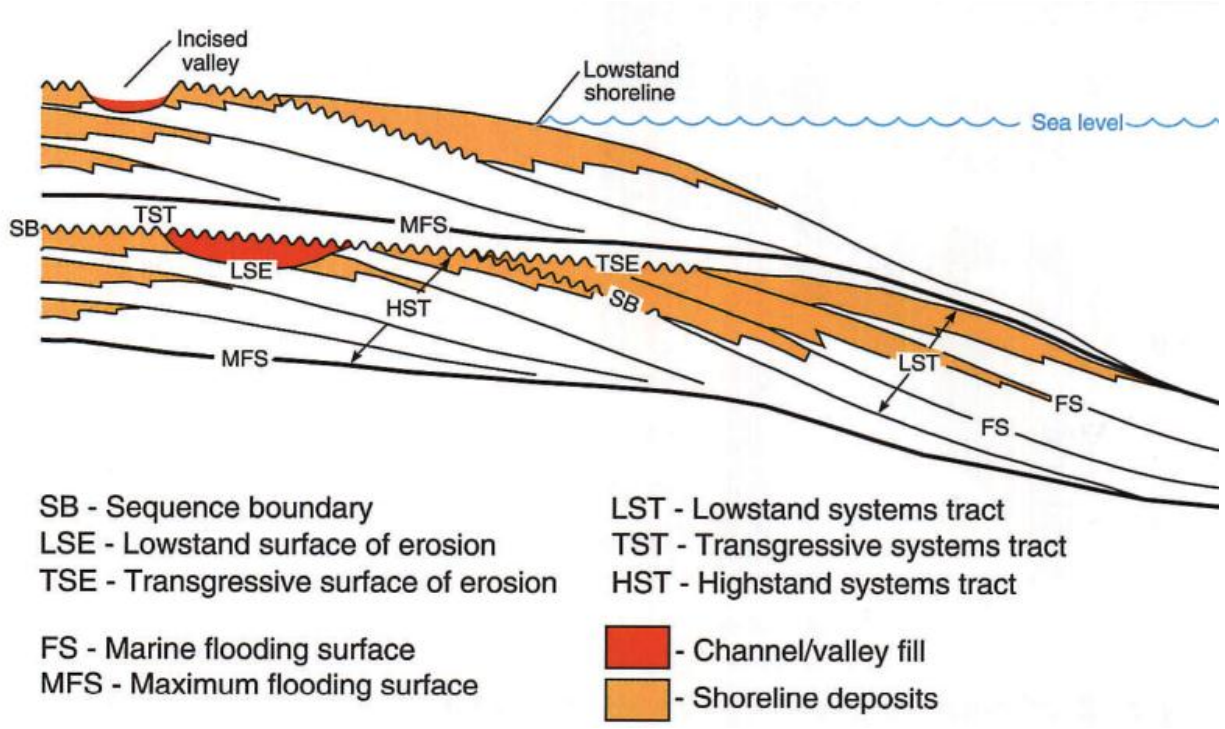


Figure 2.2 - Geometrical relationships between the highstand systems tract, transgressive systems tract, lowstand systems tract, and maximum flooding surface (MFS- Posamentier et al. 2011).

CHAPTER 3

COMPONENTS OF MECHANICAL STRATIGRAPHY

Although shale has been conventionally viewed as a single homogenous facies, the merits of defining distinct packages are coming to light. Heterogeneities within the unit can be defined on many different scales depending on the scope of interest. It is necessary to recognize this fine-scale variability, as it is apparent that it affects the completion and production results from wells to date. Through the definition of a mechanical stratigraphic framework, engineering parameters such as perforation and fracture spacing, stage number, horizontal length, and lateral landing point can be targeted based on high-graded areas of the reservoir.

The original definition for rock type is as follows:

Rock Type (Archie 1950): Units of rock deposited under similar geological conditions, having undergone similar diagenetic processes, and resulting in a unique porosity, permeability, capillary pressure, and water saturation for a given height above free water.

The definition above for distinguishing rock types clearly has limited applicability in unconventional reservoirs, as outlined by Kale (2009). In shale there is a much smaller range of porosity and permeability to distinguish different areas of the reservoir. In addition, shales occur at irreducible water saturation due to expulsion and overpressuring during hydrocarbon generation (Momper 1980). Another important mechanical factor is stratigraphic layering. Because of the quiescent conditions of deposition, sedimentary structures in deep water shales are primarily laminations, and the degree of lamination will have a strong influence on the rock properties within the unit. Changes in rock properties associated with layers will create planes of weakness, stress concentration, and are likely candidates for fracture propagation. Therefore, a new method of rock typing must be used to accurately characterize an unconventional reservoir.

Newsham and Rushing (2001) defined three different rock types; depositional, petrographic, and hydraulic. Based on these three criteria, I define a brittleness index first based on depositional conditions, then on petrographic conditions, and finally combine these two indices with the rock stress profile to generate a hydraulic rock type- the Rock Quality Index (RQI).

Formation brittleness and the corresponding Rock Quality Index (RQI) are dependent on heterogeneity within the formation, due to such factors as hydrocarbon generation, porosity, laminations, and rock property changes. These factors, along with others, can be classified under two fundamental categories to accurately characterize heterogeneity. These two categories leading to intra-shale heterogeneity are compositional variation and fabric variation, as shown in Figure 3.1.

Compositional variation is closely tied to petrographic conditions. Petrographic factors include (1) clay volume, (2) TOC (kerogen), and (3) mineralogy. Clay volume is dependent on the stratigraphic position of the reservoir, the abundance of authigenic clay minerals, and the degree of weathering. As minerals weather, illite, kaolinite, chlorite, and several expandable clays are formed. The volume of these different clay components will have an affect on overall formation brittleness. Finally, the abundance of minerals such as quartz and calcite will affect brittleness. Calcite and quartz are considered “brittle” minerals, meaning that they are more likely to break easily under increased stress. These petrographic factors will be further examined in Section 3.1.

Rock fabric variability is closely tied to depositional conditions, which are highly dependent on geological architecture, stratigraphic position, and sedimentary structures (Newsham and Rushing 2001). The depositional conditions which will be focused on in this thesis are (1) laminations and (2) natural fractures. Laminations are created as layers of clay, silt, and mud are deposited in quiet deepwater conditions. Natural fractures can be created as hydrocarbon generation causes overpressure sufficient to fracture the reservoir and allow for hydrocarbon movement through microfractures (Williams 2012). Fractures can also be created syn and post-depositionally with tectonism and deformation. These factors will be further explained in Section 3.2.

3.1 Compositional Variation- Petrographic Factors

Clays are a major constituent of mudrocks; the most common types being illite, kaolinite, chlorite, and expandable clays (Sondhi 2011). Other main constituents include siliceous minerals such as quartz, calcite, pyrite, and feldspars. A higher proportion of siliceous minerals correlate to higher values of Young’s Modulus and therefore a relatively brittle rock unit (Ross et al 2009). Higher proportions of clays are believed to reduce the brittleness of the rock (Ross et al 2009).

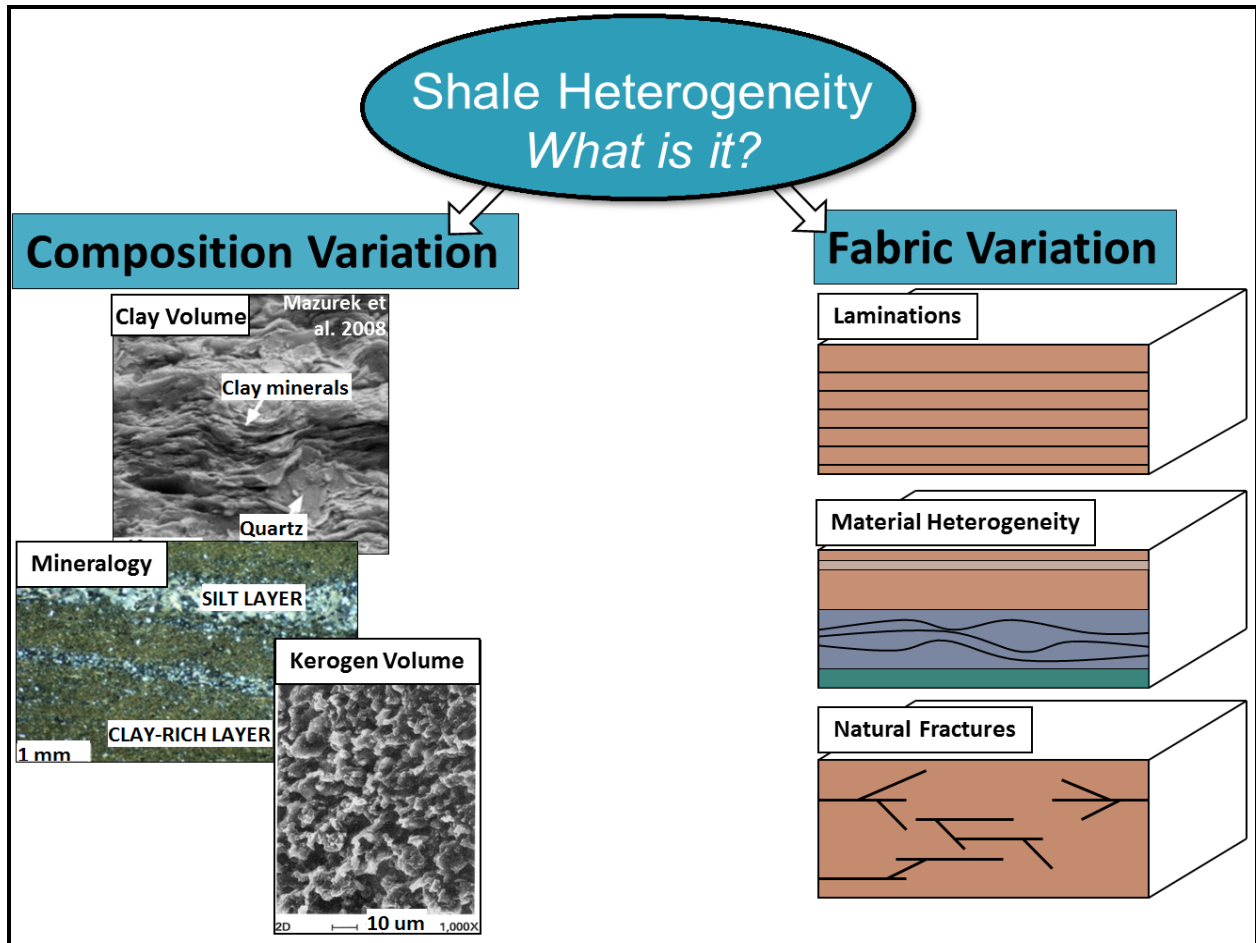


Figure 3.1- Shale heterogeneity divided into two main categories of composition and texture. Changes in the abundance of clay volume, kerogen volume, and mineralogy will affect the rock properties of the formation, as will the abundance of laminations, other sedimentary structures, and natural fractures.

An example is found in the Appalachian Basin, where in the Marcellus Shale, it is noted that increased amounts of quartz, as well as reduced clay content, results in increased brittleness in the formation. Intra-shale changes in mineralogy occur with changes in stratigraphic position. Further to the initial mineralogical conditions of the reservoir, changes will occur with the introduction of external forces and fluids into the formation. The higher proportion of calcite in the formation, the larger the decrease in Young's Modulus with exposure to fracturing fluid, due to precipitation of minerals with the fluid (Akrad et al 2011).

There is a relationship between the volume of quartz in the formation and the fabric-based heterogeneity of the reservoir; further outlined in section 3.2. The presence of quartz silt

grains has the tendency to hinder the alignment of clay particles, causing areas of lower strain and fabric anisotropy (Bandyopadhyay 2009).

3.1.1 Thermal Maturity

Total organic carbon (TOC) is a measure of the organic richness of sedimentary rocks (Jarvie 1991). Vertical variability in TOC can occur on a relatively small scale (Passey et al. 2010), and should be incorporated into rock property profiles. The three components of TOC are extractible organic matter (EOM), convertible carbon, and residual carbon. Extractible organic matter is the fraction of organic matter already generated but not expelled (bitumen). Convertible carbon is the portion of the rock remaining with the potential to generate oil and gas (kerogen). The residual carbon fraction is the portion of the rock remaining with no potential to generate oil and gas (Jarvie 1991). The convertible carbon portion of the TOC measurement is related to kerogen type and volume, and is therefore the measurement having an influence on rock brittleness.

Kerogen is formed from the remains of marine and lacustrine microorganisms, plants, and various amounts of terrigenous debris. It can be present in various forms; Type I is associated with a lacustrine source; algae in anoxic lakes, with high hydrogen:carbon ratios (>1.3) and low oxygen:carbon ratios (<0.1). This kerogen type is commonly oil-prone with up to 70% organic content. Type II kerogen is associated with marine reducing environments, and accounts for the majority of petroleum source rocks (Tissot & Welte, 1984).

As thermal maturity increases, internal structure of the shale increases, leading to more laminations and, according to some authors, more micro-porosity along bedding planes; coincident with the more ordered structure of the minerals (Ross et al 2009). With an increase in micro-porosity there is a corresponding increase in permeability, and also an increase in brittleness associated with interfaces between laminations (Ross et al 2009).

To determine TOC abundance, shale compositional breakdown is typically performed with LECO analysis. Semi-quantitative TOC values can also be calculated from trace element geochemistry; by fitting a linear regression equation (with correlation coefficient >0.8) relating selected trace elements and measured TOC. A model of TOC values can then be up-scaled to areas where LECO analysis was not performed (Ratcliffe and Schmidt 2011).

The paleo-reducing conditions of a shale reservoir will have a significant impact on the TOC values. Increased TOC is associated with anoxic basin-floor conditions. Elemental geochemistry in sediments and fluids can be used as a proxy for depositional redox conditions (Ratcliffe and Schmidt 2011). Principal component analysis (PCA) is used to distinguish between environmental effects on major and minor trace elements, such as terrigenous input, carbonate production, and authigenic enrichment from sea water. Studying these vertical and lateral changes of elements helps to constrain the sequence stratigraphic model of the formation, based on sediment origin (Ratcliffe and Schmidt 2011).

3.2 Fabric Variation- Depositional Factors

Sediment origin and deposition will affect the pore structure and fabric of a unit. Pores can be present as fossil fragments, organic pores within a kerogen, or microchannels and fractures within the shale matrix (Slatt et al 2011). The distribution and types of porosity present will lead to variability in permeability, flow pathways, and susceptibility to deformation. Depositional energy will affect how pores are distributed as well as how silt and mud layers are organized. For example, in a study of the Eagle Ford shale by Cander et al 2012, it is suggested that a drop in effective stress at the top of the formation is a function of the preservation of pore throats. This has large-scale implications for increased permeability and hydrocarbon migration at these depths. Additional pore-scale variability will be sourced from the extent of pore alignment and inclusions in the reservoir (Bandyopadhyay 2009- Figure 3.2).

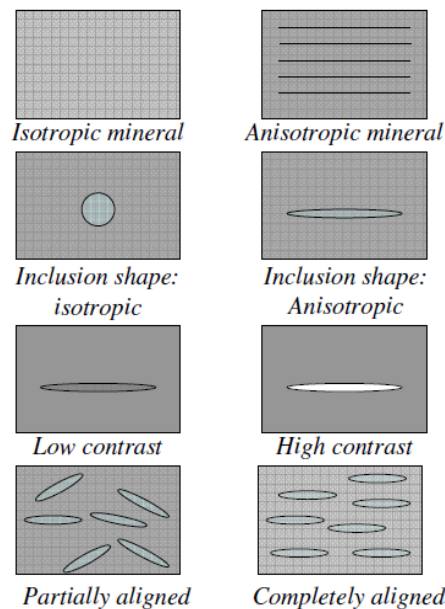


Figure 3.2- The variability in reservoir fabric which will occur with various inclusion shapes and orientations (Bandyopadhyay 2009).

3.2.1 Laminations

Individual laminations are the result of individual transport/depositional events (Slatt et al 2011). Due to the variety of transport mechanisms, variability will occur in the resulting deposits. Hyperpycnal flows, turbidity current flows, storm and wave reworking, and bottom-hugging slope oceanic currents are all methods of deepwater shale deposition (Slatt et al 2011). The degree of lamination is a critical correlation factor for determining rock property changes and barriers to fracture propagation. Laminations act as interfaces between two zones of differing properties, thereby creating a surface of stress concentration and likely candidate for rock slip. Interface weaknesses have been observed through a variety of different methods:

- (1) Mineralogical Evidence: Authigenic cement along bedding planes/laminae is often reduced or absent, created a plane more susceptible to failure (Slatt et al 2011).
- (2) Core Evidence: Core testing shows rock has reduced tensile strength when applied stresses are parallel to laminae. Young's Modulus (as measured from ultrasonic core measurements in the Woodford) is higher when measured parallel to laminations, implying more brittle rock behavior (Slatt et al 2011).
- (3) Outcrop Evidence: Fractures running perpendicular to bedding are often inhibited by interbedded ductile zones within a sequence (Slatt et al 2011).
- (4) Seismic Evidence: Records of hydraulically-induced microseismic events show that activity is more prevalent in stratigraphic intervals with thinner and more abundant laminations, rather than thicker and more competent units (Slatt et al 2011).

In all shales, laminations are commonly abundant and well-developed (Bandyopadhyay 2009). Therefore we can consider as the base case; fabric variation within a shale will be sourced from laminations if microfractures and large-scale fractures are not present.

3.2.2 Microfractures

As kerogen matures in a formation, hydrocarbon generation causes water expulsion and overpressure. Overpressuring results in tiny "cracks"; microfractures, which are a fundamental pathway allowing oil and gas migration throughout the formation (Momper 1980). However, these microfractures are in isolation not sufficient for commercial production. Larger fractures are required to provide the high-permeability pathways to the wellbore. These can be created through syn and post-deposition tectonism, or can be artificially induced through a hydraulic stimulation.

3.2.3 Large-scale Fractures

Varying scales of sedimentary layering control the density of fracturing within a unit (Figure 3.3- Zahm and Hennings 2009). Similar observations have been made in coal bed methane reservoirs, where the spacing of cleats (analogous to natural fractures) is proportional to the thickness of the bed (Meckel 2012). The scale of stratigraphic control decreases as the degree of deformation increases (Hennings 2009). In shale reservoirs, where deposition generally occurs in quiescent conditions with little-no tectonic activity, stratigraphic control therefore plays a large role in the distribution of fractures. However, this can be altered by post-depositional tectonics or hydraulic stimulation.

During burial and compaction of the formation following deposition, the overall stress state can be significantly altered. The stress state can also be changed with increasing age of a reservoir, as an increase in age generally corresponds to an increase in burial depth and compaction (Figure 3.4). Rock properties will be affected by changes in porosity and permeability occurring with diagenesis and compaction. Greater compaction will lead to consolidation and cementation of the sediment, changing the internal pore structure and likely changing the response to a hydraulic stimulation. At the same time compaction is occurring, tectonism can be occurring leading to the possibility of increased permeability with fracture and fault formation. Evidently, there is a complex relationship between reservoir transport, deposition, burial, and structural elements.

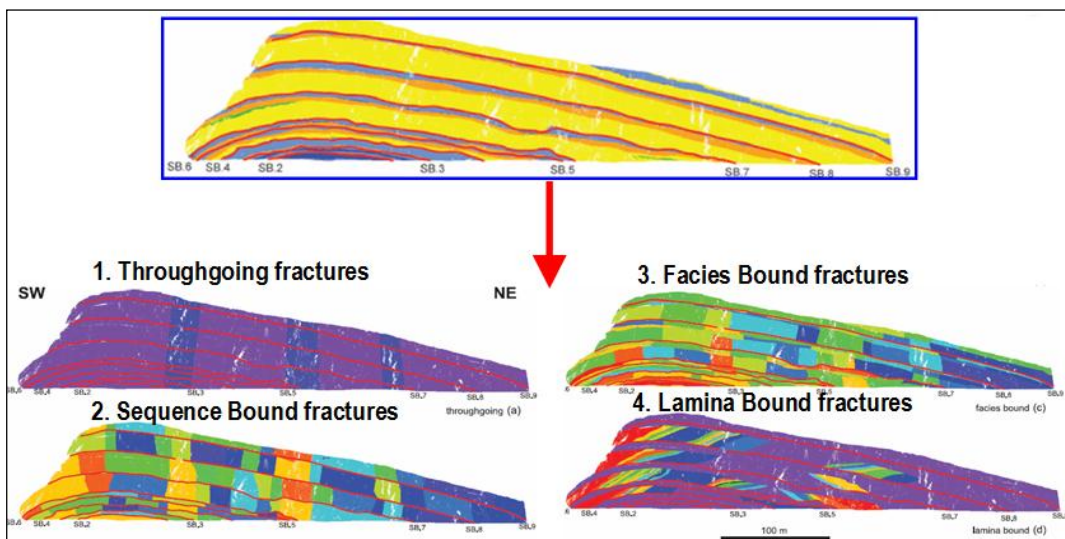


Figure 3.3- The different types of fracturing which can occur in an unconventional reservoir, from the largest scale (through-going fractures) to the finest scale (lamina bound fractures- modified from Zahm & Hennings 2009).

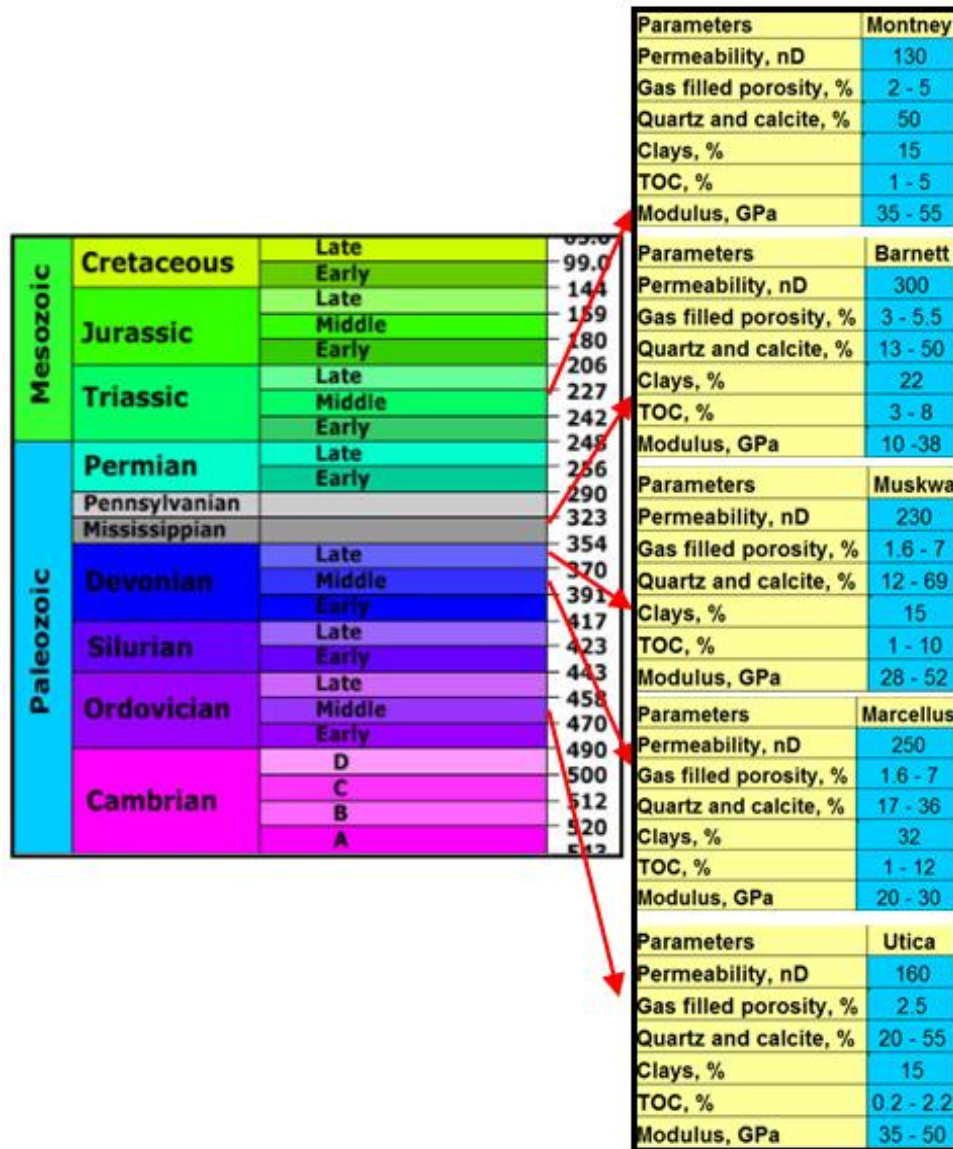


Figure 3.4- Relative ages and petrophysical parameters of North American gas shales; oldest to youngest Utica, Marcellus, Muskwa, Barnett, and Montney.

3.3 Integration of Rock Variability

In conclusion, there are many factors which can be a source of rock variability. The elements have been generalized and separated into the categories of composition (petrography, TOC) and fabric (laminations, microfractures, large-scale fractures); however this does not simplify the complex interplay. However, it can be said that any interface between variations in rock properties or stress will act as a zone of weakness. As the purpose of this thesis is to ultimately relate these weakness zones to optimal completions, defining where likely interfaces occur, regardless of their cause, is of vital importance.

CHAPTER 4

ROCK PROPERTIES & STRESS PROFILES

The regional stress regime of both Farrell Creek and Pouce Coupe is strike-slip, meaning that the overburden stress is the medial stress and the two horizontal principal stresses represent the maximum and minimum stress magnitudes (Figure 4.1). However, there are differences in the stress anisotropy between the two areas. Farrell Creek exhibits an extremely high anisotropy between the maximum horizontal stress (σ_{HMax}) and the minimum horizontal stress (σ_{hmin}). These two stresses will herein be referred to as σ_{HMax} and σ_{hmin} . This strong horizontal stress anisotropy is due to proximity to the Laramide deformation belt of the Canadian Rocky Mountains. The likelihood of critically-stressed natural fractures is high because of the strong unidirectional stress component.

In Pouce Coupe, stress anisotropy is lower and therefore likely fewer critically stressed fractures are present. However, this hypothesis cannot be validated at the borehole scale with the available dataset (lack of image logs). To gain an understanding of the fracture state in Pouce coupe, 4D time-lapse seismic was used, which will be discussed in detail in Chapter 8.

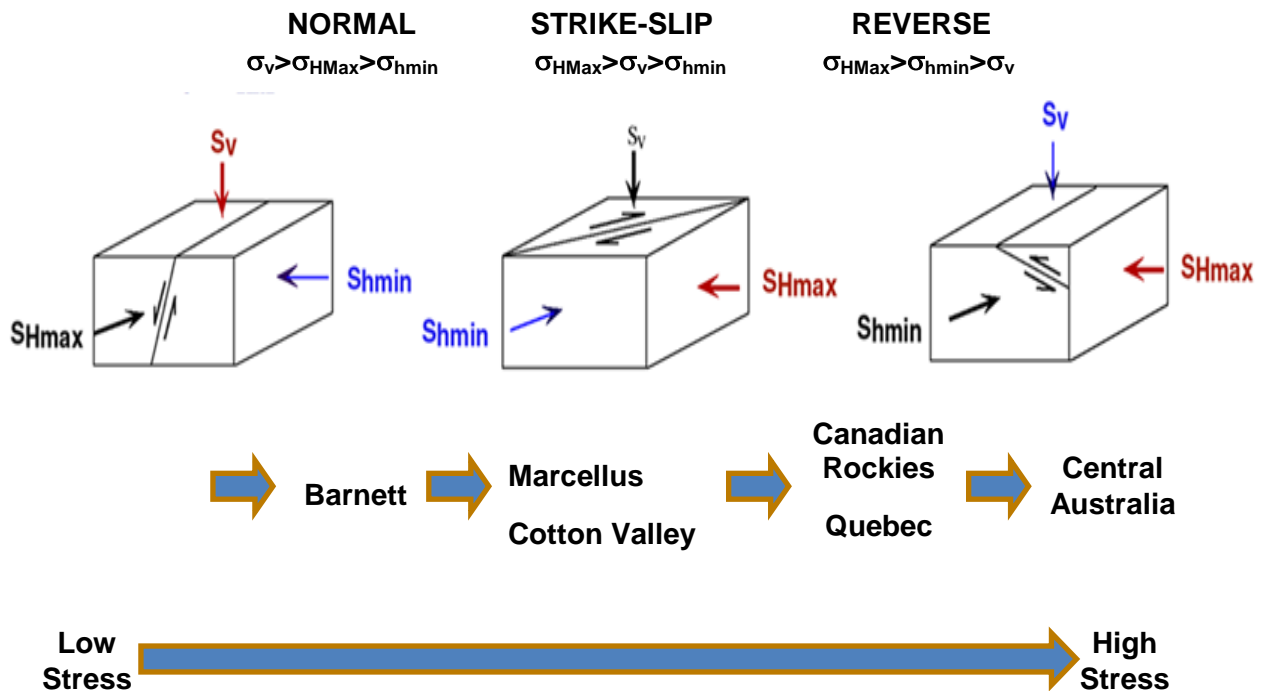


Figure 4.1- Normal, strike-slip, and reverse stress regimes, varying with relative magnitudes of the three principal stresses σ_{HMax} , σ_{hmin} , and σ_v .

4.1 Implications of Stress for the Geomechanical Model

Regional tectonics will have an influential overprint on rock variability, on both the macro-scale and micro-scale. At the macro-scale, mechanical variations due to fault and fracture systems and associated stress-strain relationships will result in a differing stress state within the area affected by the faulting/fractures (Rice 1992). Stress state has important implications early in field development; in determining the optimal well orientation and completion strategy.

Stress orientations will also have a strong correlation to fracture character and orientation, a vital aspect of low permeability shale reservoirs. At the micro-scale, regional stresses can have an impact on the diagenesis of sediments (Billingsley et al. 2006). Burial has the ability to crush grains, cause pressure solution, and decrease the porosity and permeability of a formation. Basin-scale tectonic stresses can have a similar impact (Billingsley et al. 2006). Differential compaction will occur as a direct consequence to the degree of anisotropy between the principal horizontal stresses. A weak fabric will develop in the rock, associated with compressional strain (i.e. pressure solution boundaries and vertical stylolites). These features are commonly perpendicular to the maximum horizontal stress and will be more numerous where differential compression is greater (Billingsley et al. 2006). Once again, it is ultimately the resulting changes in rock fabric, both at the macro and micro-scale, which are significant in the exploration and development of shale reservoirs.

Rock properties and the stress state of the reservoir can be derived from both log-based empirical equations and core-based triaxial testing (see Glossary of Terms). Both the defined rock properties and stress components can be used as indicators of the variability within the reservoir, as outlined in Figure 3.1. However, the elements to focus on are those factors which are related to the ideal conditions for hydraulic stimulation of a reservoir. As a continuation of Figure 3.1, Figure 4.2 shows how shale heterogeneity is related to the two main components which are considered “ideal” for stimulation; brittle rock and failing fractures. These two components will be defined through the construction of a geomechanical model and mechanical stratigraphic framework, as shown in Figure 4.3.

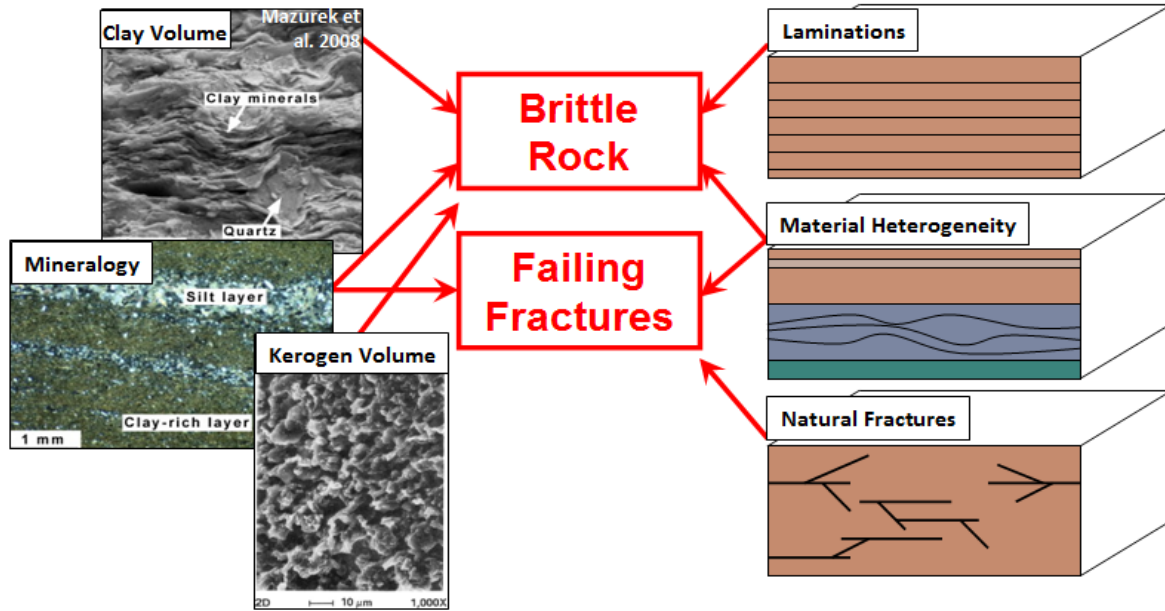


Figure 4.2- Shale heterogeneity factors as components of production factors. In a successful hydraulic stimulation, both brittle rock and failing natural fractures are desired to create a complex fracture network and provide the greatest reservoir reach.

GEOMECHANICAL MODEL

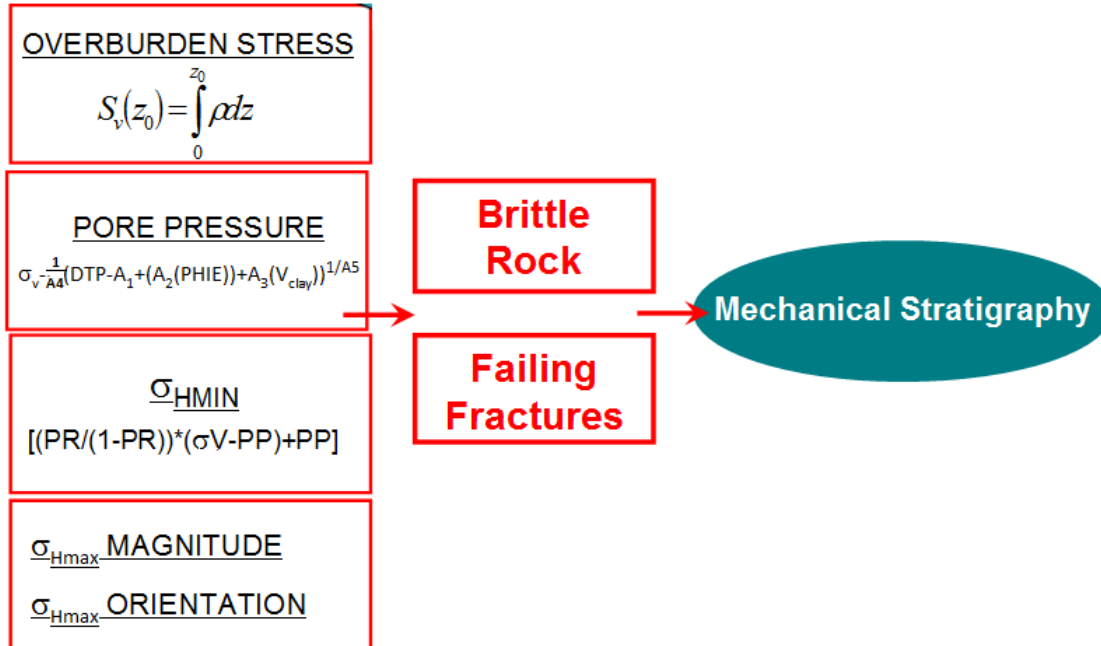


Figure 4.3- The use of a geomechanical model to define the mechanical stratigraphy of the reservoir, and ultimately relate this stratigraphy to hypothesized fracture failure and brittle zones.

4.2 Log-derived Rock Properties

Dynamic rock properties can be obtained from standard equations using the compressional and shear sonic logs for a given formation. It is assumed that acoustic velocities are related to rock elastic properties (Barree et al. 2009). However, the use of these equations must be considered in the context of the reservoir of interest. In both conventional and unconventional reservoirs, other factors will result in variability of the acoustic log; fractures and laminations, external stress, borehole conditions (i.e. breakouts, mud weight, borehole size), pore pressure, and pore fluid saturation (Barree et al. 2009). In addition, sonic logs will slow significantly due to organic content or gas saturation, which will both evolve as free gas is generated. Using these slower sonic velocities will lead to inaccurate estimates of dynamic elastic moduli. The sonic log should be corrected for gas saturation and TOC before calculations are made.

Secondly, it is important to note that rock moduli are dependent on the ratio of shear slowness squared over the compressional slowness squared (Barree et al. 2009- see Glossary of Terms). Therefore calculated rock properties will have an even greater error due to squaring of the terms in the equation.

Overall, log derived acoustic velocities fail to show the true degree of stratification present in the reservoir, and therefore log-generated stress profiles will be generalized (Barree et al 2009). Fine-scale heterogeneities evident in core should be used as a calibration point for any log-derived profiles.

4.3 Core-derived Rock Properties

Rock properties obtained from core are considered “ground-truth” and used as calibration points for dynamic values obtained from logs. However, possible inaccuracies noted for log-derived properties are also present in core-testing procedures. When a core sample is tested, the confining stress, net effective stress, stress history, pore pressure, temperature, and saturation can all affect the results (Barree et al. 2009). As cores are brought to surface, coring-induced fracturing and saturation changes can occur, and subsequent testing will not reflect the in-situ reservoir conditions. Microfractures will generally reduce the rock strength and Young’s Modulus. One method used to account for core relaxation and the development of microfractures is to stress-cycle the core sample before testing. Figure 4.4 shows a hypothetical progression of Young’s Modulus with stress cycling. Modulus E1, E3, and E5 are the initial

compaction, unloading tangent, and high net stress secant modulus respectively. These three moduli are unlikely to be representative of the reservoir stress state, which leaves E2 and E4, the low and high net stress tangent modulus respectively. The correct modulus should be chosen based on the relevant borehole stress condition (Barree et al 2009).

Another important factor is the saturation state of core samples. During hydraulic fracturing, pressure and fluid changes are introduced into a formation at very high rates. The dissipation of internal pore pressure does not occur fast enough to offset this deformation, due to the inherent low permeability of shale. As a result, rock properties are often measured on un-drained samples and compressional and shear velocities can change dramatically due to saturation. Pore pressure of a core sample will also affect whether it behaves as a drained or un-drained rock (Barree et al 2009). To illustrate this dependency on pore fluid pressure, an un-drained sample will yield a Poisson's Ratio of 0.5, the maximum possible value, indicating the sample is fluidized/ incompressible.

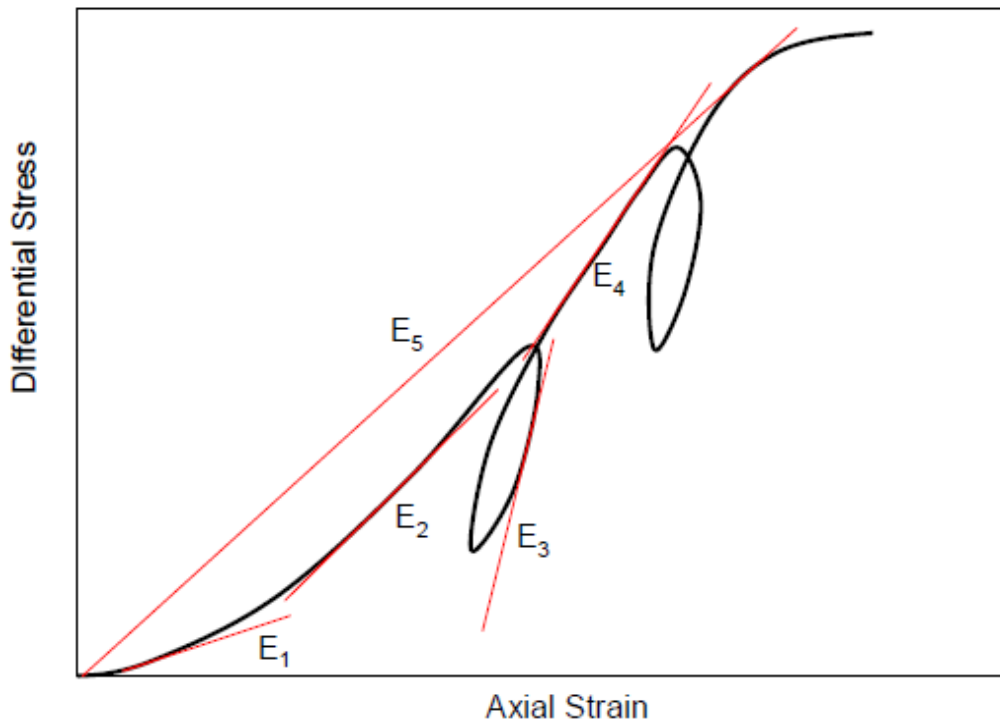


Figure 4.4 –Stress cycling of core sample, and effect on Young's Modulus. Different methods of measuring Young's Modulus values are shown by E1-E5 on the plot (Barree et al 2009).

4.4 Calibration Points

Field tests are the most accurate way to calibrate both log-derived and core-derived rock properties and stress values (Figure 4.5). Diagnostic Fracture Injection Tests (DFIT) and Mini-Frac tests available in the Farrell Creek area were used as calibration points in this study. These two tests are described below.

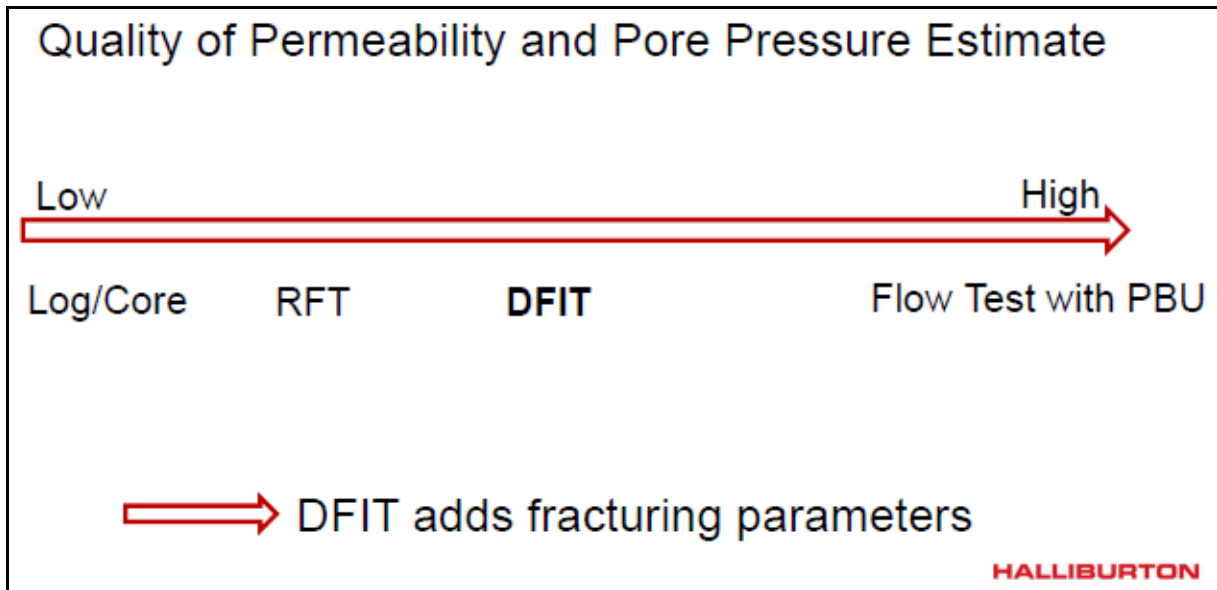


Figure 4.5- Limited amounts of engineering data will result in limited knowledge of fracture parameters, while the availability of DFIT's and flow tests allow for more accurate characterization (Mayerhofer 2012).

Mini-Frac and Diagnostic Fracture Injection Tests (DFIT) are used to determine fracture closure pressure and calibrate σ_{hmin} and rock properties obtained from logs and core. While the hydraulic fracture closure pressure is representative of reservoir σ_{hmin} , this assumes that the only variables are vertical uniaxial strain and external horizontal tectonic strain offsets (Mishra 2011). Vertical strain (α_v), approximating net effective stress, involves internal pore pressure acting against the overburden stress, and must be corrected for cementation, consolidation, and other poroelastic effects. Horizontal strain (α_h) involves internal fluid pressure, acting equally in all directions and in pressure communication with the hydraulic fracturing fluid (Mishra 2011). No poroelastic effects exist in this case. A diagram of how external stresses act on the rock is shown in Figure 4.6.

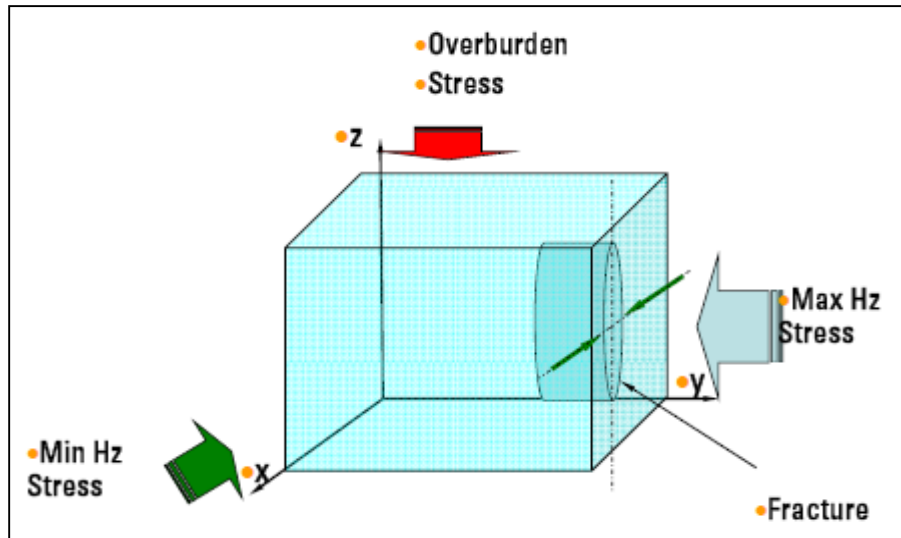


Figure 4.6- Principal stress components acting on the reservoir; overburden stress, minimum horizontal stress, and maximum horizontal stress (Mishra 2011).

During a minifrac or DFIT test, a small volume of fluid (20-80 bbls) without proppant is injected into the reservoir, at a rate sufficient to breakdown the perforations and create a small fracture (Mayerhofer 2012). This rate is generally 5 to 7 bbls/min. Following breakdown a constant rate injection of 20-80 bbls occurs (depending on zone thickness) (Mayerhofer 2012). For shale wells, the treatment is then shut-in for 10 days (on average), and isolated pressure gauges record the falloff data, to provide an estimate of pore pressure and permeability (Mayerhofer 2012). A faster but less comprehensive method is to perform this test immediately prior to the full stimulation, which will provide an upper bound for pore pressure. Permeability estimates will not be robust in this case (Mayerhofer 2012). An illustration of a DFIT/minifrac in conjunction with the full stimulation treatment is shown in Figure 4.7. Accuracy of results is highly dependent on shut-in time and achievement of fracture closure.

G-function analysis of a DFIT is useful for diagnosing fracture behavior, namely height recession, pressure-dependent leakoff (PDL), and unconfined extension (Mayerhofer 2012). Because this fracture behavior and geometry are highly dependent on stress contrasts between rock layers, it is of interest here to relate back to the mechanical stratigraphy. Fracture geometry inferred from G-function analysis will be discussed later in Chapter 7.

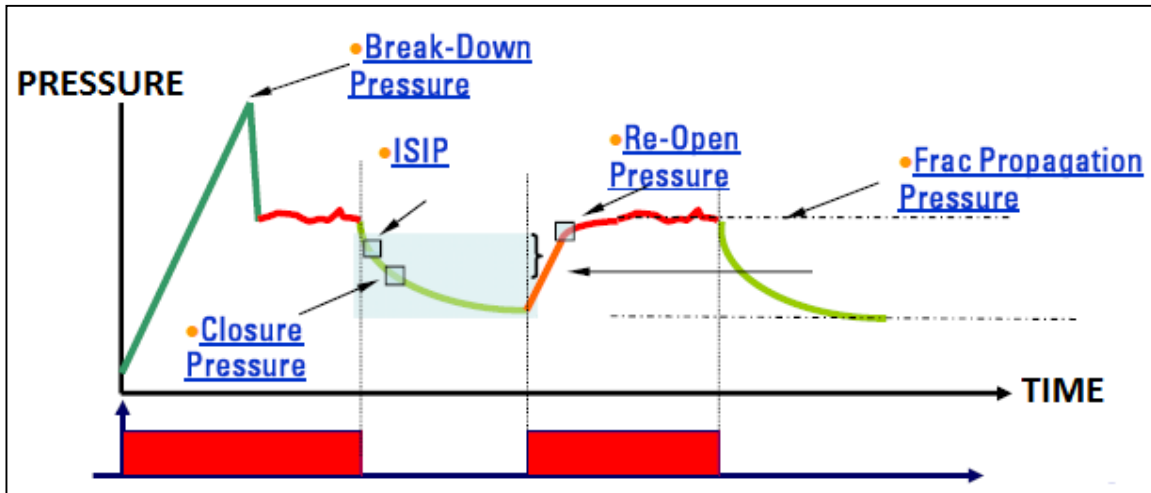


Figure 4.7- The mini-frac test is performed by injecting enough fluid to breakdown the formation (breakdown pressure). Constant-rate injection then occurs, until the treatment is shut-in (ISIP- instantaneous shut-in pressure) and following this closure pressure is determined.

4.5 Empirical Equations for Study Wells

Three wells in the Pouce Coupe study area and two wells in the Farrell Creek study area are used to generate rock properties. A shear sonic log is required for calculating log-derived rock properties, so to create a complete regional dataset two sonic logs were synthesized in the Pouce Coupe area. Values will be calibrated to core triaxial test results, which are available for all five study wells.

Pouce Coupe Study Wells: 13-12-78-11W6, 06-06-78-10W6, 05-14-78-11W6

Farrell Creek Study Wells: 16-17-83-25W6, C-85-I/094-B-01

In addition to rock properties, stress profiles were generated for the above five wells, in addition to two wells (B-15-I/094-B-01 and C-65-I/094-B-01) analyzed by Kurt Wikel previously. Stress characterization in these seven wells will provide the coverage necessary for defining regional variability. Stress and rock properties will be determined from logs using equations 4.1-4.8.

$$\text{Pore Pressure (PP): } S - [1/a_4(V - a_1 + a_2f + a_3C)]^{1/a_5} \quad (4.1)$$

$$\text{Overburden Pressure: } S(z) = g \int \rho(u) du \quad (4.2)$$

$$\text{Minimum horizontal stress: } (PR/(1-PR)) * (\sigma V - PP) + PP \quad (4.3)$$

$$\text{Poisson's Ratio } (0.5 * ((DTS(us/m)/DTC(us/m))^2 - 1) / ((DTS(us/m)/DTC(us/m))^2 - 1)) \quad (4.4)$$

$$\text{Shear Modulus: } (RHOZ(kg/m^3) * (DTS^2)) / 100000000 \quad (4.5)$$

$$\text{Dynamic Young's Modulus: } ((2 * \text{Shear Modulus}) * (1 + PR)) \quad (4.6)$$

$$\text{Internal Friction Angle, Lal (1999): } \mu_i = \tan(\arcsin((V_p - 1) / (V_p + 1))); \quad V_p \text{ in km/s} \quad (4.7)$$

$$\text{Internal Friction Coefficient (Lal 1999): } \text{Tangent (Internal Friction Angle)} \quad (4.8)$$

Cohesion and internal friction angle will be calibrated to values derived from core triaxial testing (see Glossary of Terms) on well C-85-I/094-B-01 and image logs from the area. Mohr-Coulomb failure analysis was performed on this well. Three independent analyses of this core (by the author, Senergy Consulting, and TerraTek labs) were averaged to obtain cohesion and internal friction angles for the Montney Formation. In addition, cohesion values were derived from image logs in the area. Unconfined compressive strength was determined using a proprietary empirical equation from Kurt Wikel for unconventional shales and sandstones.

4.6 Pore Pressure

Pore pressure is determined using a rock physics equation (equation 4.1- after Sayers) (Doyen et al 2004). The equation incorporates P-wave velocity, overburden stress, porosity, and clay content at the depth of investigation, therefore providing a robust analysis tool incorporating multiple rock parameters. Constants a_1 - a_5 will vary depending on the formation of study. In the case of the Montney, a value of 1 was used for a_1 - a_3 , a value of 10 was used for a_4 , and a value ~2 was used for a_5 , varying slightly for each well. This equation allows for the sensitivity of the pore pressure output to be examined in the context of each individual input variable (Doyen et al 2004), and proves to be very robust in providing an accurate profile of pore pressure (Figures 4.8 and 4.9 below). These profiles were compared to real-world kick data from drilling and reservoir pressure gauges.

To determine the clay volume parameter for equation 4.1, relative deflection of the gamma ray log was used as an indicator of shale volume. The gamma ray curve was scaled to its maximum and minimum values within the Montney, and a Gamma Ray Index was generated using equations 4.9 through 4.11.

$$\text{Gamma Ray Index (I}_{GR}\text{): } GR - GR_{min} / GR_{max} - GR_{min} \quad (4.9)$$

$$V_{clay} \text{ (Stieber): } 0.5(I_{GR}) / (1.5 - I_{GR}) \quad (4.10)$$

$$V_{clay} \text{ (Clavier): } 1.7 - (3.38 - (I_{GR} + 0.7)^2)^{1/2} \quad (4.11)$$

4.7 Results

Below are the stress profiles for the Pouce Coupe and Farrell Creek areas, as well as values for log corrections to core.

4.7.1 Pouce Coupe

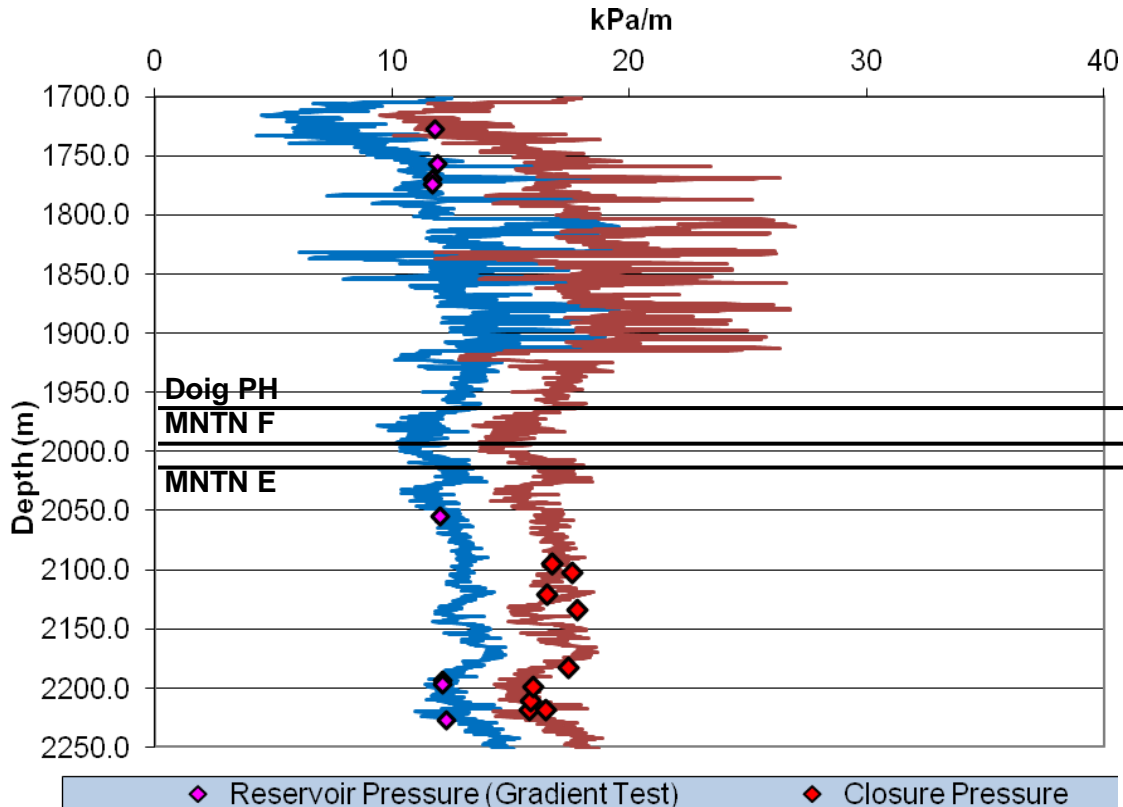


Figure 4.8- Pouce Coupe Stress Profile, with predicted pore pressure shown by the blue curve and predicted σ_{min} shown by the red curve. Calibration points for pore pressure and σ_{min} are pink diamonds and red diamonds respectively.

06-06-78-10W6

Dynamic Young's Modulus (Synthesized Sonic) x 0.55=Core Dynamic Young's Modulus

Synthesized Sonic x 1.43= Core Sonic (us/m)

UCS: Average 117 Mpa for the Montney in its entirety.

05-14-78-11W6

Dynamic Young's Modulus (Synthesized Sonic) x 0.56=Core Dynamic Young's Modulus

Synthesized Sonic x 1.39= Core Sonic (us/m)

UCS: Average 136 Mpa for the Montney in its entirety.

4.7.2 Farrell Creek

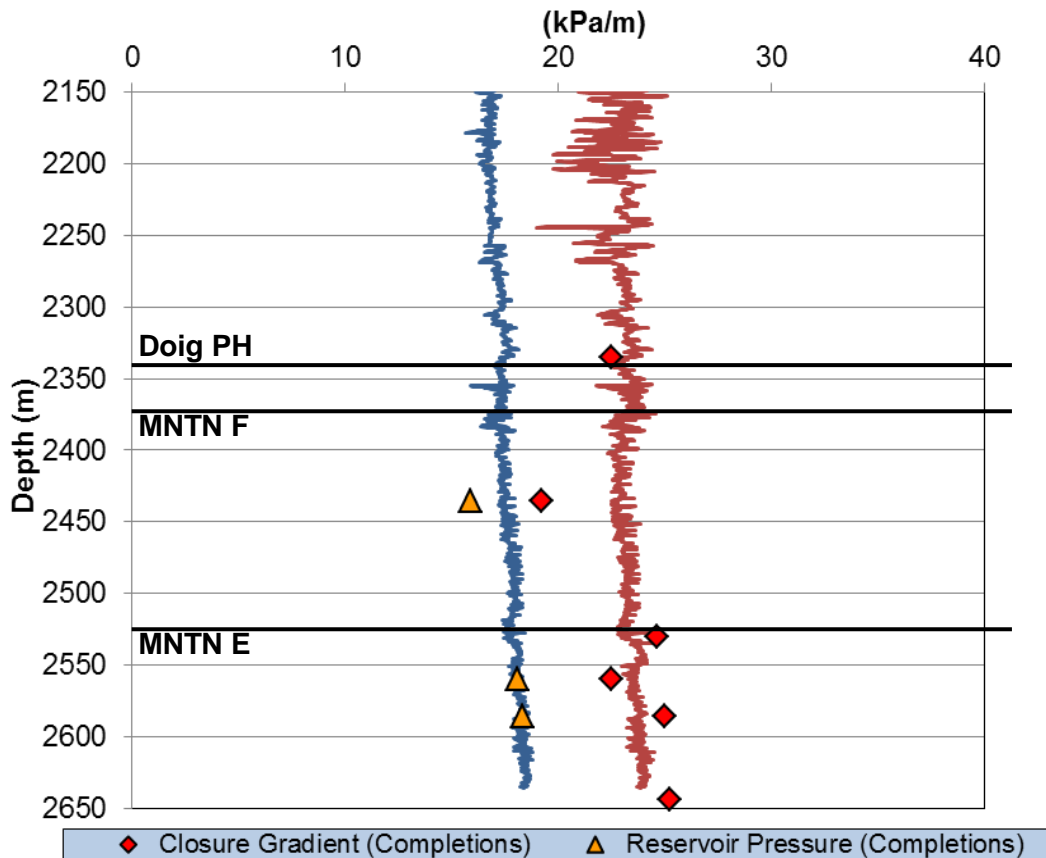


Figure 4.9- Farrell Creek Stress Profile, with predicted pore pressure shown by the blue curve and predicted σ_{hmin} shown by the red curve. Calibration points for pore pressure and σ_{hmin} are orange triangles and red diamonds respectively.

The determination of stress profiles and rock property relationships in both study areas allows for accurate characterization of the mechanical stratigraphy. Knowledge of rock property and stress variation is vital for predictions of rock behavior, and calibration to core and reservoir pressure tests is important for understanding uncertainties in the data.

CHAPTER 5

MONTNEY MECHANICAL STRATIGRAPHY

Highly detailed core facies descriptions for wells 16-17-83-25W6 and C-85-I/094-B-01 in Farrell Creek were used as the primary tool for formulating relationships. Additional general facies descriptions from wells 05-14-78-11 and 13-12-78-11 in Pouce Coupe were used as data points.

In the context of the reservoir depositional history and stress regime, mechanical stratigraphy is defined using a standard suite of logs, rock properties as determined through equations in Chapter 6, and the brittleness index described in Section 7.1. The gamma ray, density, and sonic logs are used in conjunction with the Young's modulus and Brittleness Index curves to define rock types in the reservoir, as shown in Figure 5.1. Stratigraphy was additionally calibrated to core rock properties and image logs, where available.

I observed that patterns in rock brittleness relate to stratigraphic cycles. Within each cycle, the lowermost zone above the underlying maximum flooding surface was relatively more ductile. Due to stratigraphic superposition, as the formation transitions to lower gamma ray values and more proximal sediments, the brittleness increases. This increase in brittleness is consistent with information presented earlier in Chapter 3; a higher proportion of siliceous minerals corresponding to a more brittle rock. At the top of the cycle where the next flooding surface appears, there is in some cases a condensed section. Because of the starved sediment conditions within the condensed zone, beds and laminations are much thinner, resulting in a larger number of interfaces. The corresponding contrast in rock properties at each interface will act as a zone of weakness and overall create a highly brittle zone. These three broad mechanical zones; (1) relatively ductile, (2) relatively brittle, and (3) condensed sections, were assigned a corresponding color for simplification; yellow, red, and blue respectively. As these zones exhibited a consistent correlation throughout the zone of interest in the study wells, this definition was taken throughout the study area, to wells with limited datasets.

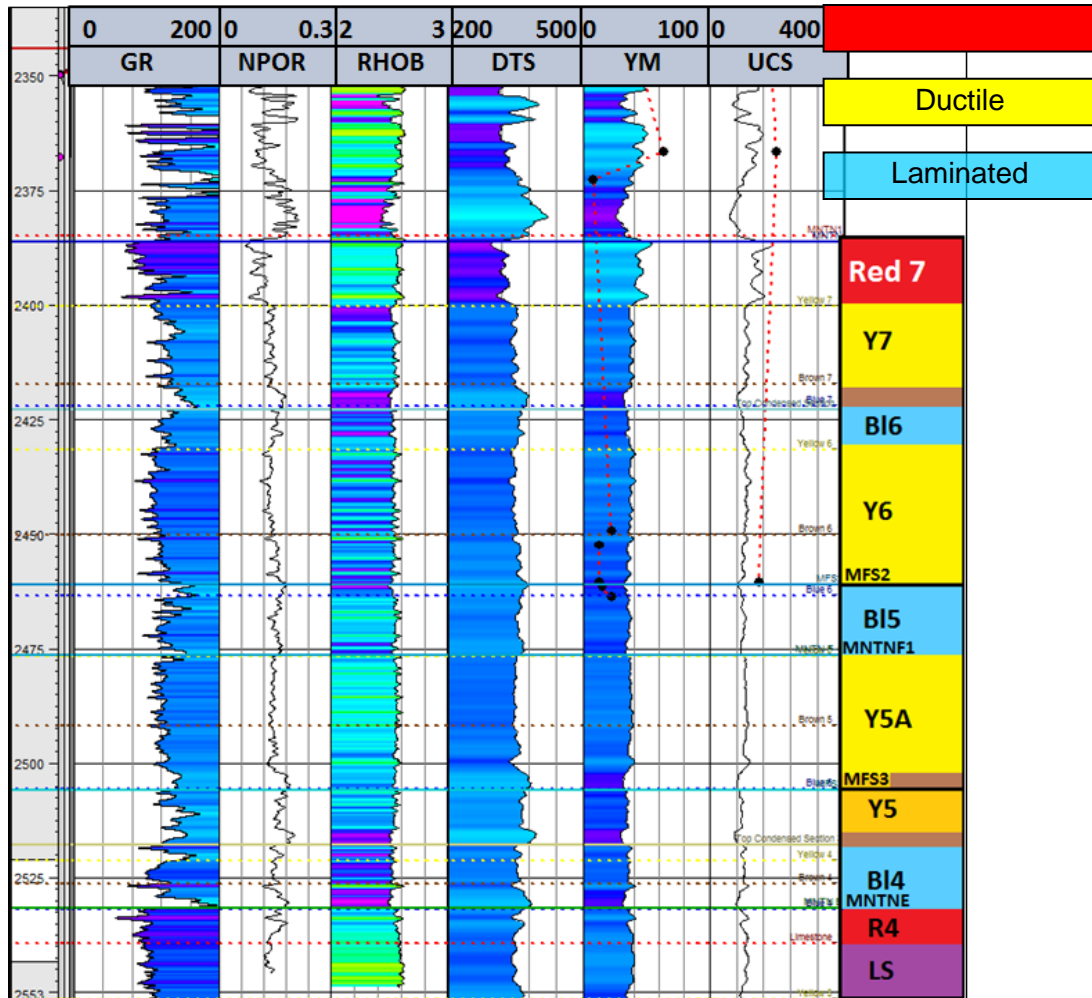


Figure 5.1- Farrell Creek mechanical stratigraphy definition. Yellow facies are relatively ductile, red facies are relatively brittle, and blue facies are relatively laminated/brittle. The pre-defined MNTN E and F1 horizon and maximum flooding surfaces (MFS2, MFS3) are also shown.

In Pouce Coupe, the stratigraphic definition is slightly modified. Because of the change in stratigraphic setting to a position further up the slope, the presence of condensed sections is absent. The overall number of relatively brittle zones is therefore fewer. This stratigraphic definition is shown in Figure 5.2. The condensed section may act as a propagation barrier to a hydraulic fracture, and could result in lower height growth within the formation. To investigate in detail the behavior of the blue brittle zones, further investigation was conducted. First, I formulated a Rock Quality Index (RQI) based both on stress and formation rock properties. This Rock Quality Index (RQI) assists in better definition of the behavior of red, yellow, and blue zones, and will be expanded on in Section 5.1. Secondly, microseismic events were analyzed in

the context of the mechanical stratigraphic framework, to further understand hydraulic fracture propagation in the reservoir. This analysis will be expanded on in Chapter 6.

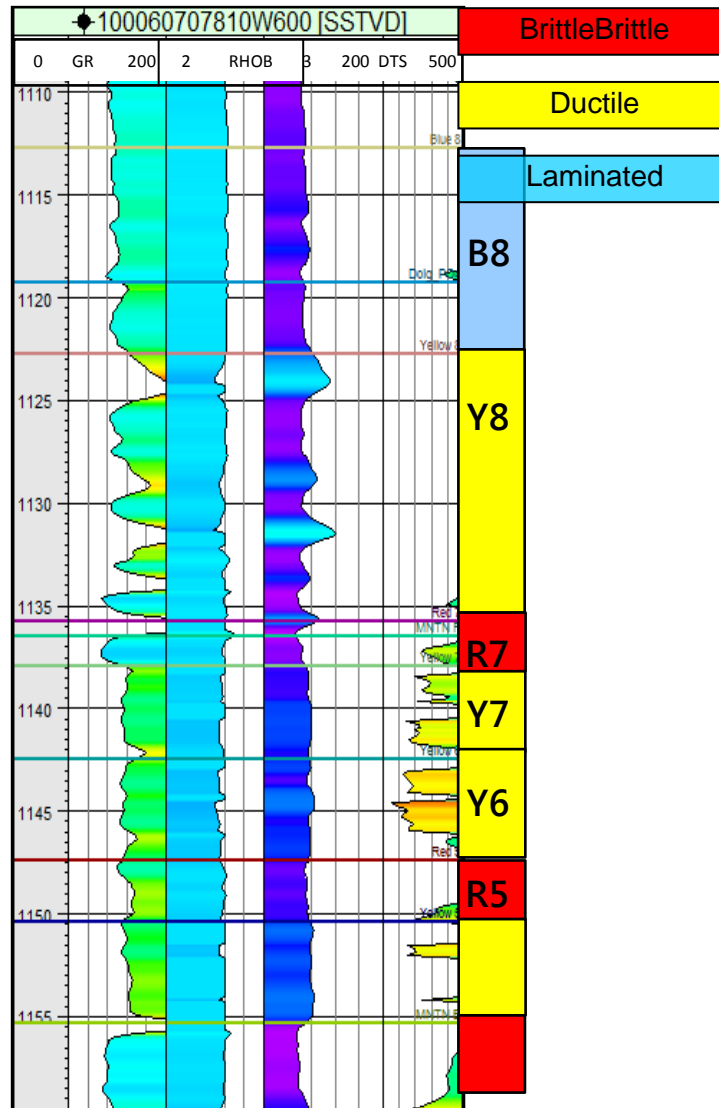


Figure 5.2- Pouce Coupe mechanical stratigraphy definition. Yellow facies are relatively ductile, red facies are relatively brittle, and blue facies are relatively laminated/brittle.

5.1 Rock Quality Index

The purpose for defining the various parameters in Chapter 4 was primarily to provide the geomechanical context of the reservoir. The definition of stress and rock properties provides the necessary link for understanding rock property variation in conjunction with stratal surfaces. Within this context, further characterization of the defined mechanical stratigraphic zones is needed to accurately predict hydraulic fracture behavior in the reservoir. Therefore, a new

parameter, describing both reservoir brittleness and reservoir stress state, is defined here to understand both the ideal stress condition and rock property condition for hydraulic stimulation, as introduced previously. I termed this parameter the Rock Quality Index (RQI). It is a combination of fabric-based brittleness, composition-based brittleness, and reservoir stress differential. It is theorized that areas of low stress and relatively brittle rock are the most likely to enable a successful hydraulic stimulation. The reasoning behind this assumption is expanded on below:

Stress Factors:

- (1) A hydraulic fracture will preferentially propagate to areas along the wellbore with a lower stress state (Warpinski 2011). High stress makes breaking down the formation more difficult, and fractures will be more likely to close rapidly following stimulation (Norton et al 2011).
- (2) Both lower overall stress state (low mean σ) and lower anisotropy between horizontal stresses ($\Delta\sigma_{HZ}$) will encourage the growth of a complex fracture network and propagation of a hydraulic fracture. While it is difficult to calculate the overall stress state due to ambiguity in estimates of σ_{Hmax} , σ_{hmin} is used here as an approximation of the stress state.

Rock Property Factors:

- (3) Areas of higher brittleness (higher Young's Modulus) are expected to break more easily than areas of higher ductility.
- (4) Layer interfaces, which in a shale lithology most commonly take the form of laminations, are features which create anisotropy with a rock mass (Teufel et al. 1984). Interfaces can take one of two forms; perfect bonding interface, equivalent to no mechanical discontinuity, or unbonded interface; at which tensile strength will be minimized and failure is likely (Teufel et al 1984).
- (5) The amount of shear stress transmitted across an interface is dependent on the inherent shear strength (cohesion) and frictional properties at the interface (Teufel et al 1984). Where detailed core mineralogy data was available a full RQI was defined, however this data was not available for all wells and therefore the fabric-based approach, using only P-wave brittleness is used (equation 5.1-5.3). The additional equation used for defining compositional-based brittleness is shown by equation 5.4.

- (6) Mechanical interfaces can occur both within a single zone (i.e. a condensed section facies) and between zones (i.e. transition from a yellow to blue facies).
- (7) An increase in the frequency of interfaces will result in an increase in the stress state, due to high formation variation.

Combining the above factors together, it can be said that the ideal hydraulic fracture environment would be one with a low stress state, a low number of mechanical interfaces, and a high brittleness. However, there are inherent complications in this definition of “ideal”. A zone which is highly brittle is likely to also have interfaces within it, which are in turn likely to increase the mean stress of that zone and interfere with the growth and propagation of a hydraulic fracture. To say that the best zone is one of high brittleness is a generalization. While high brittleness is desired, is it the relative brittleness or ductility of the target zone that matters, or is it in fact the variation in ductility or brittleness within the zone that is of paramount importance? Chapter 9 will examine this question further.

Therefore, a Fabric Brittleness Index (BI) based on P-wave velocity (over-consolidation ratio) was calculated (Holt et al 2011), using equations 5.1- 5.3. The Fabric Brittleness Index (BI) was further combined with the Composition Brittleness Index (BI- equation 5.4) and the stress state to create the overall Rock Quality Index (RQI- Figure 5.3).

Fabric-Based Brittleness:

$$\text{Brittleness Index } B_7 = \text{OCR}^b \rightarrow \text{OCR} = (\sigma_{V(\text{max})} / \sigma_V)^* \tag{5.1}$$

$$((\sigma_{V(\text{max})} (\text{mpa})) = 8.6C_0(\text{Mpa})^{0.55*} \tag{5.2}$$

$$C_0(\text{Mpa}) = 0.77 V_p(\text{km/s})^{2.93*} \tag{5.3}$$

*The over-consolidation ratio (OCR) and variables used to generate it are further defined in the Glossary of Terms.

The Fabric Brittleness Index ranges on a scale from 0-1, and this index is closely approximated by variations in Young’s Modulus. Therefore, Young’s Modulus can be used as a proxy for the formation brittleness due to *fabric* variation. Composition Brittleness Index utilizes mineralogy and TOC data, where available (equation 5.1.4- Walles 2010, personal communication).

Composition-Based Brittleness:

(1.3)Quartz + Feldspar + Plagioclase + (1.2)Carbonates

$$((\text{numerator} + (2) V_{\text{mixed I/S}} + (1.5) V_{\text{illite + chlorite + kaolinite}}) + \text{others})(1 - \text{TOC}_{\text{pd}}) + \text{TOC}_{\text{pd}} \quad (5.4)$$

Resulting brittleness and stress values were normalized to the maximum value within the formation of interest. Combining the two normalized Brittleness Indices with the normalized stress state (σ_{hmin}), the Rock Quality Index (RQI) was determined. The Rock Quality Index (RQI) required inputs from all previously defined rock property and stress data, as shown in Table 5.1. An equation representation of this index is shown in Figure 5.3, and a diagrammatical example is shown in Figure 5.4.

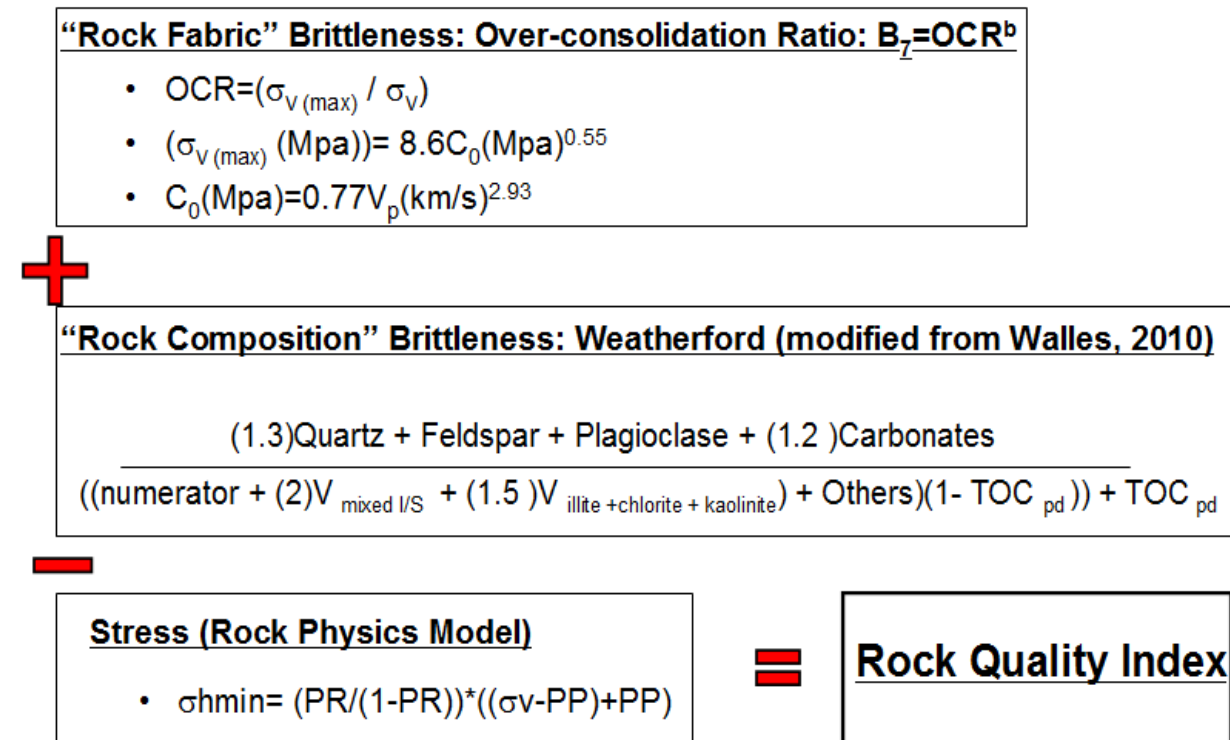


Figure 5.3- Parameters for defining the Rock Quality Index (RQI). Rock fabric and rock composition-based brittleness terms are added together, and then minimum horizontal stress is subtracted to generate the Rock Quality Index (RQI).

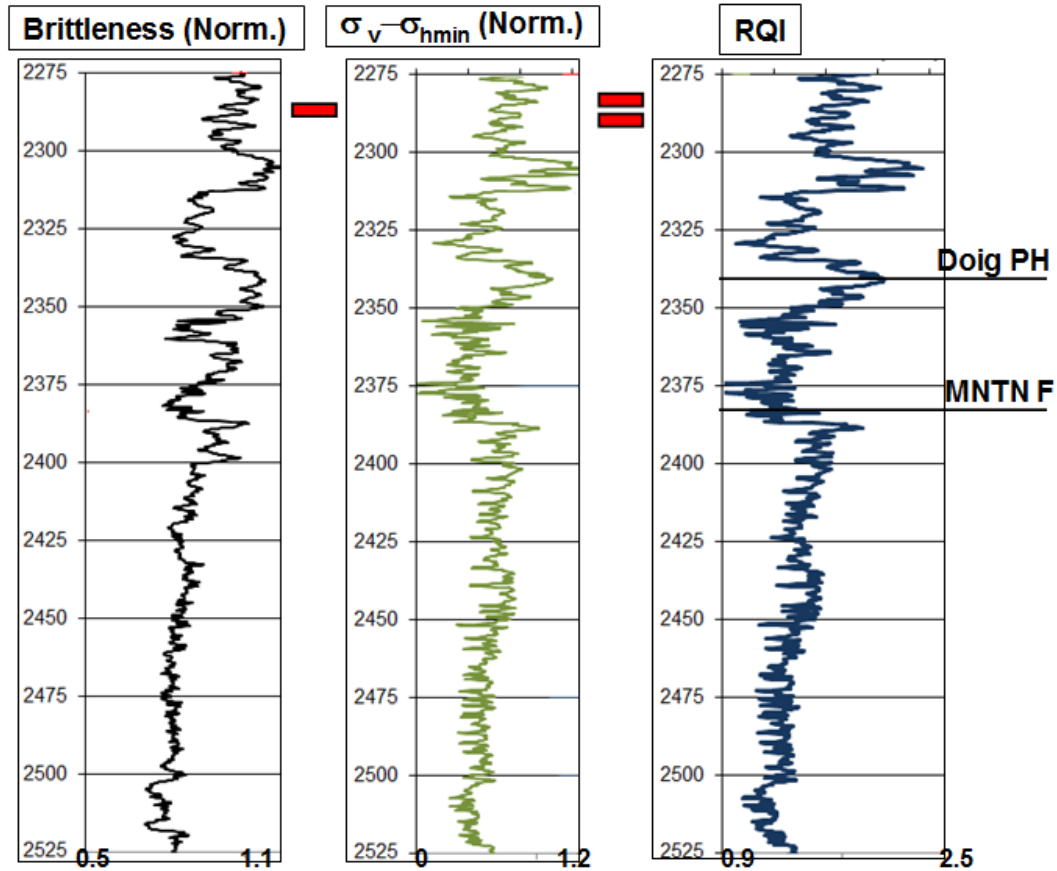


Figure 5.4 - Log representation of Rock Quality Index (RQI), with normalized total brittleness on the far left and normalized stress differential in the center.

The resulting Rock Quality Index (RQI) from the procedure shown in Figure 5.3 is highly dependent on the brittleness inputs. Because stress gradients, while variable, will remain relatively constant within the formation of interest, they have a smaller influence on the end results. Due to this observation, a Modified Rock Quality Index (RQI) was formulated to amplify the variations in stress. The equation was modified to examine the stress differential, rather than the magnitude of σ_{hmin} . The normalized stress differential provides a more variable input into the Rock Quality Index equation, and therefore reflects stress variations more accurately.

Ideally, the horizontal stress differential would be determined, however constraining the magnitude of the maximum horizontal stress at a fine scale is very difficult. While a general definition of maximum horizontal stress magnitude was defined for several wells in Farrell Creek based on image logs, it is not at the fine scale necessary here. Therefore, the difference between the overburden stress and minimum horizontal stress are used. This stress differential defines an important element of the reservoir. As mentioned in Chapter 4, the stress state in the

Montney Formation is strike-slip. However, with an increase in pore pressure in the reservoir; for example, due to the initiation of the hydraulic stimulation, σ_{hmin} will increase at a rate two-thirds that of the pore pressure (PP) increase (see Glossary of Terms).

$$\Delta\sigma_3=2/3\Delta PP \quad (5.5)$$

When σ_{hmin} becomes larger than the overburden stress, the stress regime becomes reverse (Figure 5.5). Therefore, the smaller the difference between σ_{hmin} and the overburden, the higher the likelihood of a shift to a reverse stress regime. A shift to a reverse stress regime is coincident with “pancake frac” behavior (Soh 2012), meaning a large amount of lateral reservoir growth will occur but little height growth will be observed.

A hydraulic fracture would ideally have both adequate height and lateral growth, and a Rock Quality Index (RQI) which defines [Brittleness Index (Norm.)]+ [overburden- σ_{hmin} (Norm.)] will high-grade areas where proximity to a reverse stress regime is lower. The natural log of the stress differential was calculated to further amplify variability [Brittleness Index (Norm.)] /ln [(overburden- σ_{hmin}) Norm.]. The natural log of a number will rapidly approach negative infinity as the number approaches zero. Because the stress differential has been normalized to a scale of 0 to1, the natural log will display the differential variability more accurately. Using division of the terms means that areas of higher brittleness and higher stress differential will result in a more negative number. The modified Rock Quality Index (RQI) is shown in Figure 5.6. The correlation between this hypothesis and the behavior of fractures as inferred from DFIT analysis will be further discussed in Section 7.6.

Both the initial Rock Quality Index (RQI) and modified Rock Quality Index (RQI) have merits for defining reservoir “quality”; however the modified Rock Quality Index (RQI) will be displayed and discussed here. The modified index is better for displaying material heterogeneity in the reservoir; the merits of which will be discussed further.

A pseudo Rock Quality Index (RQI) was defined for wells 07-07-78-10W6, 06-06-78-10W6, and 02-07-78-10W6 in Pouce Coupe. Because of the lack of mineralogy/ thermal maturity data, it was not possible to define a full Rock Quality Index (RQI), and brittleness was based on the P-wave Brittleness Index (BI) only. While the pseudo definition is less accurate than the full definition, reservoir heterogeneity is still reflected correctly, as shown in Figure 5.7. The availability of lateral logs for well 02/07-07-78-10W6 allowed for comparison between the

pseudo-Rock Quality Index (RQI) and the 4D time-lapse response to stimulation. This work will be further described in Chapter 9.

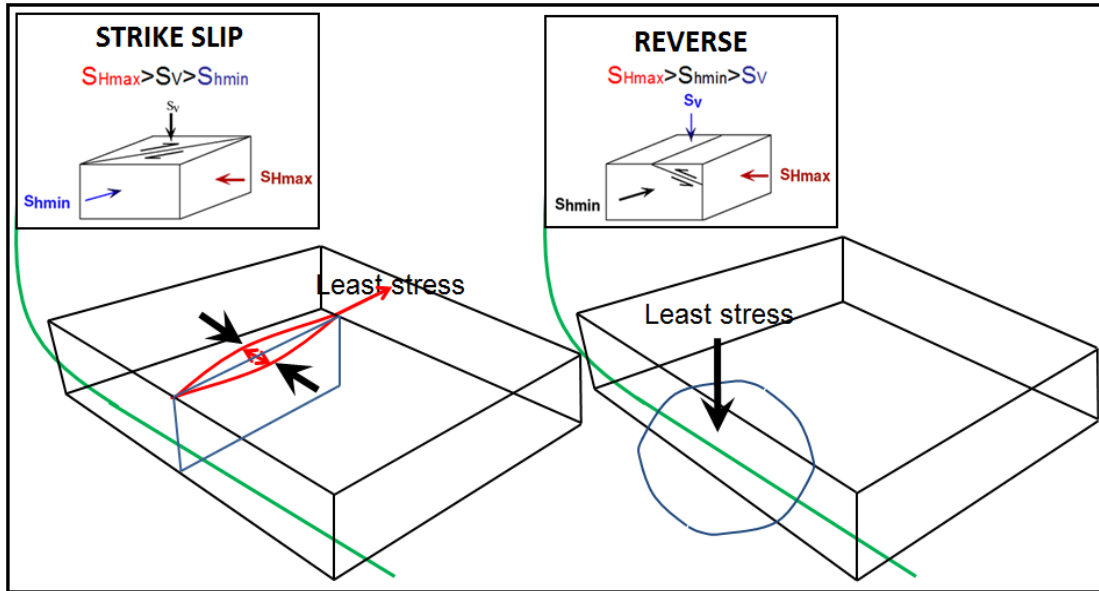


Figure 5.5 - The change in hydraulic fracture character with stress regime shift; from vertical transverse fracture (left) to horizontal pancake fracture (right). On the left, least stress is σ_{hmin} and therefore the hydraulic fracture propagating from the wellbore (blue plane) is vertical. On the right, least stress is now σ_v and the propagating hydraulic fracture is horizontal.

“Rock Fabric” Brittleness: Over-consolidation Ratio: $B_z = OCR^b$

- $OCR = (\sigma_{v(max)} / \sigma_v)$
- $(\sigma_{v(max)} (Mpa)) = 8.6C_0(Mpa)^{0.55}$
- $C_0(Mpa) = 0.77V_p(km/s)^{2.93}$

+

“Rock Composition” Brittleness: Weatherford (modified from Walles, 2010)

(1.3)Quartz + Feldspar + Plagioclase + (1.2)Carbonates

((numerator + (2) $V_{mixed\ I/S}$ + (1.5) $V_{illite+chlorite+kaolinite}$) + Others)(1- TOC_{pd})) + TOC_{pd}

LN [Stress Differential($\sigma_v - \sigma_{hmin}$)]

=

Modified Rock Quality Index

Figure 5.6- Modified Rock Quality Index (RQI) equation. The original stress term (σ_{hmin}) has been modified to the normalized stress differential ($\sigma_v - \sigma_{hmin}$), to amplify changes in stress.

Table 5.1- Log and Data requirements for Geomechanical characterization.

LOG-BASED GEOMECHANICS		CALIBRATION DATA	
Required Logs	Equation	Required Data	Result
RHOZ	$S_v(z_0) = \int_0^{z_0} \rho dz$		
DTP	Vclay (from GR Index)	ECS, XRF, XRD, LIBS, Qemscan (SEM) Log	Quantitative mineralogy
N/A	PP: $sv - 1/A4 (DTP-A1+(A2(PHIE))+A3(Vclay))1/A5$	Pressure Test/gauge	Reservoir Pressure
DTS, DTP	Poisson's Ratio: $(0.5*((DTS/DTP)^2) - 1)/(((DTS/DTP)^2)-1)$	Triaxial Test	Static Poisson Ratio
RHOZ, DTS	Shear Modulus: $(RHOZ)*((1 \times 10^8)/(DTS^2)/(1 \times 10^9))$	Triaxial Test	Static Shear Modulus
N/A	Dynamic Young's Modulus: $(2*SM)*(1+PR)$	Triaxial Test	Static Youngs Modulus
DTP	IFA (Lal 1999): $\mu_i = \tan(\text{asin}((Vp-1)/(Vp+1)))$	Core MC failure	IFA
DTP	UCS (Hosrud 2001): $0.77(304.8/dTC)^{2.93}$ (Equation for high porosity Tertiary shales)	Core MC failure	UCS, Cohesion
DTS, DTP	UCS (Modified Davey 2012): $0.77(304.8/(dTP*(0.85*S/P)))^{2.93}$	Core MC failure	Failure envelope**
N/A	σ_{hmin} : $[(PR/(1-PR))*(sV-PP)+PP]$	DFIT, Mini-frac	σ_{hmin}
N/A	σ_{Hmax} Magnitude: $\sigma_v, \sigma_{hmin}, PP, IFA, UCS$	Wellbore MW and azimuth/deviation	σ_{Hmax} Magnitude
N/A	σ_{Hmax} Orientation	Image logs- breakouts and tensile fractures	σ_{Hmax} Orientation
N/A	Fabric-based Brittleness Index $B7=OCRb$	Post-completion data	Rock Quality Index
N/A	Eqn 7.1.1- $OCR=(\sigma_v(\text{max}) / \sigma_v)$		
N/A	Eqn 7.1.2- $(\sigma_v(\text{max}) (\text{Mpa}))= 8.6C0(\text{Mpa})^{0.55}$		
N/A	Eqn 7.1.3- $C0(\text{Mpa})=0.77Vp(\text{km/s})^{-2.93}$		
XRD/SRA	Mineralogy- based Brittleness Index- Eqn 7.1.4	Post-completion data	Rock Quality Index

*All log-based calculations are dependent on sonic velocity error due to organic content.

Poisson's ratio strongly dependent on the fluid saturation of the core sample.

**Core sample must be taken to the failure point, and stress cycling of the sample should be performed to ensure accurate results.

A full Rock Quality Index (RQI) was defined for the logged zone in C-85-I/094-B-01 in Farrell Creek. This well therefore serves as the primary basis for correlation between the stratigraphy and rock quality (Figure 5.8).

Table 5.2- Abbreviation list for Table 5.1.

ECS	Elemental capture spectroscopy
XRF	X-Ray Fluorescence
XRD	X-Ray Diffraction
LIBS	Laser-induced breakdown spectroscopy
SEM	Scanning Electron Microscopy
UCS	Unconfined Compressive Strength
Co	Compressive Strength
σ_v	Overburden Stress
PHIE	Effective permeability
DTS	Shear wave travel time (us/m)
DTP	Compressional Wave travel time
Vp	Compressional wave velocity
Vclay	Clay Volume
RHOZ	Bulk density (kg/m ³)
PP	Pore Pressure
PR	Poisson Ratio

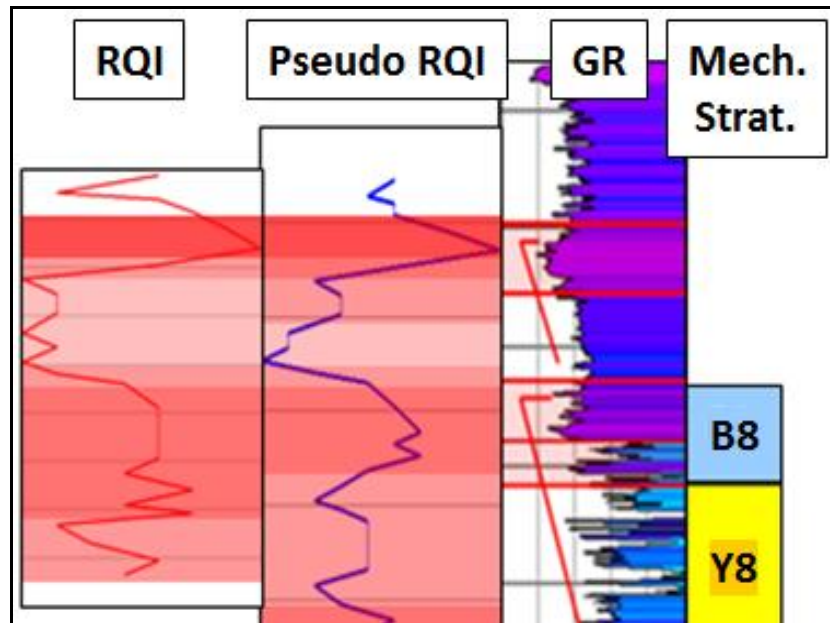


Figure 5.7 - Comparison of results of full (left) and pseudo (right) Rock Quality Index (RQI) analysis for well C-85-I.

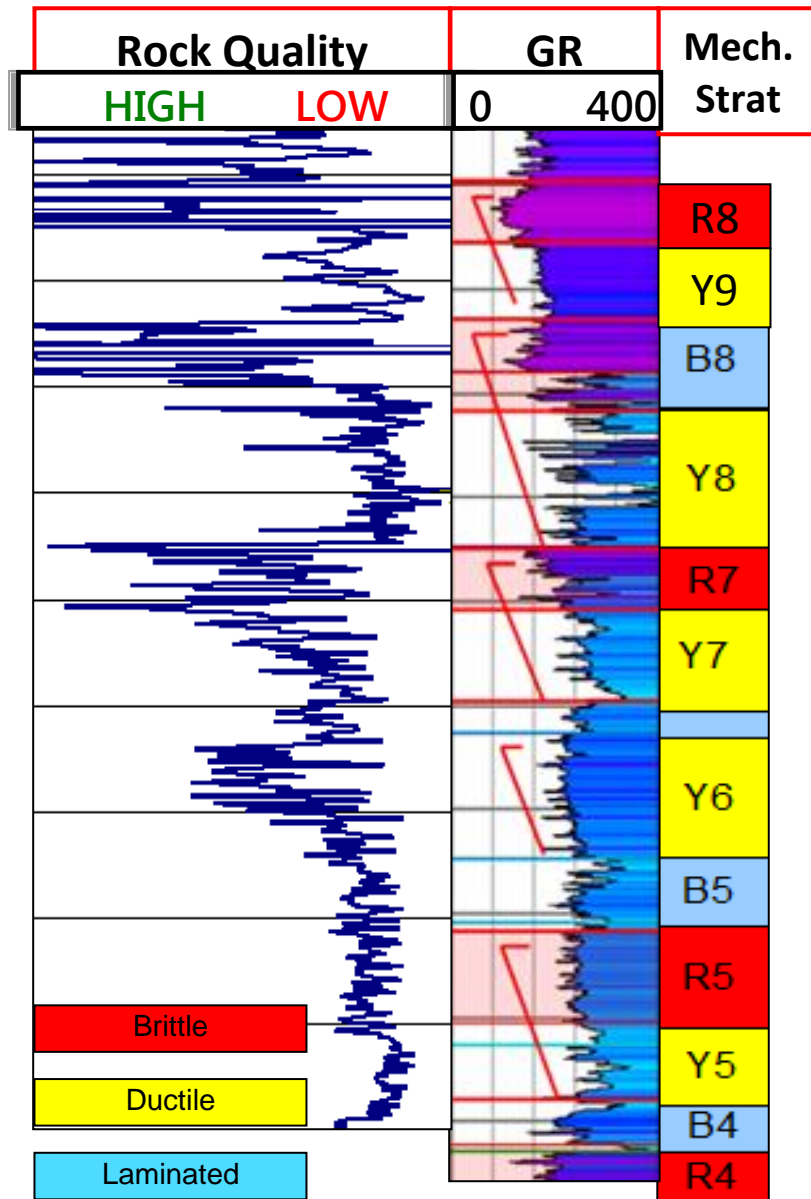


Figure 5.8 - C-85-I Modified Rock Quality Index (RQI- left log), plotted with the gamma ray curve (center, on a scale from 0-400 API), and the mechanical stratigraphy.

CHAPTER 6

MICROSEISMIC

6.1 Microseismic Background Theory

In-situ natural fracturing is an integral part of productive shale reservoirs. Compositional changes within a formation, due to shifts in stratigraphic position and increasing thermal maturity (and therefore increasing pore pressure), will create textural changes, in the form of microfractures due to overpressure. Further fracturing can occur with external tectonic forces and regional stress shifts. In each shale reservoir, these changes and the corresponding density, orientation, and connectivity of in-situ fractures can provide critical information about how the rock may respond to a hydraulic fracture treatment.

Fracturing results from several types of “deformation” within a reservoir, namely:

- (1) Induced hydraulic deformation
- (2) Natural shear slip (through increased pore pressure)
- (3) Aseismic background deformation

Induced hydraulic deformation involves the re-activation, growth, and connection of fault and fracture networks, which results and/or contributes to deformations (2) and (3). As shale reservoirs are highly heterogeneous, the response to stimulation can vary greatly both laterally and vertically. Distinguishing deformation types from one another is challenging, but necessary to fully understand how reservoir connectivity is established.

Microseismic activity is defined as events generated by instantaneous geomechanical strain/slip (Maxwell et al 2011). As stress changes during the injection period of a hydraulic fracture treatment, acoustic emissions are generated. Monitoring these emissions is based on the theory of earthquake seismology. The signatures of compressional and shear waves are recorded by geophones in the monitoring well, and integrated and processed to estimate the source location. An accurate velocity model, incorporating vertical reservoir heterogeneity, must be constructed to precisely determine the source location (Maxwell 2009). Additional sources of error lie in arrival times and raypath polarizations. Arrival time residuals (difference between

“observed” and computed arrival times from the event location) can be used for quality control of the velocity model (Maxwell 2009).

Microseismic can record all three types of deformation as outlined above, however not all these types of deformation will contribute to the fracture network that will be drained by production. Natural shear slip will occur in any reservoir with in-situ fractures. The strong S-wave component of microseismic events indicates that most events are dominantly shear (Maxwell 2011). Aseismic background deformation describes deformation occurring without recorded seismicity (for example, amplitudes too small to be detected or very slow opening mode failure). Warpinski et al (2005) have argued that microseismic events occurring close to a hydraulic fracture treatment represent indirect deformation triggered by pore pressure changes of the dilating hydraulic fracture, and Rutledge et al (2004) have showed that bends in a seismicity trend are areas of stress concentration, exhibiting anomalously high event counts changing fluid viscosities or pump rates.

These observations suggest that shear failure can be present as an aseismic “background” signature, with little input needed from induced completion effects. Therefore, due to shear slip, aseismic deformation, and uncertainty inherent in microseismic event locations, the stimulated reservoir volume estimated through microseismic can be excessive (Maxwell et al 2011). The microseismically active volume is a sum of the hydraulic volume plus the volume of the surrounding stress-activated fracturing. Shear slip on these in-situ fractures creates a falsely inflated estimation of SRV, while it is likely that after slip occurs these fractures will not remain open. The remaining conductive effective fracture network is what is actually needed for proper modeling of the stimulated reservoir volume (Maxwell 2011).

For a fracture to be an effective element in the overall network, it must have a large enough aperture to accommodate fluid and proppant. A shear microseism therefore must have a significant tensional component at some point. Fracture dilation is the proposed method for accommodating injected fluids (Maxwell et al 2011). Evidence for natural fracturing accommodating fluid is shown through fluid recovery rates in shale gas completions; Ehlig-Economides et al. (2011) cite fluid recoveries of 10-40%. Current theory is that fluid remains in natural fractures and acts as a proppant in itself (water and sand have similar compressibility factors). This theory is further supported by microseismic maps showing widely dispersed events, suggested pressure and fluid fronts interacting with natural fracture systems. However

the likelihood that these events are reflective of production drainage area is low. These microseismic events can occur at distance up to 30% of the horizontal well length, while production data analysis (PDA) shows half-lengths ranging from 2-4% of the horizontal well length (Ehlig-Economides et al. 2011). Determining the real stimulated rock volume is the goal.

Source characteristics of events can provide additional information about the nature of deformation which resulted in the microseismic activity. For this purpose, methods are applied from earthquake seismology; however limitations lie in this application as often only a single monitoring well is employed for microseismic monitoring, limiting the directionality of source radiation and increasing location uncertainty.

Moment Tensor Inversion (MTI). MTI relates the radiation pattern observed from a microseism to the mode of failure responsible for that event. Microseismic records instantaneous strain; coinciding with the first motions of the events at the hypocenter (earthquake initiation point within the Earth). Motion can be isotropic (tensile opening/closing), double-couple (DC- shear slip on a fracture surface), or compensated linear vector dipole (CLVD) (Maxwell et al 2011). Often these source mechanisms can vary throughout a single hydraulic fracture treatment. In addition, fracture orientation can be determined based on the type of deformation. Issues with this analysis include local borehole anomalies, seismic attenuation issues, energy partitioning with seismic wave reflection, multiple phases, background noise, and single well monitoring.

Shear vs. Tensile Deformation. During tensile deformation, formation breakdown during injection results in increased injectability, and as fluid volume continues to increase within the reservoir the fracture continues to grow. Post-injection the pressure is reduced and fractures close. With shear deformation, formation breakdown occurs under shear/hybrid shear stress, and increased permeability is a result of topography differences between the contacting fracture surfaces. While permeability has been observed to increase on shear fractures that are critically-stressed or have sheared, repeated shear events will reduce permeability by grinding off asperities on fracture faces and producing fracture-filling fines. Repeated shear failure during production may also lead to problems such as casing shear (Geoff Rait, personal communication).

B-Value Analysis. By plotting the frequency of microseisms versus magnitude on a logarithmic scale, the slope of the graph can give insight into the mechanism of seismicity. Slopes of ~1

correspond to activation of in-situ features, while slopes of ~ 2 correspond to hydraulic fractures (parallel to the maximum horizontal stress direction). By identifying the slip mechanism present, those areas activated by the treatment itself can be confirmed. These activated areas are the portion of the volume effectively stimulated; that which will ultimately impact total EUR.

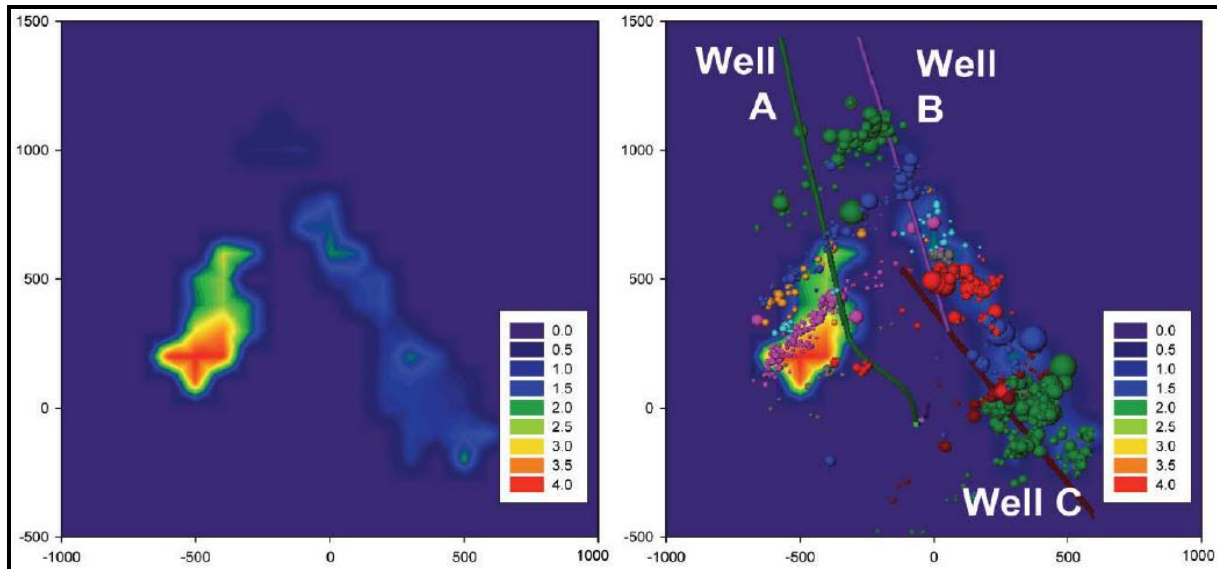


Figure 6.1 - B-Values (left), on a scale of 0-4, superimposed with microseismicity (right), indicating different fracture activation mechanisms in different areas of the hydraulic treatment (Maxwell 2011). Higher b-values are associated with the propagation of a hydraulic fracture while lower b-values are associated with natural fracture re-activation.

6.2 Montney Microseismic

The tool for correlating microseismic events to the stratigraphic framework was the mechanical stratigraphy defined in Chapter 7 (Figure 6.2). A Rock Quality Index (RQI) for the formation was further defined in section 7.1 and 7.2. These two formation definitions bring forth the question of whether overall zone brittleness governs hydraulic fracture propagation, or whether it is the intra-zone interfaces of rock variation which govern fracture propagation. The interplay between overall rock “brittleness” and intra-formational interfaces is complex; however microseismic event analysis provides further confirmation of behaviour.

It is expected that the laminated condensed section facies (blue), being both highly brittle and containing abundant laminations, would break easily internally, but act as barriers to fracture propagation. High Young’s Modulus facies (red) are expected to propagate a hydraulic

fracture; however the extent will be dependent on the frequency of intra-zone mechanical interfaces. Lower Young's Modulus "ductile" facies, while not having the desired brittleness to break easily under increased pressure, generally have less variation in rock properties and therefore their homogeneity may allow for hydraulic fracture growth. Microseismic event data was analyzed to determine the correlation of events to stratigraphic zones. The primary focus in this case was the number of events; however additional parameters such as moment magnitude and b-values of events will be further examined in Sections 6.6 and 6.7.

6.3 Datasets

The dataset used is from three well pads in the Farrell Creek area of the Montney Shale; the 89-I well pad, 87-I well pad, and 85-I well pad, and is outlined in Table 6.2. All stages were monitored using vertical arrays to obtain the most accurate depth control. Events were correlated to mechanical stratigraphy (Figure 6.2 and Table 6.1) based on the depth and the dip of the formation. The main questions in this study are as follows:

1. How does perforation placement vs. stratigraphy affect event location?
2. Are zones more preferentially prone to shear failure (and therefore microseismic activity)?
3. Does the microseismic event distribution show a correlation to the defined mechanical stratigraphy and Rock Quality Index (RQI)?

6.4 Bulk Analysis

The first step involved analysis of all events occurring during the stimulation treatment. The event distribution for all events is shown in Figure 6.3, indicated by the grey bars overlying the stratigraphic framework. Figure 6.3 indicates that there is an overall increase in event count with depth, and both laminated and brittle facies have high event counts in the lower portion of the section. As there was no distinction between brittle, ductile, and laminated facies evident in the total event counts, data was further analyzed to determine variation.

6.5 High-graded Analysis

From the bulk event dataset, "high-graded" events were chosen based on both signal to noise ratio (SNR) and distance from the monitoring arrays. Events with SNR greater than 5, and distance from the receivers less than 500 meters were used as the high-graded dataset. The event distribution of high-graded events is shown in Figure 6.4. Table 6.3 shows the percentage of total events which remained in the high-graded dataset.

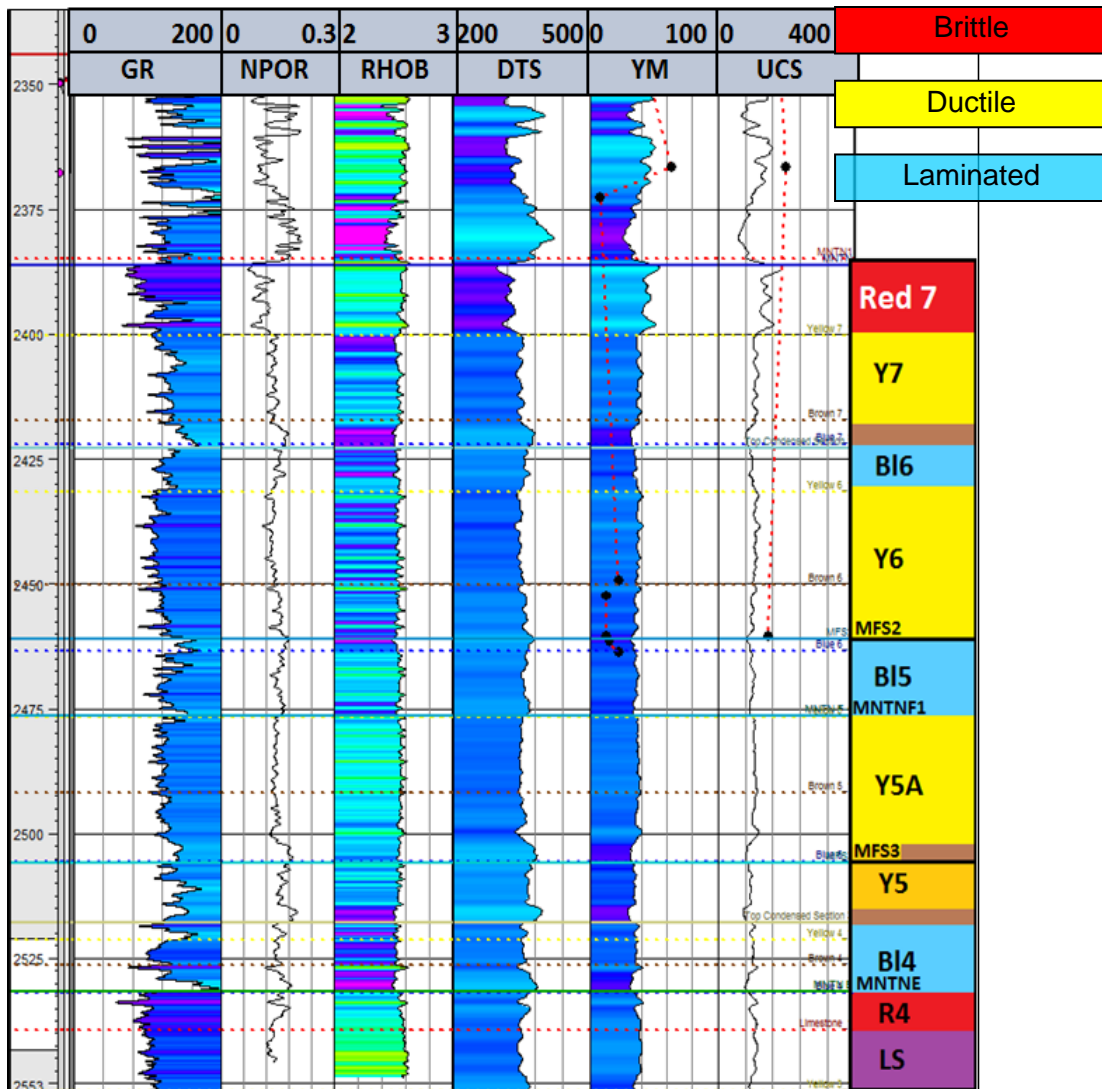


Figure 6.2- Mechanical stratigraphy defined for Farrell Creek, the Montney Shale, BC.

It is important to note that further reference to homogeneity vs. heterogeneity in the Rock Quality Index (RQI) is referring to this index only, not the reservoir itself. Homogeneous RQI corresponds to a state of little *stress* and *brittleness* variation. This is not necessarily coincident with a portion of the reservoir which is homogenous in terms of fracturing or sedimentary structures.

Table 6.1: Mechanical stratigraphic zones, depths, and thicknesses.

	Thickness	Depth Range (TVD m)	Mid-Point (TVD m)	Legend
Red 7	15.3	2385-2400.3	2392.65	Brittle
Yellow 7	16.9	2400.3-2417.3	2408.8	Ductile
Brown 7	4.7	2417.3-2422	2419.65	Ductile
Blue 6	9.5	2422-2431.5	2426.75	Laminated
Yellow 6	29.5	2431.5-2461	2446.25	Ductile
Blue 5	13	2462-2475	2468.5	Laminated
Yellow 5A	30	2475-2505	2490	Ductile
Yellow 5	15	2505-2518	2511.5	Ductile
Blue 4	13.5	2518-2531.5	2524.75	Laminated
Red 4	7.5	2531.5-2539	2535.25	Brittle

Table 6.2 - Data used for microseismic event analysis.

DATA FOR EVENT COUNT ANALYSIS	
<i>Criteria: Vertical array monitoring for depth control</i>	
WELL	STAGES
C-A85-I/094-B-01	Stage 1-5
C-B85-I/094-B-01	Stage 3-9
C-C85-I/094-B-01	Stage 3-12
C-D85-I/094-B-01	Stage 7-14
C-D89-I/094-B-01	Stage 3-12
C-E89-I/094-B-01	Stage 1-11
C-F89-I/094-B-01	Stage 1-11
D-87-I/094-B-01	Stage 1-7
DATA FOR MAGNITUDE & B-VALUE ANALYSIS	
<i>Criteria: SNR>5, Distance <500m from receiver array</i>	
WELL	STAGES
C-A85-I/094-B-01	Stage 4, 5
C-B85-I/094-B-01	Stage 10, 11, 12
C-C85-I/094-B-01	Stage 9, 10, 12
C-D85-I/094-B-01	Stage 10-14
D-87-I/094-B-01	Stage 3,5,6,7

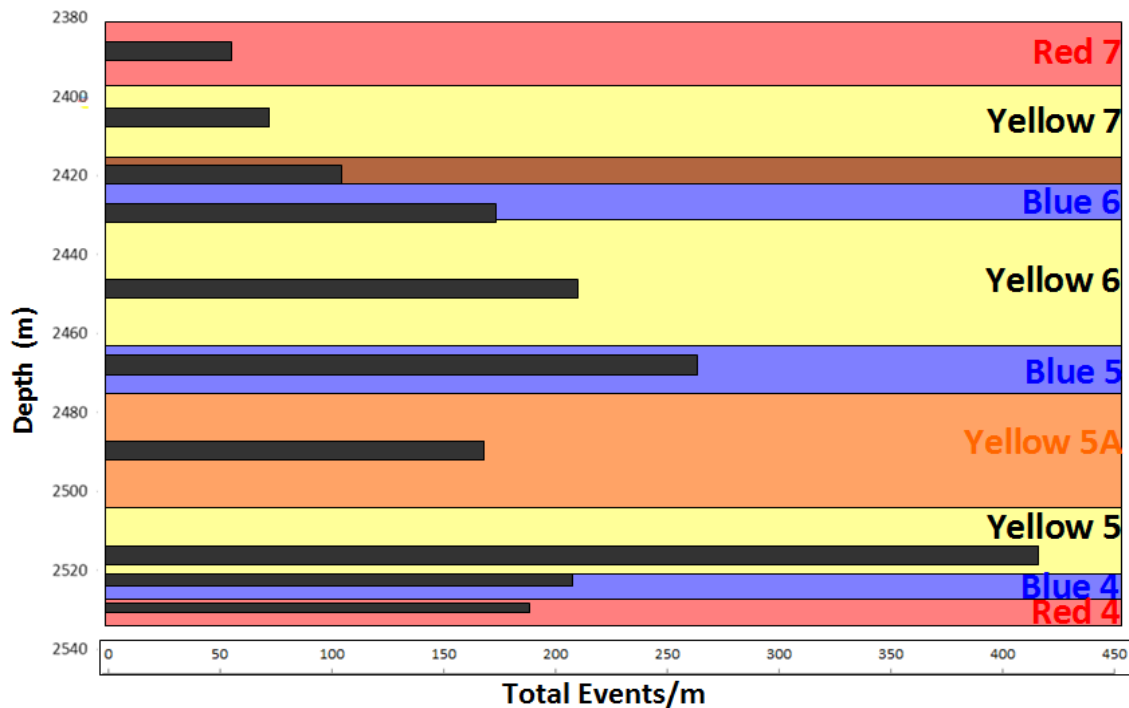


Figure 6.3- Total event counts for all well pads are shown by the grey bars, on a scale of 0-450 events. Mechanical stratigraphy previously defined is shown by the background colors.

It can be observed that in the Yellow 5A, Yellow 5, and Blue 4 facies a significantly higher percentage of events remain in the high-graded dataset. Numerous high-graded events in these facies tell the observer several important things about the stratigraphy. Firstly, microseismic in the Yellow 5A, Yellow 5, and Blue 4 facies are manifested as “louder” events near the wellbore, due to rock breakdown during the propagation of the dilating hydraulic fracture. It is logical that within these facies, where two stacked zones of similar properties (Yellow 5A, Yellow 5) are present, internal heterogeneity would be lower, and hydraulic fractures would be easier to propagate and grow. As the hydraulic fracture propagates, any natural fractures present would be more likely to be activated due to their proximity to large stress and pressure changes. These failures would be manifested as these louder proximal microseisms.

Secondly, in the zones above Yellow 5A, a large reduction in the event numbers close to the wellbore indicate most of the events are occurring at distance, with a low SNR ratio, meaning they are likely representative of aseismic background deformation. These events could be abundant small shear events occurring at formation interfaces, which could shear at any

point where the rock is critically stressed. These events would likely be smaller, more dispersed, and triggered by smaller stress perturbations, while the events we see in the lower facies are a result of tip effects and pressure changes of the main hydraulic fracture (Agarwal et al 2012).

As referred to in Section 7.1, the traditional theory that high brittleness is desired may require alteration. It is hypothesized here that it is not the absolute brittleness of the zone, but the variation within brittleness/rock properties within the zone that is of most importance. This appears to be the case according to this analysis, and will be further examined and corroborated in Chapter 8. The relationship between high-graded events and the modified Rock Quality Index (RQI) is shown in Figure 6.5.

Table 6.3 shows quantitatively that a significantly larger portion of total events remains in the Yellow 5A through Blue 4 facies, indicating that more shear events close to the wellbore are occurring in these lower facies. This is likely due to a large induced pressure perturbation from the hydraulic stimulation in these lower facies.

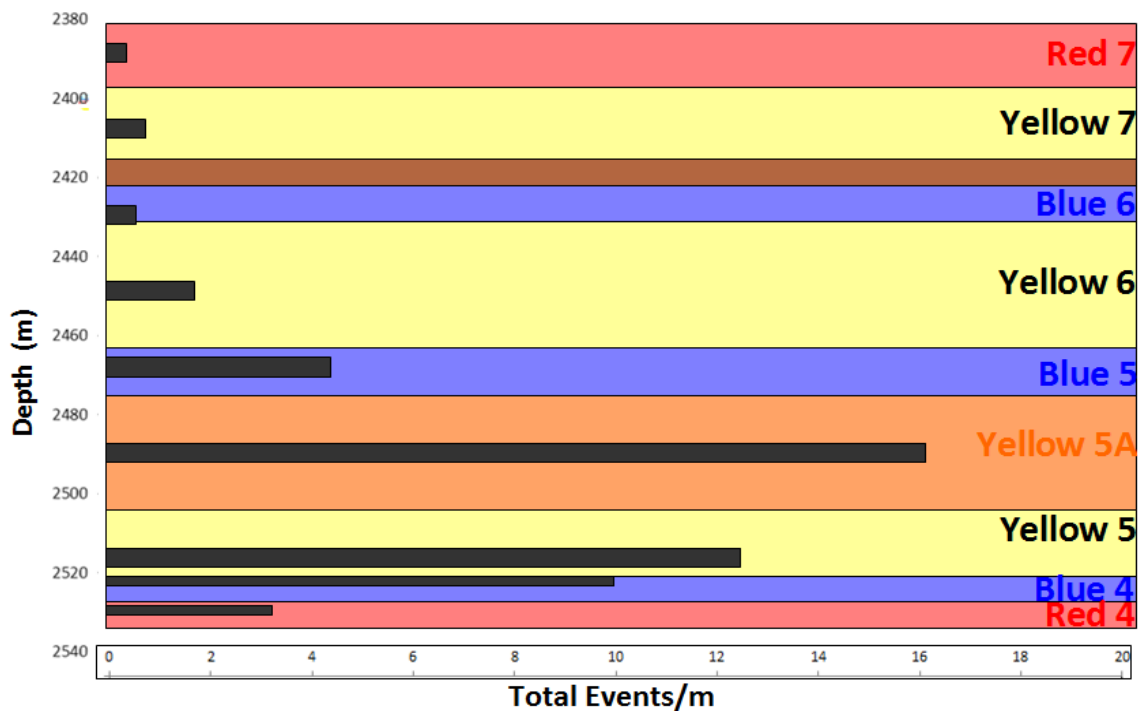


Figure 6.4 - High-graded event dataset. High-graded event counts for all well pads are shown by the grey bars, on a scale of 0-20 events. Mechanical stratigraphy previously defined is shown by the background colors.

Table 6.3- Percentage of total events with SNR >5 and distance <500m from the monitoring array.

	High-graded Events/m	All Events/m	Fraction
	85, 87, 89	85, 87, 89	%
Red7	0.39	57.25	0.68
Yellow7	0.71	75.38	0.94
Blue6	0.52	173.69	0.30
Yellow6	1.49	213.97	0.70
Blue5	4.54	266.54	1.70
Yellow 5A	16.07	171.40	9.37
Yellow 5	12.40	414.53	2.99
Blue4	7.48	209.78	3.57

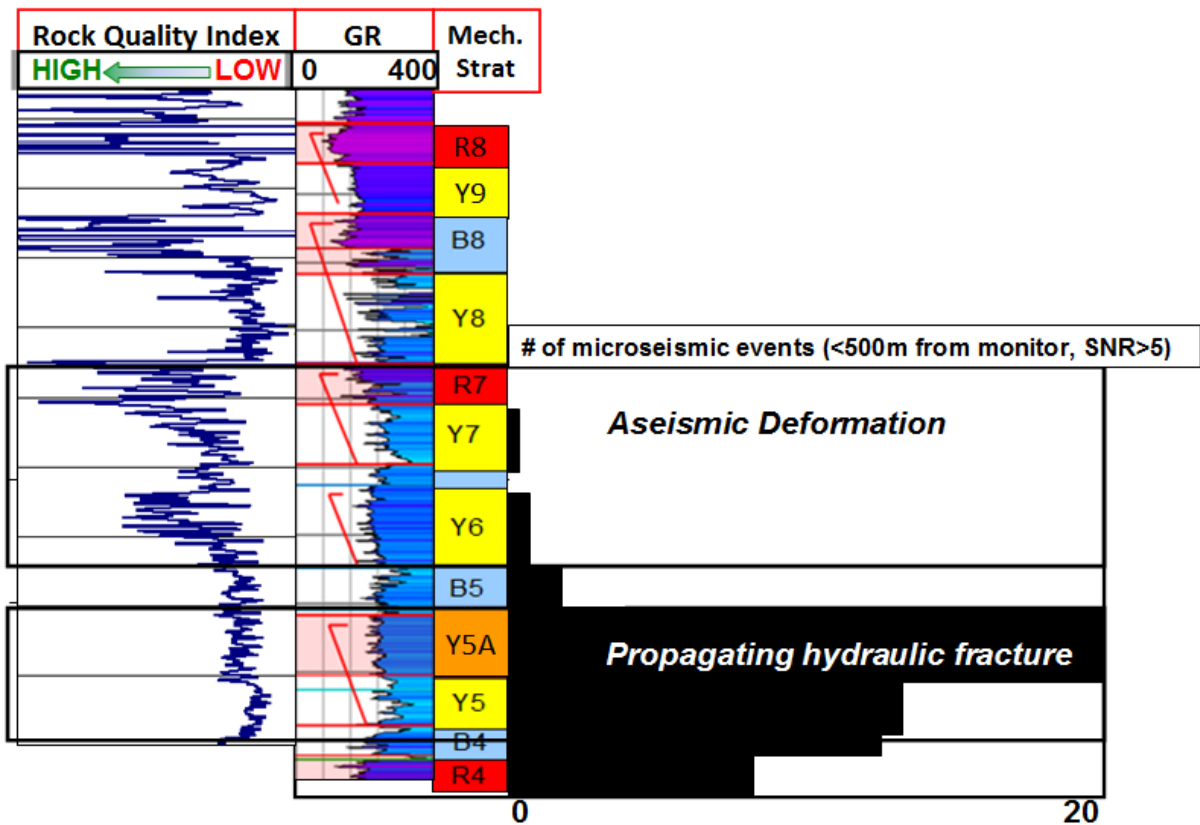


Figure 6.5 - Correlation of high-graded events to mechanical stratigraphy. In the Yellow 5A and Yellow 5 facies high event counts remain, which correlated with the lowermost homogenous zone in the Rock Quality Index (RQI) log.

The Blue 5 facies appears to represent a special case. It is both a laminated/brittle facies, and has a relatively homogenous RQI, whereas other blue and red facies generally have a highly variable RQI. Give that this facies has both desirable conditions; brittleness and homogeneity, it would be expected to be highly productive. This hypothesis will be examined further in Section 6.6.

6.6 B-value Analysis

The hypothesis has now been established that abundant large magnitude events remaining in the lower stratigraphic zones (B4 through B5) are associated with stress perturbations occurring during the propagation of a hydraulic fracture. In addition, the Blue 5 facies appears to be desirable both in terms of brittleness and Rock Quality Index (RQI). To further understand the relationships between these lower facies, the frequency-magnitude relationships of the high-graded microseisms were further analyzed. When frequency-magnitude relationships of high signal to noise ratio (SNR) microseisms are further analyzed, the b-value of the zones can be determined. The b-value is derived from the equation formulated by Gutenberg and Richter (1944):

$$\log N = a - bM \quad (6.1)$$

N= earthquake count

M= magnitude

Constants a= describes seismic activity, b= tectonic parameter; properties of medium.

The b-value can provide an indication of both the stress state and fracture activation mechanisms in the reservoir. Higher b-values correspond to a lower stress state, lower material heterogeneity, and hydraulic fracture propagation (Kulhanek 2005). Lower b-values are associated with a higher stress state, higher material heterogeneity, and re-activation of natural fractures. B-values correlated with stratigraphy are shown in Figure 6.6. For the upper three zones, a limited number of usable events meant an accurate estimation of b-value could not be made. In the Yellow 6 and Blue 5 facies, we see lower b-values compared to the Yellow 5A, Yellow 5, and Blue 4 facies.

These observations would suggest that in the lower zone we have hydraulic fracture propagation, less activation of natural fractures, and a lower material heterogeneity. This behaviour correlates well with the RQI results (Figure 6.7); where above the Yellow 5A facies the abundance of brittle zones is greater and a lesser number of large events near the wellbore

are observed. In the Yellow 5A facies and below, a low material heterogeneity and large number of events near the wellbore is observed. Hydraulic fracture dilation, propagation, and height growth is more dominant in the lower facies, while in the upper facies small shear events and aseismic background deformation is dominant.

Returning to the specific examination of the Blue 5 facies, the large change in b-value from the underlying zone indicates a different fracture activation mechanism. This zone is site of abundant fracture failure, and also a barrier to further upward propagation of the hydraulic energy. Fracture behaviour; hydraulic fracture growth and propagation, versus natural fracture re-activation and shear, are shown in Figure 6.8.

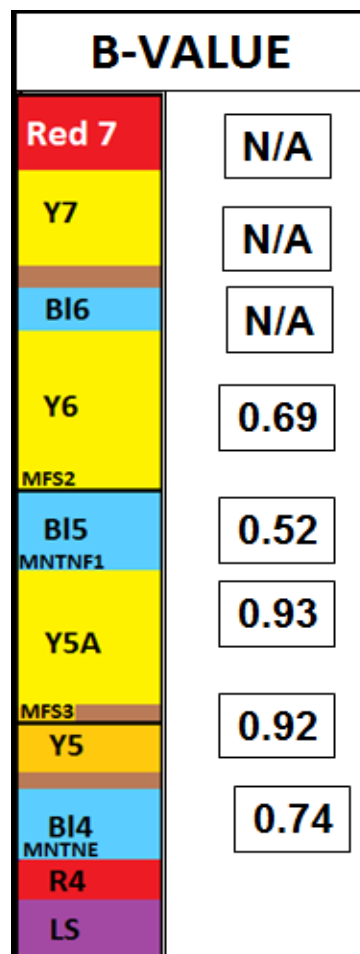


Figure 6.6- B-values correlated to mechanical stratigraphy. Higher b-values, corresponding to the propagation of a hydraulic fracture and lower material heterogeneity, are seen in the Yellow 5 and Yellow 5A facies, strengthening the argument that growth of a hydraulic fracture is most prolific here. A much lower b-value is seen starting at the Blue 5 facies, indicating a stress change and different fracturing mechanism.

In addition to a change in stress and fracturing mechanisms at the Blue 5 facies, stress shadowing likely plays an additional role in the change in character. Stress shadowing theory states that with each hydraulic stage introduced into the reservoir, pressurization is an additive effect. Therefore, as pressure increases and the perturbation propagates upward with the stimulation, when it reaches the highly laminated Blue 5 facies they are abundant interfaces for this energy to dissipate and release. This interaction of the propagating hydraulic energy and abundant laminations/natural fractures will be discussed further, and appears to correlate to high production.

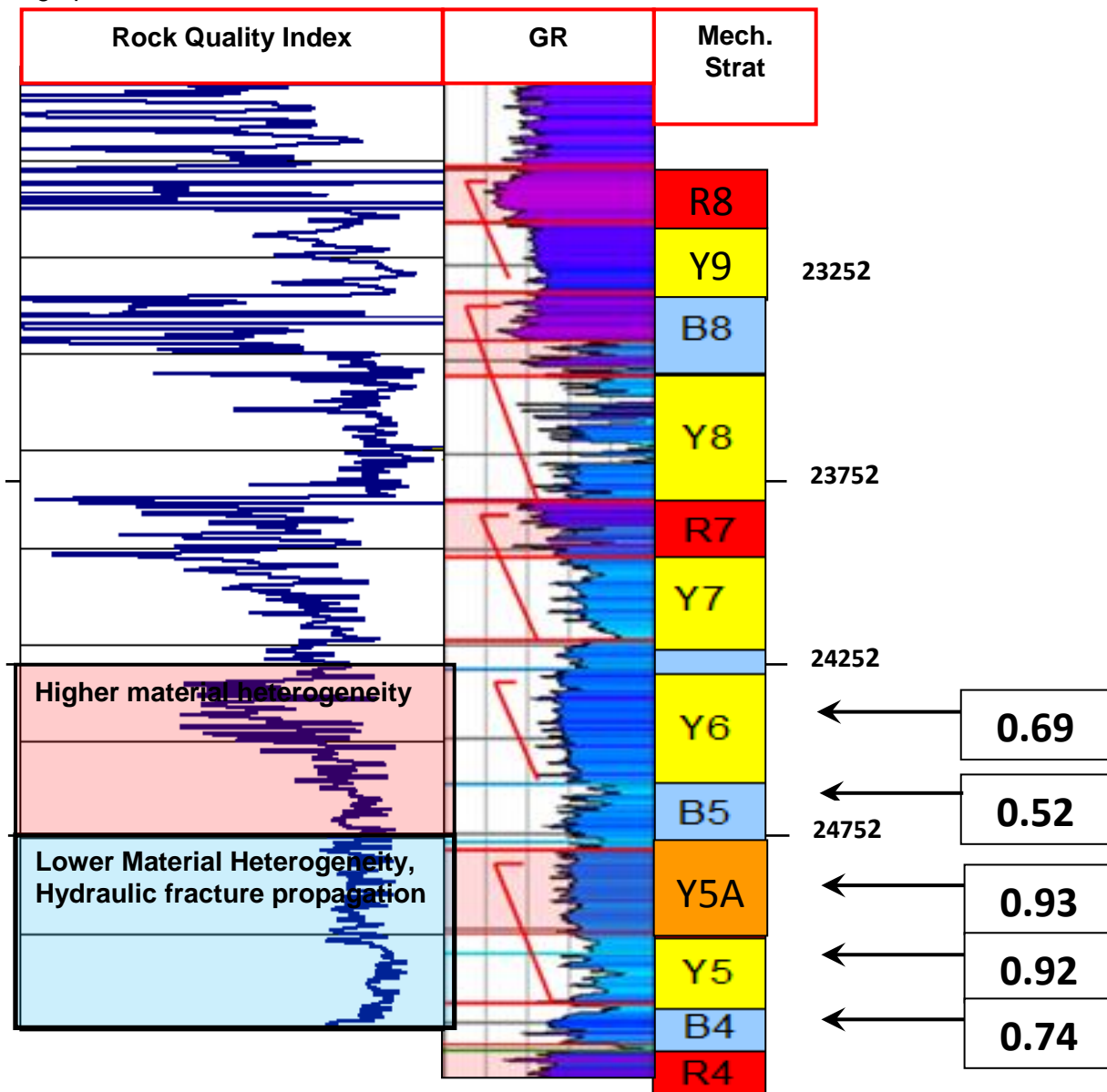


Figure 6.7- B-values correlating to mechanical stratigraphy and Rock Quality Index (RQI).

6.7 Seismic Moment

To further substantiate the above hypotheses, the seismic moment release of the 25 highest-magnitude events was determined in each zone. The moment release is an indication of seismic deformation which may correlate to fracture density (Maxwell 2009). The results of this analysis are shown in Figure 6.9.

Once again, it is observed that where lower material heterogeneity is present large microseisms occur. These large events are likely the result of the large stress perturbations induced by the hydraulic fracture.

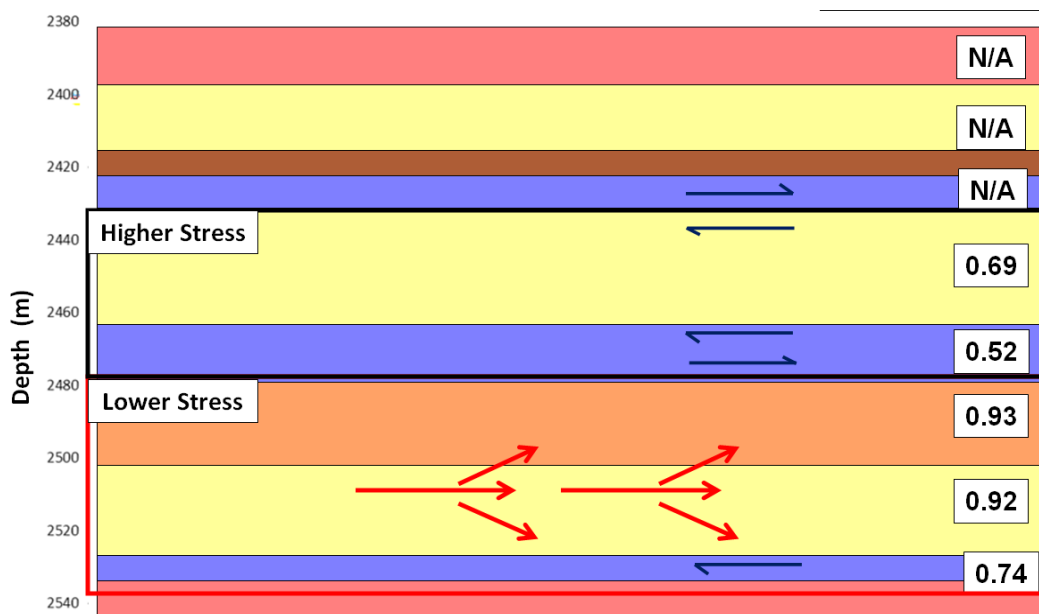


Figure 6.8- Hydraulic fracture propagation in lower stress zone (red arrows); natural fracture reactivation and shear in higher stress zone (blue arrows). The point of interaction between these two fracturing mechanisms, at the Blue 5 facies, appears to be an area of prolific production.

6.8 Perforation Placement

The final analysis examines how fracture placement affects event distribution. Figure 6.10 and Figure 6.11 provide examples of this analysis. From this analysis, it appears that when a treatment is placed in a brittle zone, event counts are elevated within the zone and proximal laminated/brittle zones, but do not propagate far from the brittle zone. Considering the large number of events occurring in the Yellow 5A and Yellow 5 facies, and the fact that these two facies are bounded by the Blue 4 and Blue 5 facies, this again gives support to the observation

of a large number of events in this lower zone. It is likely that the two brittle zones act as a barrier to pressure propagation from the bounded Yellow facies.

This analysis supports the idea that evenly-spaced perforations along a horizontal or vertical wellbore may not result in the most effective stimulation or highest production. Specifically targeting areas where a homogenous facies interacts with a laminated/fractured facies appears to be the most likely way to create a complex network and greater reservoir reach. To date, the strategy in unconventional shale reservoirs has been to space perforations evenly along the wellbore and use an equal amount of proppant and fluid for each stage. The comparisons here between mechanical stratigraphy and microseismic events show that differential spacing and fluid/proppant volumes may be advantageous for production. In addition, there is the potential to re-fracture wells which currently have equally-spaced perforations, resulting in greater reservoir reach not achieved with the previous strategy.

6.9 Implications of Analysis

The analysis of microseismic events provided very good evidence for the hypotheses proposed based on mechanical stratigraphy and Rock Quality Index (RQI). A larger proportion of high-energy events occur close to the wellbore in facies where mechanical interfaces are minimized and the zone is more homogenous. These zones of high microseismic activity are not always consistent with the mechanical stratigraphic definition of the zones with highest “brittleness”. It appears that the overall stress state and abundance of mechanical interfaces governs the propagation of a hydraulic fracture, rather than the brittleness itself. Higher internal variability within a zone appears to hinder hydraulic fracture growth, and therefore it is the *frequency of change* in brittleness between zones, rather than the brittleness itself that determines how a hydraulic fracture stimulation will perform.

B-value analysis confirms different fracture activation mechanisms in the upper and lower portions of the stratigraphy, and perhaps differences in the stress state based on the events seen. Further discussion of fracture activation and stress changes will be discussed in Chapter 9.

The most prolific zones in terms of production occur where a homogenous zone, allowing for the growth and expansion of hydraulic fracture energy, meet at an interface with a highly laminated or fractured zone, allowing for dissipation and propagation of this energy along layers. The correlation between this zone interaction and production is further confirmed with

spinner gas flow rates in Chapter 9. The importance of the interface between homogenous and heterogeneous zones also comes into play when considering re-fracture treatments in previously completed wells.

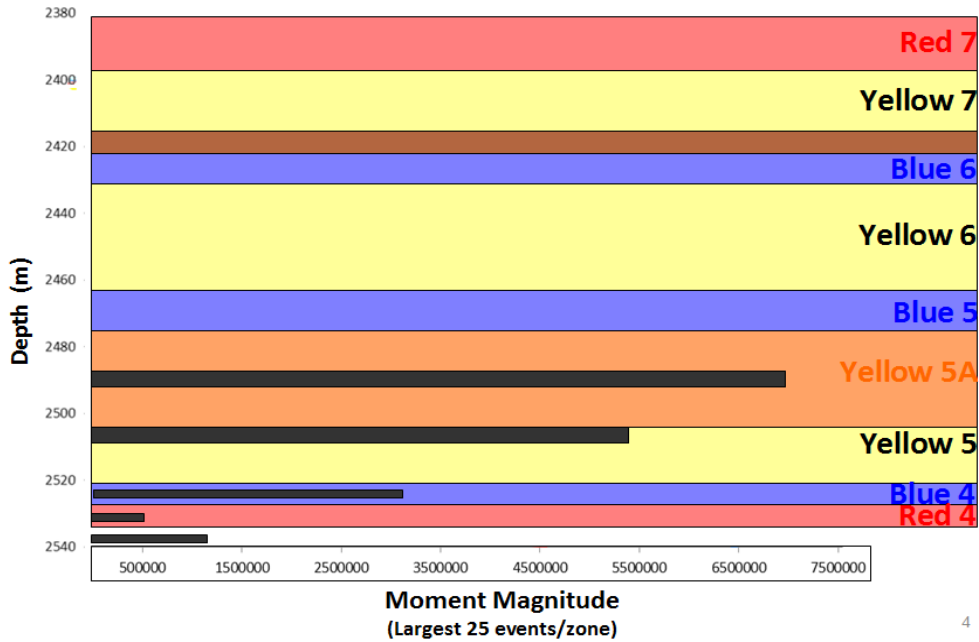


Figure 6.9- Moment magnitude of largest 25 events per zone.

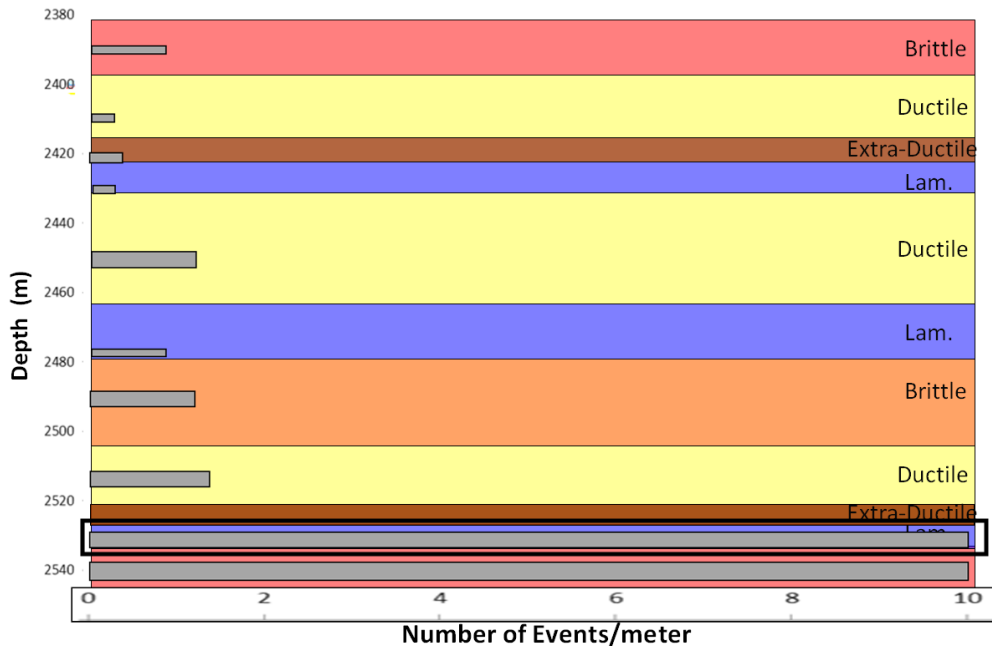


Figure 6.10 - Stage placement indicated by black box, event distribution indicated by grey bars, overlying mechanical stratigraphy as previously defined. In this case, stage placement in a brittle facies results in little hydraulic growth outside this facies.

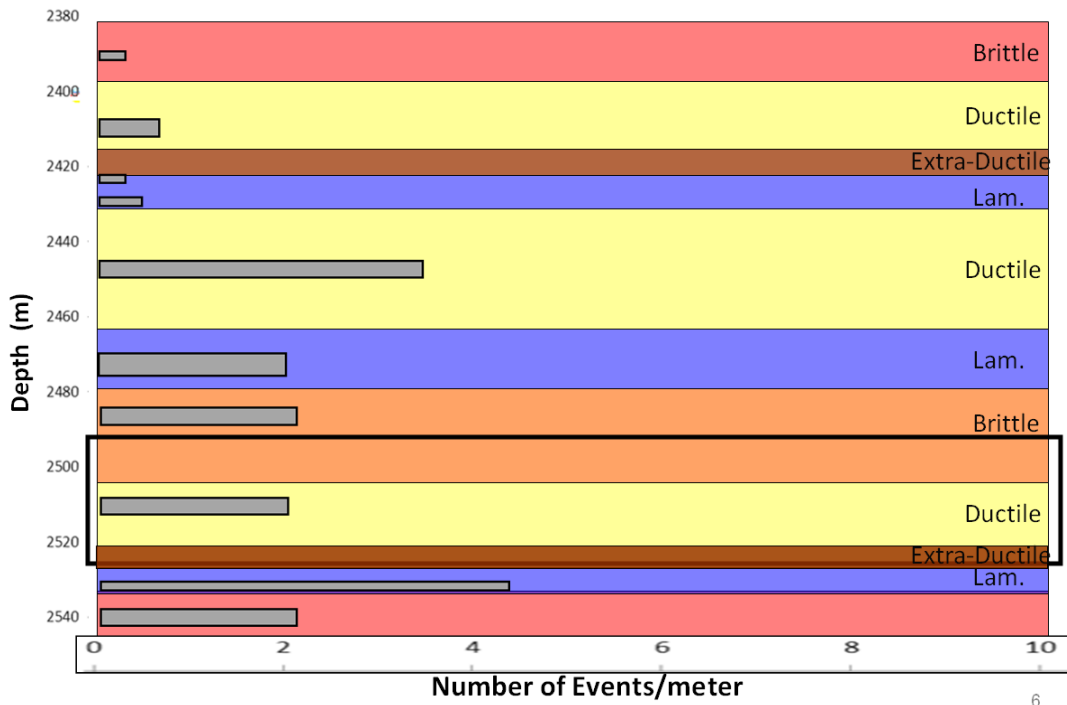


Figure 6.11- Stage placement indicated by black box, event distribution indicated by grey bars, overlying mechanical stratigraphy as previously defined. In this case, stage placement in a more ductile but homogenous facies results in more distributed hydraulic fracture energy in all facies.

CHAPTER 7

NATURAL FRACTURES

The failure of natural fractures was discussed in Chapter 6. It is assumed that any natural fractures present in a reservoir will interact with an introduced hydraulic stimulation. However, it is necessary to examine natural fracture failure at a detailed scale. Geomechanical modeling utilizes the fundamental principles of structural geology and rock mechanics to examine stress-strain relationships in the reservoir. Modeling must also incorporate textural variation at multiple scales, first as fine-scale kerogen pores, alignment of these pores, and laminations of these organic-rich layers with other layers (Bandyopadhyay 2009). These analyses examine a snapshot in time; however the history of the basin is also important. One way to infer basin history is through records of past history, which occur as textural variation. Therefore, natural fractures give insight into rock evolution, and therefore provide a predictive tool for future fracture behavior in the present day stratigraphy and stress state.

Hydraulically fracturing a low-permeability formation creates high permeability conduits. Fluid associated with the hydraulic fracture elevates reservoir pressure, thereby reducing effective stress and causing failure of in-situ natural fractures. This allows for natural and hydraulic fracture linkage and a pathway for hydrocarbon flow to the wellbore. Other studies have observed induced hydraulic fracturing affecting the stability of natural fractures. It is theorized that induced slip can increase the conductivity of the fracture network (Warpinski et al 2005).

Proppant acts as a high porosity “matrix” and maintains the aperture of the fractures. However, the role of natural fractures is difficult to quantify due to their scale within the overall petroleum system (Billingsley et al 2006). This issue of scale will be further discussed in Chapter 8. In this analysis, Mohr Coulomb failure theory is used to define how natural fractures are contributing to reservoir completion and production behavior.

7.1 Relationships between Rock Quality Index and Natural Fracture Failure

The Brittleness Index (BI), Rock Quality Index (RQI), and associated formation behavior previously defined in Chapter 5 describes the overall susceptibility of a zone to failure. How

natural fractures additionally influence formation failure is equally important and intrinsically related to the stress state which helps define the Rock Quality Index (RQI). Failure occurs as either:

- (1) A shear fracture- single fracture surface inclined to the principal stress
- (2) An extensional fracture- separation occurs normal to the failure surface (usually optimally oriented normal to the minor principal stress).

In both cases, the nature of failure is strongly dependent on the confining pressure. A brittle fracture is a discrete event in which the failure of the rock occurs without significant prior deformation and without warning, at a particular stress level (Kolymbas 2003). Of particular interest here is the stress level at which fracturing will occur. When a layered material is loaded with a uniaxial stress oriented normal to the interface (Figure 7.1), as is the case with a hydraulic stimulation, lateral expansion of individual layers will occur (Teufel et al 1984). If slip does not occur at the interface, the expansion of each layer will be affected by the expansion of each adjacent layer.

Therefore, the interface between two differing layers will experience differential contraction/extension and result in a horizontal stress differential. Compressive horizontal stress develops in the high Poisson Ratio layers, where expansion is greater and therefore constraint is greater, and tensile horizontal stress develops in the low Poisson Ratio (high modulus) layer, where expansion is less and the layer is therefore extended (Teufel et al 1984). This is shown diagrammatically in Figure 7.2.

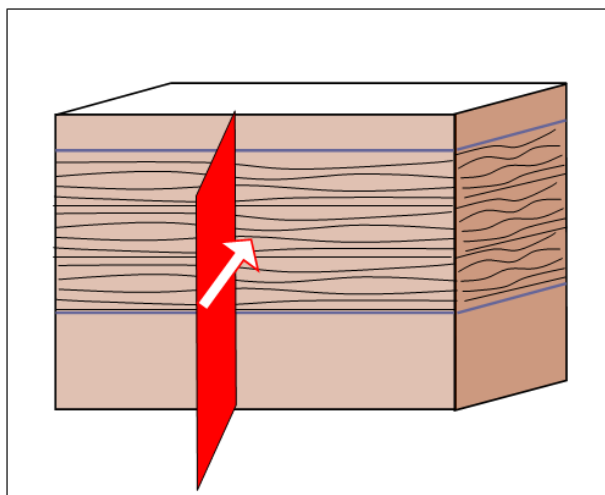


Figure 7.1- Layered rock formation “loaded” with the stress of a propagating hydraulic stimulation (red plane).

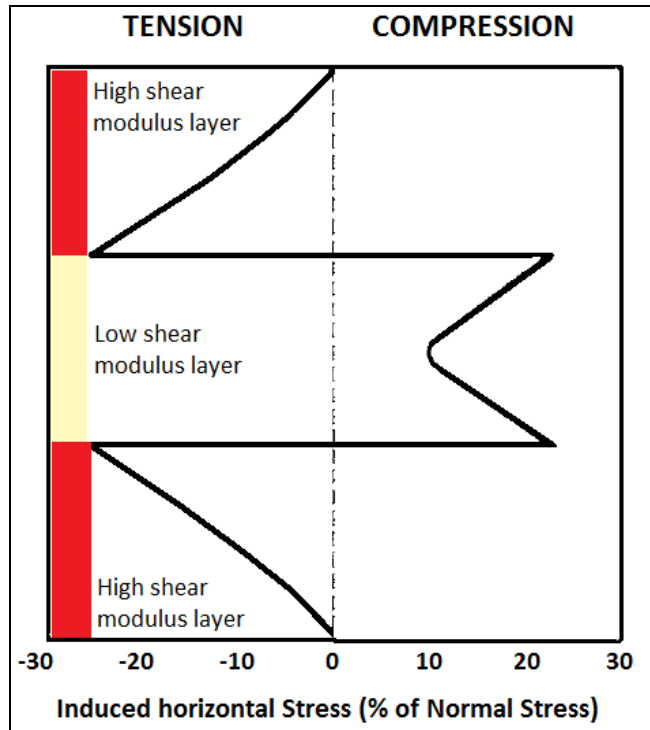


Figure 7.2- Changes in layer properties with loading (modified from Teufel et al 1984). The induced change in horizontal stress is compressional in a low shear modulus layers while in high shear modulus layers the horizontal stress is compressional.

Throughout the history of a formation, changes in contraction and extension of layers are directly linked to the over-consolidation ratio (equation 5.1), which was used to define the “fabric-based” brittleness index. The over-consolidation ratio is a ratio of the present stress level divided by a previously applied stress level, memorized in the fabric of the rock. By defining the stress state and expected failure of natural fractures in the present-day stress state, the brittleness index and subsequent Rock Quality Index (RQI), can be related to the natural fractures of the formation.

7.2 Quantitative Fracture Failure

In Chapter 6 the hypothesized behavior of the formation, based on mechanical stratigraphy and Rock Quality Index (RQI), was substantiated with microseismic event analysis. This correlation was largely qualitative, providing an idea of zones where the rock mass reacts differently to a hydraulic stimulation. As the reservoir properties change with introduction of fluid and proppant, the rock mass fails. Why this failure occurs was related back to the rock properties and stress state in the different zones. But how this failure occurs cannot be determined based solely on the microseismic and mechanical stratigraphy. A more detailed

quantitative picture of where natural fractures occur in the formation provides an indication of how these fractures interact with the dominating hydraulic fracture. Changes in pressure due to the hydraulic stimulation will induce failure. Image logs are used to determine the orientation and abundance of natural fractures existing in-situ in the reservoir. In conjunction with pressure data from the completions program, an accurate determination of when and at what pressure these natural fractures fail provides vital information about their ability to affect the propagation of the hydraulic fracture.

Through image log analysis, it was determined that in general, each image log contained two dominant natural fracture orientations, one roughly parallel to σ_{Hmax} and one roughly perpendicular (Figure 7.3). For each well, one of these orientations contained approximately 65% of the total fractures in that wellbore; meaning there was a dominant orientation per well. Of interest here was determining whether one of these dominant orientations was more likely to fail than the other. This will be further examined in Sections 7.4- 7.6.

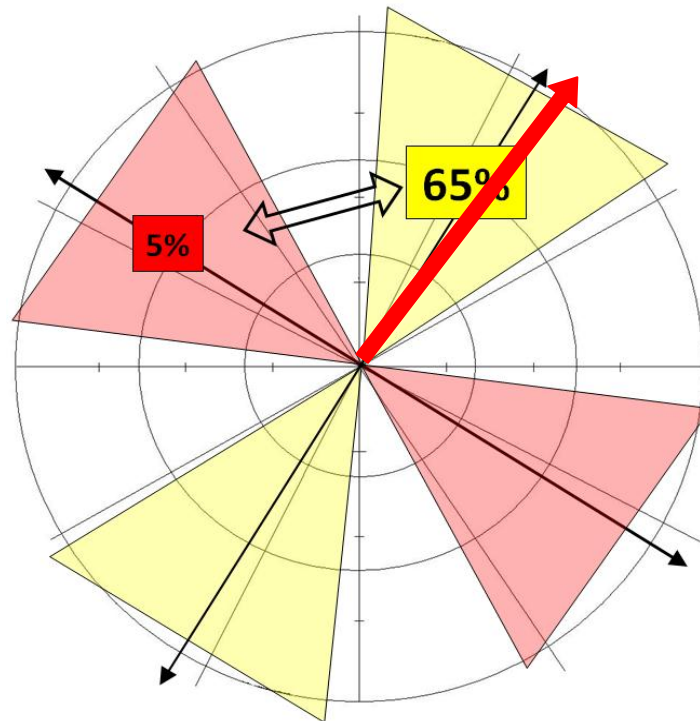


Figure 7.3 - Dominant natural fracture orientations, sub-parallel to minimum horizontal stress (red outline) and sub-parallel to maximum horizontal stress (yellow outline). Orientation of maximum horizontal stress (N40E) shown by red arrow.

7.3 The Importance of Natural Fractures- Analogous Case Study

The performance of low permeability fractured reservoirs is controlled by two factors; the in-situ stress state and distribution and orientation of natural fracture and fault systems (Tezuka et al 2002). Because of the strong stress and strength anisotropy associated with these fracture networks, reservoir characterization using conventional logging techniques is often not sufficient for predicting reservoir production. It is difficult to define a clear correlation between productivity and well orientation, or field location (Tezuka et al 2002). The Yufutsu Gas Field is a low permeability fractured reservoir occurring at depths of 4000-5000 meters, composed of alluvial/fluvial Eocene conglomerates underlying marine sedimentary rocks and volcanic units. Maximum horizontal compressive stress (σ_{HMax}) is approximately N30E, similar to the orientation of σ_{HMax} in the Montney; N40E. Production in the Yufutsu Field varies from highly productive to non-productive.

Through image log analysis, two populations of dominant fractures were determined; NE-SW (steeply dipping to the NW/SE), and NW-SE (moderately dipping to the SW/W). These fracture trends are strikingly similar to the dominant fracture trends identified in image logs at Farrell Creek. Coulomb failure analysis revealed that optimally-oriented critically stressed fractures largely occurred in the NE-SW fracture set. These stressed fractures are preferentially oriented for shear failure, and controlled reservoir permeability and therefore fluid flow to the wellbore (Tezuka et al 2002). Overall, the Yufutsu study concluded that higher productivity wells occurred when there were an increased number of NE-SW striking fractures, and additionally where “mega” fractures were intersected by the wellbore (having centimeter-order apertures). These mega fractures act as a conduit for hydrocarbon flow from smaller “major” and “minor” fractures. The idea that a “mega” fracture aligned with the maximum horizontal stress direction is necessary for flow from smaller secondary fractures has important implications for analysis in the Montney. Since a hydraulic stimulation will result in a hydraulic fracture aligned with σ_{HMax} ; the “mega” fracture, it is hypothesized here that smaller secondary fractures in an orthogonal direction would result in higher production. The hydraulic fracture will provide the high permeability conduit for flow while orthogonal natural fractures will provide the complex network needed for full reservoir reach. This hypothesis is further examined in section 10.4.

Following the theory and workflow presented in this Yufutsu study, both image log analysis and Mohr coulomb failure analysis were performed in the Montney study area. Results were additionally corroborated with Diagnostic Fracture Injection Tests (DFIT).

7.4 Mohr Coulomb Analysis

To incorporate Mohr-Coulomb failure theory, the shear and normal stresses on natural fracture faces in their in-situ stress state were determined. This allows for fractures to be plotted on a two-dimensional Mohr-Coulomb diagram and a predictive failure model to be made.

Mohr-Coulomb failure is based on the assumption that when some component of the dynamic stress field δT (e.g. a seismic event or hydraulic stimulation) is added to the local stress field T , this added stress can push a critically-stress fracture or fault beyond the Coulomb failure threshold.

$$T(t) = T + \delta T(t) \tag{7.1}$$

The Coulomb failure threshold is defined through Byerlee's Law for rock friction (Byerlee, 1978):

$$T(t) = \pm [C + \mu \sigma_n(t)] \tag{7.2}$$

C , μ = cohesive strength and coefficient of static friction respectively

$T(t)$, $\sigma_n(t)$ = shear and effective normal stress components acting on the fault under the stress field $T(t)$. The advantage of the Mohr-Coulomb circle is its two dimensional graphical representation of the Mohr-Coulomb failure criteria. Failure occurs when the Mohr circle touches the Coulomb failure envelope with the tangent point (R_c, θ_c) giving the orientation of a fault optimally oriented for failure in the given stress field (Hill 2008). However, because natural fractures in Farrell creek are not all perfectly aligned with the principal stress direction, the shear and effective normal stress components will be slightly altered. To determine the true stress state, Euler angle rotation was used to align the principal stress components with the natural fracture face.

7.5 Euler Angle Rotation

Stress rotation utilizes a right-hand coordinate system; where x points North (σ_{HMax}), y points East (σ_{hmin}), and z points down (σ_v). In this computation the principal stresses must be rotated from the aligned with σ_{Hmax} , σ_{hmin} , and σ_v (x,y,z) to a system aligned with the fracture face (x',y',z'). Therefore, rotation takes place around three angles (ϕ , θ , ψ) to reach the coordinate system of the natural fracture (Figure 7.4 and 7.5). One angle will equal zero, as the

initial stress field contains only vertical and horizontal components, and the strike of fracture is along a horizontal direction ($l' = \sigma_{HMax}$, $j' = \sigma_{hmin}$, $k' = \sigma_v$).

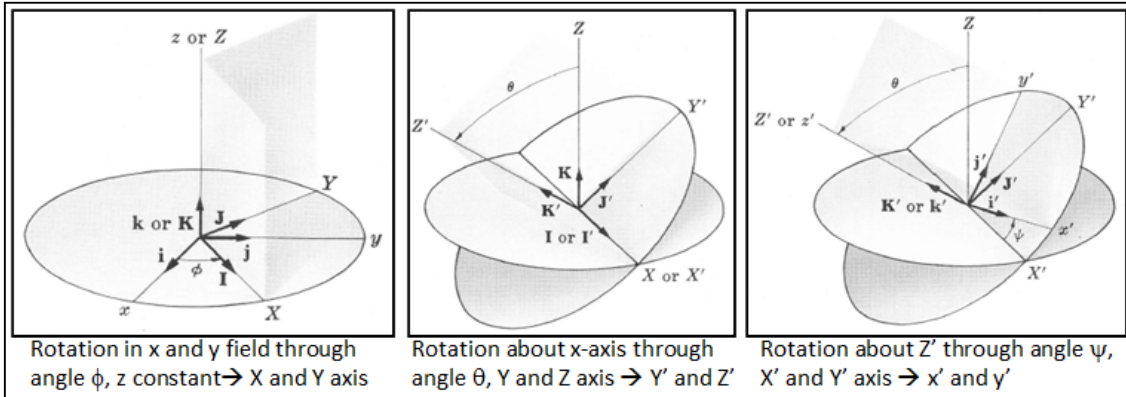


Figure 7.4- Process of Euler angle rotation about the principal axes.

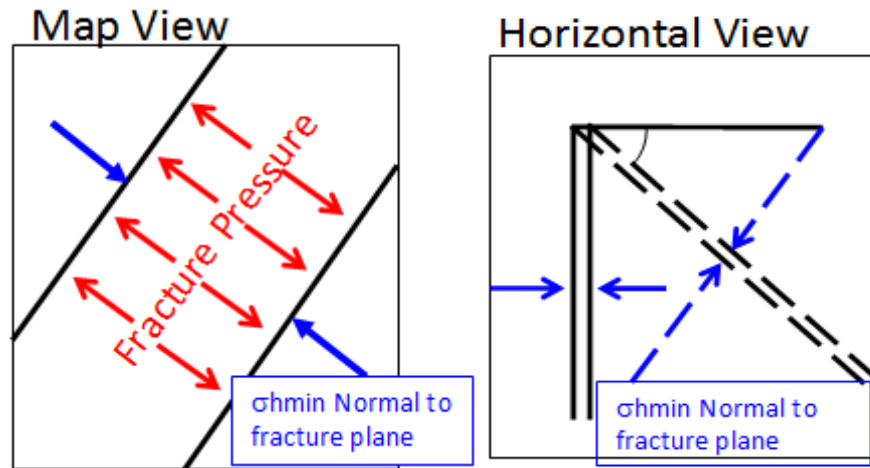


Figure 7.5- Representation of stress rotation. The principal stress σ_{hmin} will be slightly altered depending on the orientation of a natural fracture face. The magnitude of this stress aligned with the fracture plane itself must be defined.

7.6 Hydraulic Stimulation

Following computation of fracture face stresses, the next step was to determine the change in stress state that will occur with stimulation. Stress evolution will be dependent on the initial conditions (pre-stimulation), material properties of the reservoir, overlying and underlying units, and the reservoir geometry (Sayers 2006). Together these factors will define the “reservoir stress path parameters”. Pore pressure drop will occur with fluid drop according to Terzaghi’s equation:

$$\Delta\sigma'_v = \Delta\sigma_v - \alpha\Delta P \quad (7.3)$$

$$\Delta\sigma'_h = \Delta\sigma_h - \alpha\Delta P \tag{7.4}$$

As hydraulic fracture fluids and proppant are introduced into the reservoir, increased pore pressure will lead to a reduction in effective stress, as shown in Terzhagi's effective stress equation. A reduction in effective stress will cause a shift of the reservoir's stress state to the left, as shown in Figure 7.6, making the probability of critically-stressed fractures (and fracture failure) more likely. Understanding the stress evolution during reservoir production is important for predicting reactivation of faults, pore collapse, bedding-parallel slip, casing deformation and seismic activity. Stress shifts at Farrell Creek are examined for three wells using image logs, Mohr-Coulomb failure, and Euler angle rotation. The results are correlated to microseismic and DFIT's. However, in Pouce Coupe, such data is not available and therefore a different approach must be taken to characterize the stress evolution. Here, a 4D time-lapse seismic survey is used to examine shifts in stress during and following stimulation, and will be examined in Chapter 8.

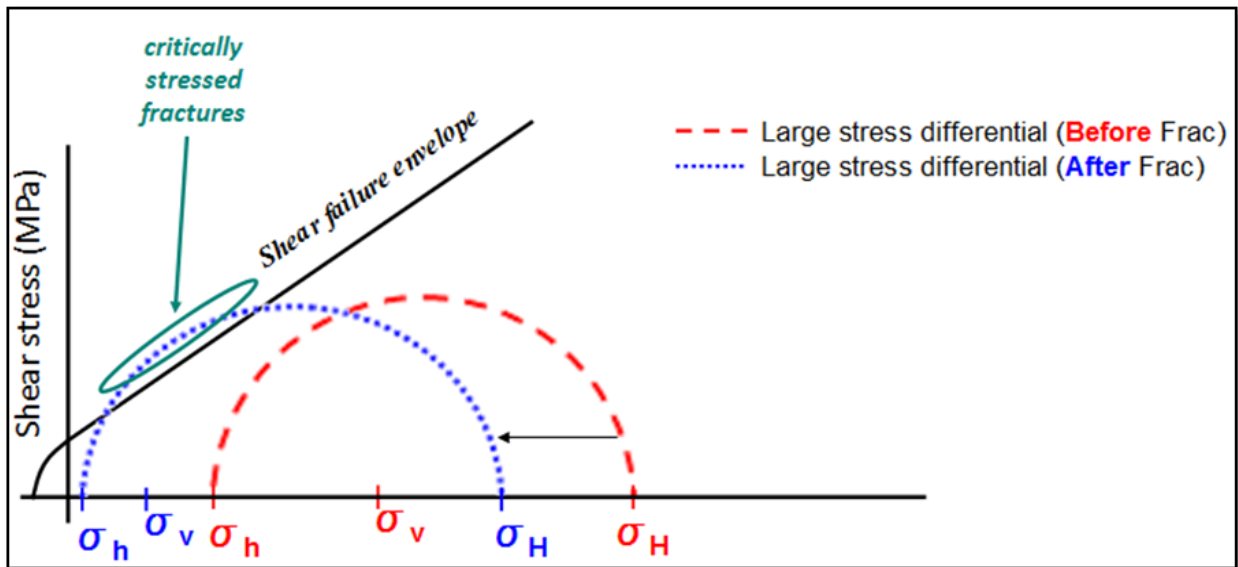


Figure 7.6 - Mohr-Coulomb failure theory. Effective normal stress is along the x-axis, as represented by equation 7.3-7.4. With an increase in the pore pressure term in this equation, a reduction in effective stress occurs and the stress state shifts to the left, from the original reservoir state (red circle) to the elevated pressure state (blue circle). At this point, any fracture lying on the portion of the semi-circle which surpasses the shear failure envelope will be critically-stressed.

The pressures used in this analysis were determined by looking at the treatment schedule of the completions in the study area. While each well will have a slightly different pressure profile, all will go through a common sequence, beginning with the breakdown pressure as fluid enters the formation from the wellbore. Following breakdown, the hydraulic fracture is propagated at the treating pressure, and finally the well is shut-in (at the ISIP point in Figure 7.7) after which reservoir pressure will drop to levels slightly elevated from the pre-fracture state (fracture closure pressure in Figure 7.7). Therefore, the stress state on natural fracture faces was examined at the breakdown pressure, treating pressure, maximum treating pressure, and closure pressure for each well with image log data.

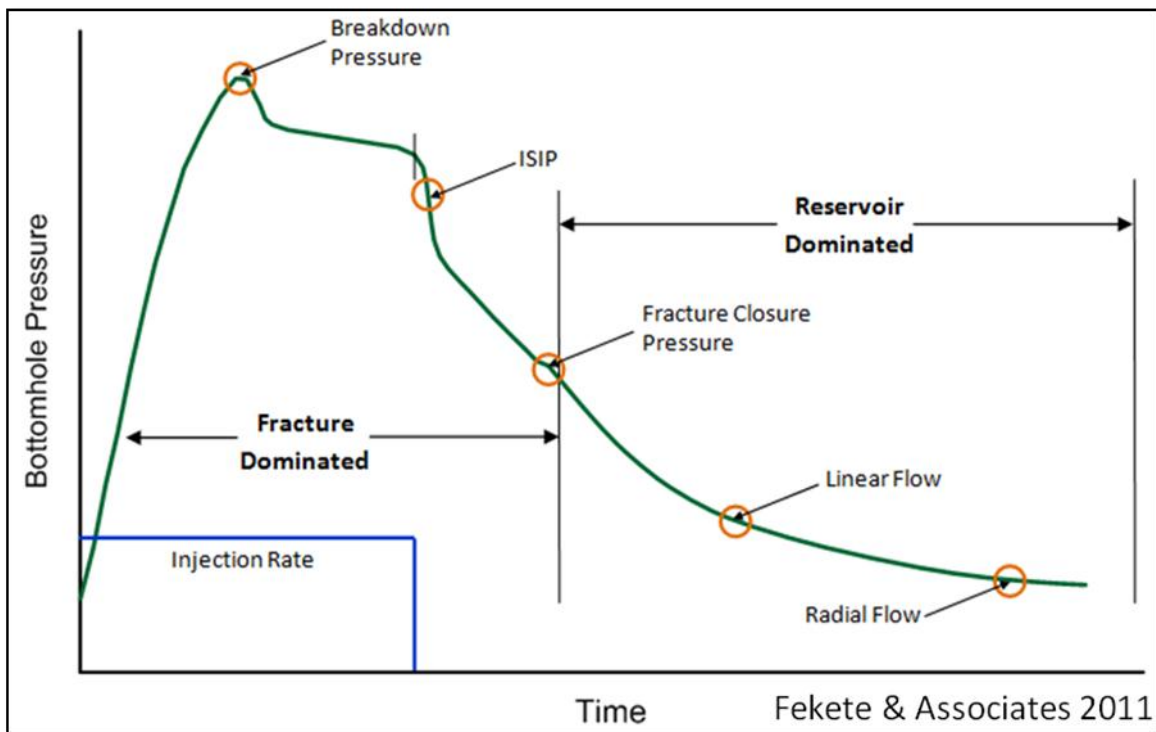


Figure 7.7- Pressure progression of a hydraulic fracture treatment (Jones & Britt 2009).

This procedure allowed for delineation of the pressure elevation required to fail in-situ natural fractures. Figure 7.8- 7.10 shows examples of the stress state of natural fractures at the point of in-situ reservoir pressure, breakdown pressure, treating pressure, maximum treating pressure, and net pressure. It is observed that certain natural fractures are surpassing the failure envelope and slipping in shear, in some cases even in the in-situ reservoir conditions.

In addition to the failure of fractures during stimulation, an important conclusion of this study is the recognition of critically-stressed fractures; fractures which are shearing in the in-situ

reservoir state with no added pressure. This is an important distinction from the Pouce Coupe study area. In Farrell Creek, the difference between the principal horizontal stresses is very large, and the magnitude of σ_{hmin} is also elevated. Because of the proximity of σ_{hmin} to the overburden stress, the likelihood of this stress overcoming the vertical stress is probable. If the overburden stress becomes the least stress, the overall stress regime becomes a reverse rather than strike-slip.

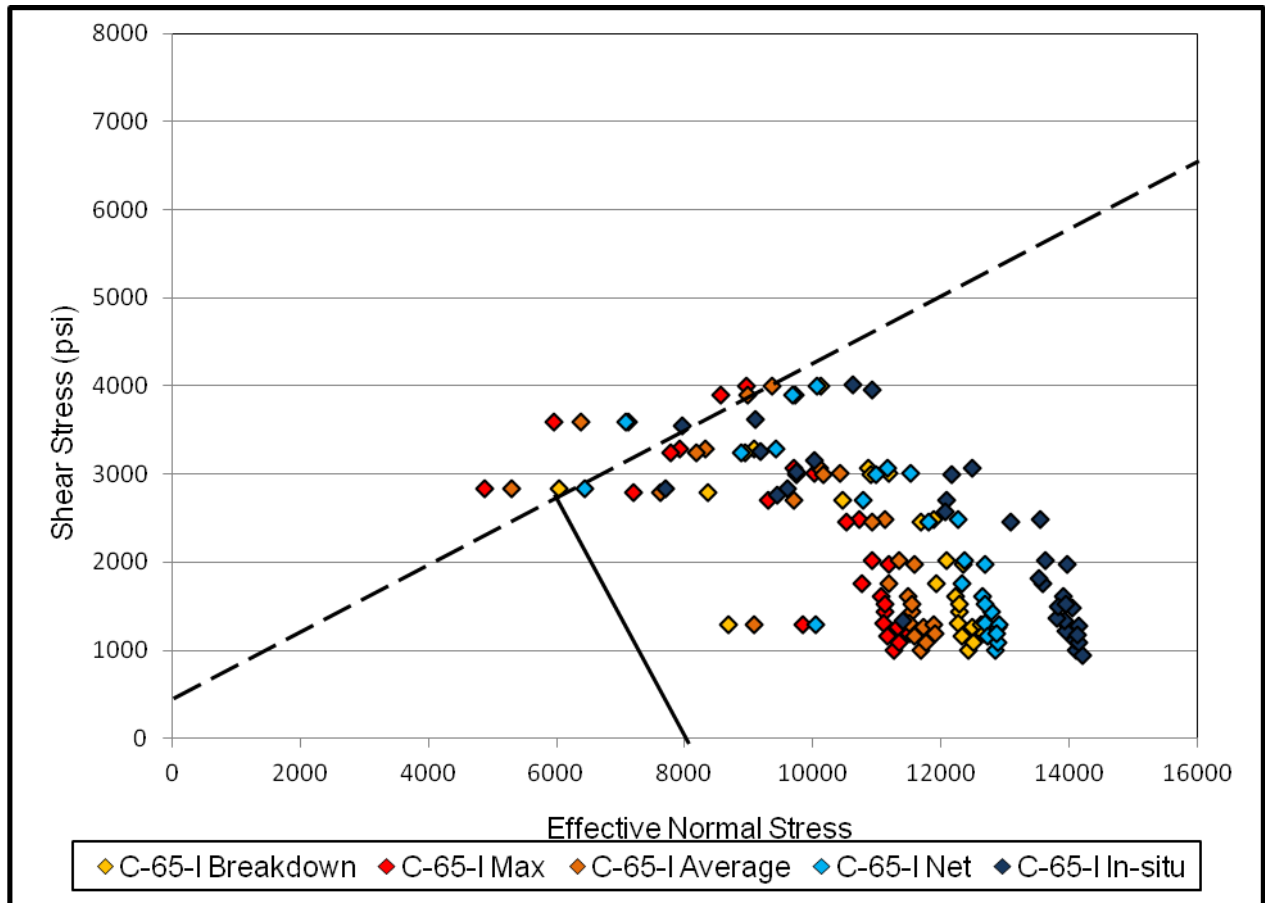


Figure 7.8- C-65-I Fracture failure progression. The original reservoir stress state on natural fractures is shown by the dark blue diamonds. Elevated pressures are shown by the yellow diamonds (breakdown pressure), orange diamonds (average treating pressure), red diamonds (maximum treating pressure), and light blue diamonds (net pressure).

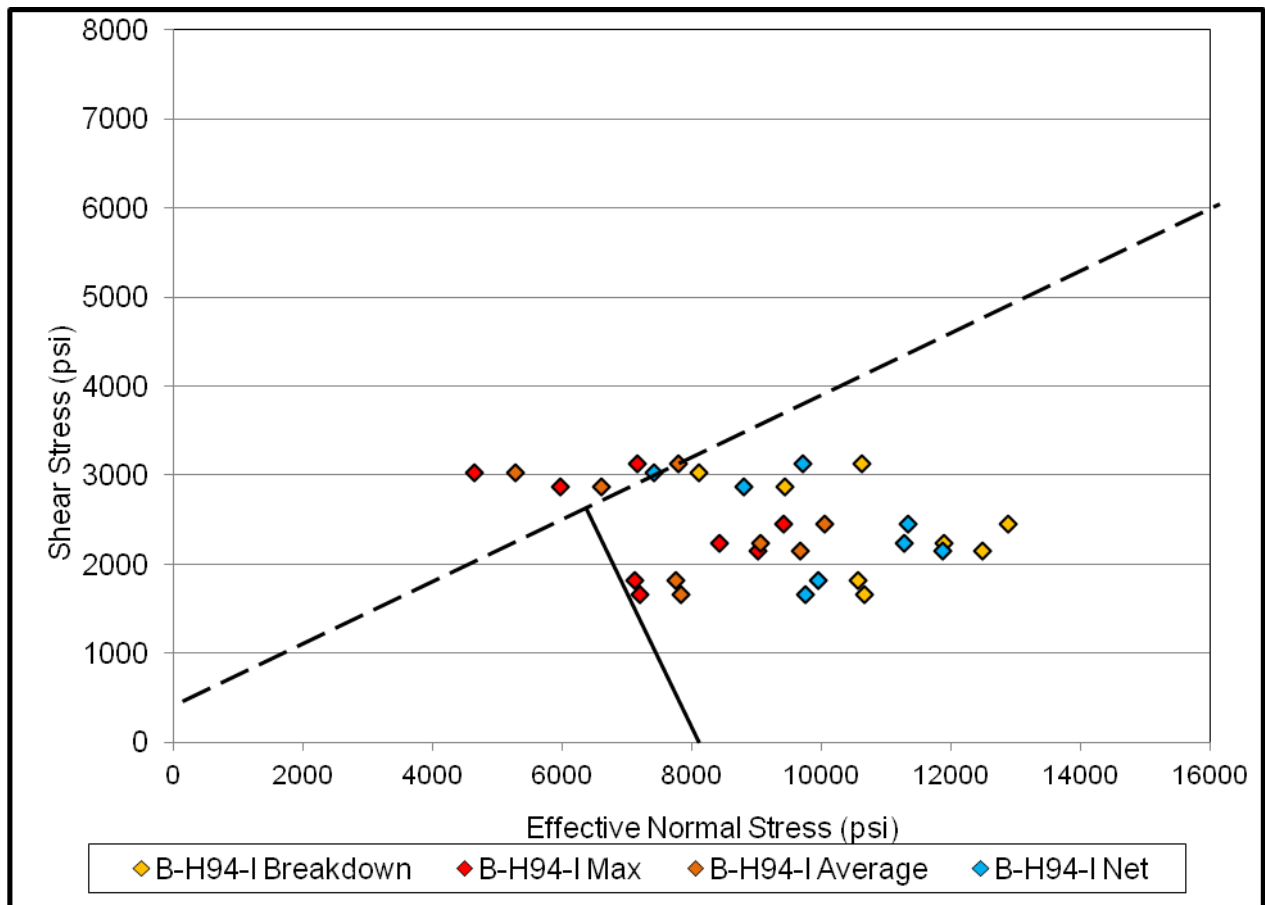


Figure 7.9 - B-H94-I Fracture failure progression. Elevated pressures are shown by the yellow diamonds (breakdown pressure), orange diamonds (average treating pressure), red diamonds (maximum treating pressure), and light blue diamonds (net pressure).

These observations are vital for defining possible fracture networks within the reservoir, and the pressures necessary to open and maintain a complex network. Furthermore, certain orientations of natural fractures may be more prone to failure and therefore better suited to stimulation than others. If it can be discerned what fracture orientations fail first in a given pressure regime, and ultimately relate these orientations to well production in the field, this provides us with a correlation between fracture orientation and the ultimate success of a well.

It was found that fractures failing first were those occurring in orientations roughly parallel to the direction of minimum horizontal stress (Figure 7.11). There are several possible reasons for this failure progression. Lajtai and Allison (1979) performed residual stress experiments in laboratory conditions, and observed that weaker planes of micro-fractures formed perpendicular to the principal stress direction. Fracturing associated with the orthogonal

orientation to σ_{Hmax} could be attributed to the unloading process. As a hydraulic stimulation ends, the reservoir closes on the proppant-filled hydraulic conduit, increasing the stresses oriented parallel to σ_{hmin} . Due to these increased stresses, any shear events along natural fracture planes oriented parallel are more likely. Therefore, critically-stressed fractures will likely develop in this orientation.

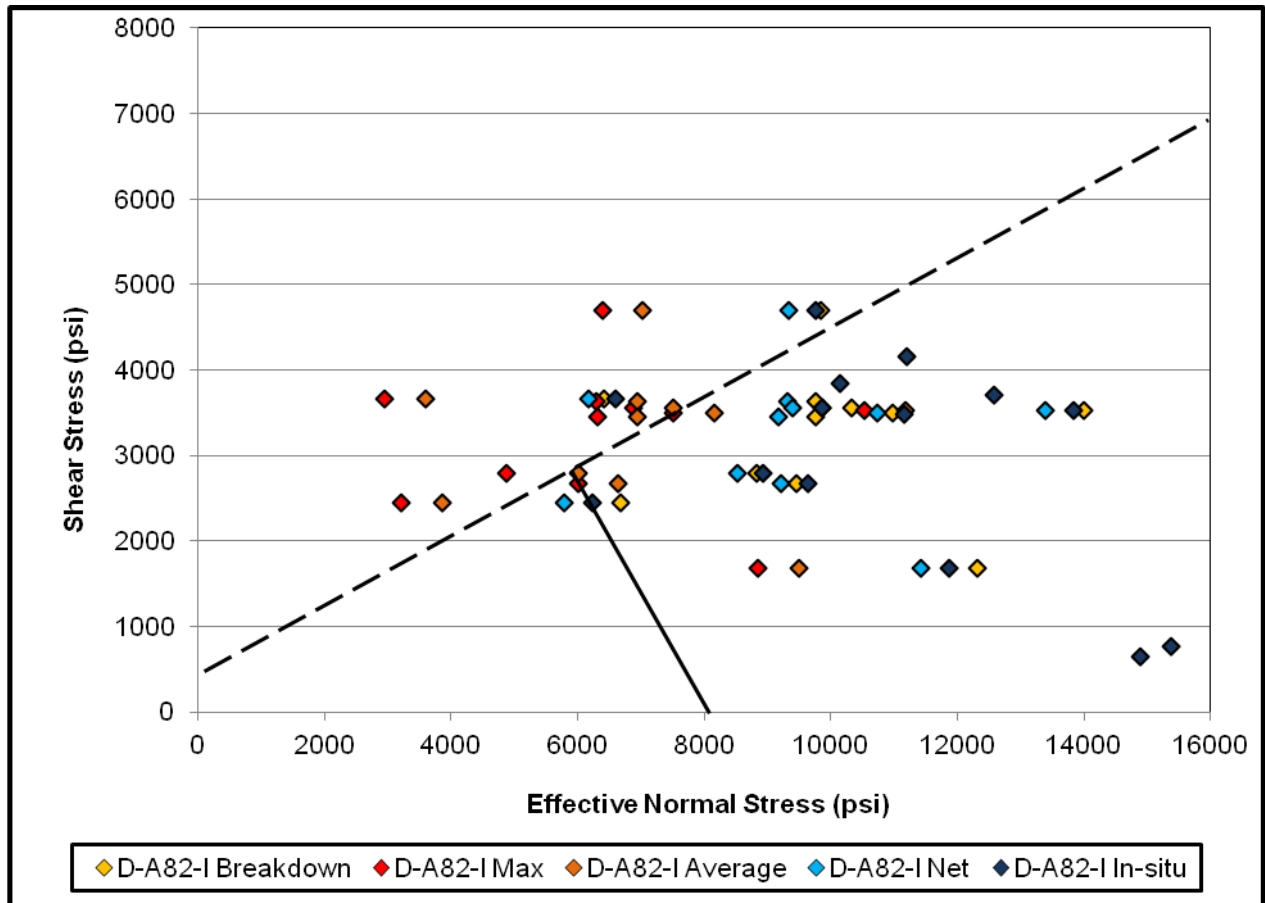


Figure 7.10 - D-A82-I Fracture failure progression. Elevated pressures are shown by the yellow diamonds (breakdown pressure), orange diamonds (average treating pressure), red diamonds (maximum treating pressure), and light blue diamonds (net pressure).

Given that a hydraulic fracture is expected to propagate parallel to the maximum horizontal stress direction, natural fracture failure and hydraulic fracture failure are occurring orthogonal to one another (Figure 7.12). This style of interaction is consistent with a model for microseismic events proposed by Maxwell et al (2011). Two end-member models; with the natural fracture either parallel or perpendicular to the hydraulic fracture, are presented, both

assuming that microseismic events are associated with a hydraulic fracture interacting with a natural fracture (Maxwell 2011).

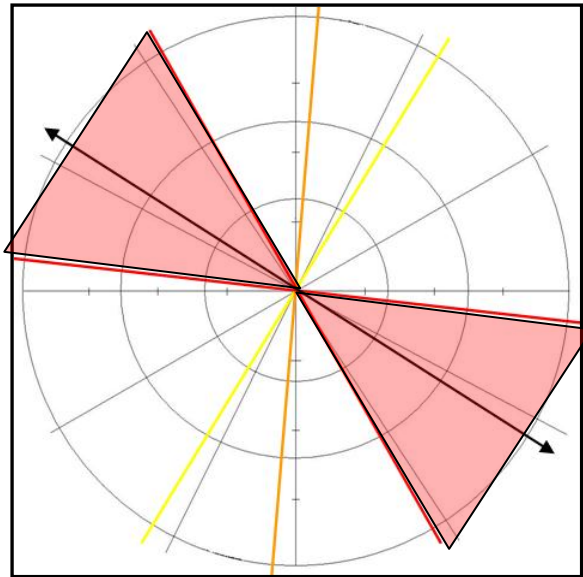


Figure 7.11- General orientation of fractures which are critically stressed in the Montney lie within the zone outlined in red.

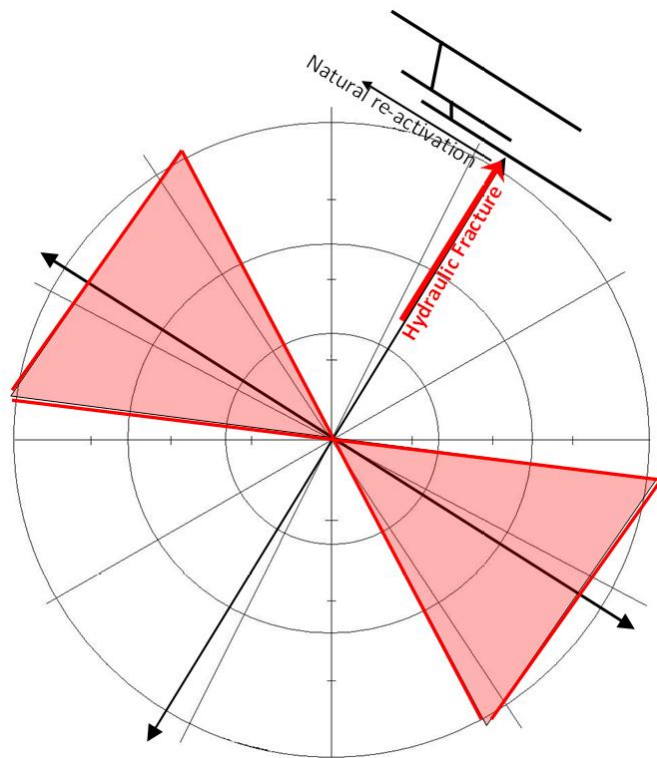


Figure 7.12- Orthogonal natural fracture (black lines) and hydraulic fracture (red arrow) interaction.

A model of interest in this case represents a natural fracture orientation perpendicular to the hydraulic fracture orientation. Because the two planes are orthogonal to one another, this style of fracture interaction has the capability of creating a complex network. Hydraulic fracture initiation into the reservoir can induce sufficient pressure perturbations to prompt shear movements along natural fracture faces. These shear events can continue following stimulation, as outlined above. During stimulation, microseisms would most probably occur at the edge of the deformation front where the hydraulic fracture tip meets natural fractures, and shear stresses are highest (Snedn 1946).

Once the hydraulic fracture reaches the natural fracture, fluid infiltration into the natural fracture results in pressurization, however dilation will be restricted due to fissure opening against maximum horizontal stress. Pressure build-up within the natural fracture will further increase, resulting in “stick-slip” microseismic events; repeated events with similar characteristics and locations (Raymer et al 2008). This pressure build-up provides the mechanism for microseismic activity behind the edge of the deformation front.

However, in low permeability reservoirs such as the Montney Shale, any events occurring behind the fracture tip will likely occur on or very near to the hydraulically active conduit, due to inherently low permeability (Agarwal et al 2012). Consequently, any microseismicity observed is likely to be the byproduct of the propagating hydraulic fracture (Cipolla et al 2011). Fluid leakoff into natural fractures, resulting in slip, dilation, and branching of the main hydraulic fracture, is less likely once the main extensional fracture has been opened and tip effects are the dominant method of fracture movement (Agarwal et al 2012). Once the stimulation ends, heightened stresses due to closure on proppant is another method for events behind the fracture tip. These theories are supported by the results of Chapter 6, where the propagating hydraulic fracture maintained a strong control on the location of natural fracture shear.

As orthogonally oriented natural fractures are expected fail first, higher production (due to greater reservoir reach through natural fractures) would be expected. Through production analysis of four wells with available 200 day production rates, it was confirmed that the highest production is associated with a greater percentage of orthogonal natural fractures.

As a final correlation tool, Diagnostic Fracture Injection Tests (DFITs) were used, providing ground-truth values of reservoir pressures. During a DFIT a small volume of water is pumped down the wellbore to determine leak-off type, pore pressure, permeability, and closure pressure (Mullen et al. 2010). The difference between the closure pressure from a DFIT and the instantaneous shut-in pressure (ISIP) is known as the Process Zone Stress (PZS). PZS provides insight into the nature of natural fractures in the reservoir. If the DFIT closure pressure is lower than the ISIP, it is likely that the stimulation reopened pre-existing places of weakness. If PZS is greater than 0.1 psi/ft, there is the possibility of causing multiple fractures at the tip or reducing the width of the hydraulic fracture (Mullen et al 2010).

The main reason for examining process zone stress, in the context of this thesis, is that the stress required to re-activate an existing weakness in a reservoir is equal to the closure stress, or deactivation stress on that mechanical weakness (Mullen et al 2010). Therefore PZS gives insight into whether or not multiple fractures are likely to propagate from the main hydraulic fracture.

As seen in the DFIT example of Figure 7.13, the type of fracture behavior observed in all five DFITs available is fracture height recession. Fracture height recession indicates that initially hydraulic fracture growth occurred out of zone, possibly as a system of transverse fractures into high-stress bounding layers (Barree & Associates 2012). These fractures are forced to close first with shut-in of the treatment, due to higher net pressure acting upon them. The closure of these fractures causes a decrease in treatment height and recession back into the zone of initial propagation. This phenomenon can be explained by returning to the behavior observed in both Chapter 5 and Chapter 6. In Chapter 5, we saw that the variability in Rock Quality Index (RQI) and mechanical stratigraphy is high within the Montney, to the extent the microseismic events preferentially occur in certain horizons and not others. The dominance of microseismic activity in facies Yellow 5A and Yellow 5 indicates the preferred location of the hydraulic stimulation here. Hydraulic fracture propagation into the overlying high stress Blue 5 zone and subsequent recession could be the reason for the height recession behavior observed. In addition, as mentioned in Chapter 4, the stress regime is strongly anisotropic in Farrell Creek, and σ_{hmin} is very close in magnitude to that of the overburden stress. In addition to Terzhagi's effective stress equation described in equations 7.3- 7.4, there is an additional stress relationship which becomes very important when considering stimulation effects in the reservoir. This equation describes the pore pressure-stress coupling effect through the equation:

$$\Delta\sigma_3=2/3\Delta PP$$

(7.5)

This equation tells us that as pore pressure increases during a hydraulic stimulation, minimum horizontal stress also increases at a rate equal to 2/3 the rate of the pore pressure. When we consider the proximity in magnitude of the minimum horizontal stress and the overburden stress, it would not take a large increase in pressure to cause σ_{hmin} to overcome the overburden. If this occurs, so called “pancake fractures” will occur, meaning energy will propagate laterally but not vertically in the reservoir. This occurs because the overburden is now the least stress and is literally “lifted” by the horizontal stresses, allowing abundant lateral movement of pressure and energy. A pancake fracture stimulation could contribute to the height recession behavior observed here.

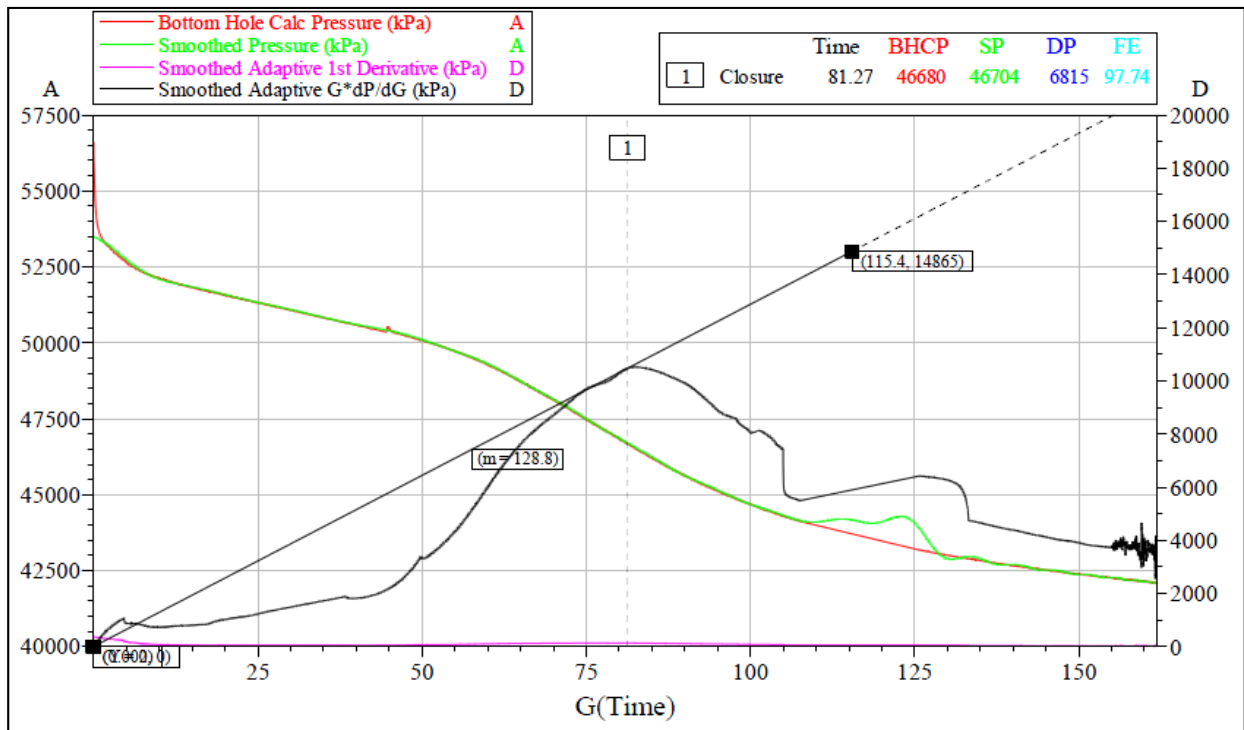


Figure 7.13 - DFIT Fracture height recession example. G (time) is plotted on the x-axis, pressure is plotted on the y-axis.

CHAPTER 8

UPSCALING TO SEISMIC

When considering the comparison of a wellbore to a seismic survey, the discrepancy in scale is large. Measurements of rock properties from point in a reservoir, and measurements of rock properties averaged over large portions of the reservoir, can hardly be considered comparable. Fortunately, there are aspects of a shale reservoir which are well suited to correlation at these widely differing scales. As stated throughout this thesis, natural fractures are of paramount importance to the overall success of the reservoir. They have been examined at the two scales thus far; firstly at the borehole through image log identification and Mohr Coulomb failure analysis. This borehole scale examination was also related to the formation Rock Quality Index (RQI).

Secondly, fractures were examined at the field scale correlating microseismic events to the Rock Quality Index and expected failure of fractures. G-function analysis was used to further confirm the results from an engineering perspective. From here, the next logical step would be to examine natural fractures at the seismic scale. While no single tool has the ability to detect the distribution of natural fractures at the seismic scale, we attempt here to relate the failure patterns seen in microseismic and image logs to the failure inferred from shear wave velocity anisotropy (SWVA), examined through a time-lapse multicomponent seismic survey.

Shear wave velocity anisotropy (SWVA) analysis capitalizes on the fact that shear waves are highly sensitive to open fractures (Steinhoff 2012). When encountering an open fracture set, an incident shear wave will split into a fast (PS1) and slow (PS2) component, aligned parallel and perpendicular to fractures respectively. The earliest arrivals within sinusoidal events correspond to the PS1 (fast) direction, and later arrivals correspond to the PS2 (slow) direction (Steinhoff 2012). These time delays can be used to understand the degree of fracturing present. A more in-depth analysis of fracture orientations and seismic polarization directions can be done through shear wave splitting anisotropy (SWSA) analysis. In addition to the minimum and maximum arrival times of the sinusoidal events, the polarization directions of the fast and slow shear waves can be determined (Steinhoff 2012). Using this method, the location and orientation of natural fractures can be inferred. For an in-depth analysis of the SWVA/SWSA methods and processing, see Steinhoff 2012.

The seismic methods outlined above, while unable to directly examine fracture failure, provide insight into the tectonic history of the reservoir, as well as a broader scale perspective on fracture geometry. Geomechanical modeling utilizes fundamental scientific principles to theorize the past history and expected future behavior of natural fractures. By using the strengths of both scientific techniques, we hope to examine natural fractures within the framework of the seismic scale analysis. The correlations presented here utilize the orientation of anisotropy in the baseline survey, thus correlating to the SWSA (shear wave splitting anisotropy) analysis. Comparisons to the monitor surveys examine the degree of anisotropy present, not the orientation, and therefore will be referred to as SWVA (shear wave velocity anisotropy) anomalies.

N.J. Price first described and modeled the method of relating brittle failure to faults and natural fractures in 1966. Unlike sedimentary facies and their corresponding depositional environments, rock failure is not directly observable as it occurs in the subsurface (Billingsley et al 2006). The range of mechanical variation in real world subsurface geological environments is numerous, as is their progression through time. These two factors must both be simulated accurately. In the geomechanical realm, measured rock properties and a generated system of equations are used to project the behavior of rock under subsurface conditions (Billingsley et al 2006). However, these experiments occur over a much shorter duration than geologic time, and projecting these relationships into the past is inaccurate and does not mimic this second condition; temporal variation, accurately. To compensate for the inability of geomechanical experiments to observe rock failure temporally, seismic time-lapse analysis is utilized to determine how the reservoir changes. Shear fractures in brittle reservoirs often develop at depth, around mapped discontinuities where mean and differential stresses associated with displacement are high. Their occurrence would be higher where rocks have been previously disrupted by folding and faulting (Billingsley et al 2006).

A time-lapse multicomponent seismic survey was shot over a two section area in Pouce Coupe before and during stimulation of the Montney C and D units. The operational timeline is outlined in Figure 8.1 and Table 8.1. Seismic data consists of a baseline survey, occurring after the drilling of two horizontal NW-SE oriented wells (02/02-07-78-10W6 and 02/07-07-78-10W6) and two monitoring surveys, occurring after stimulation of these two horizontal wells.

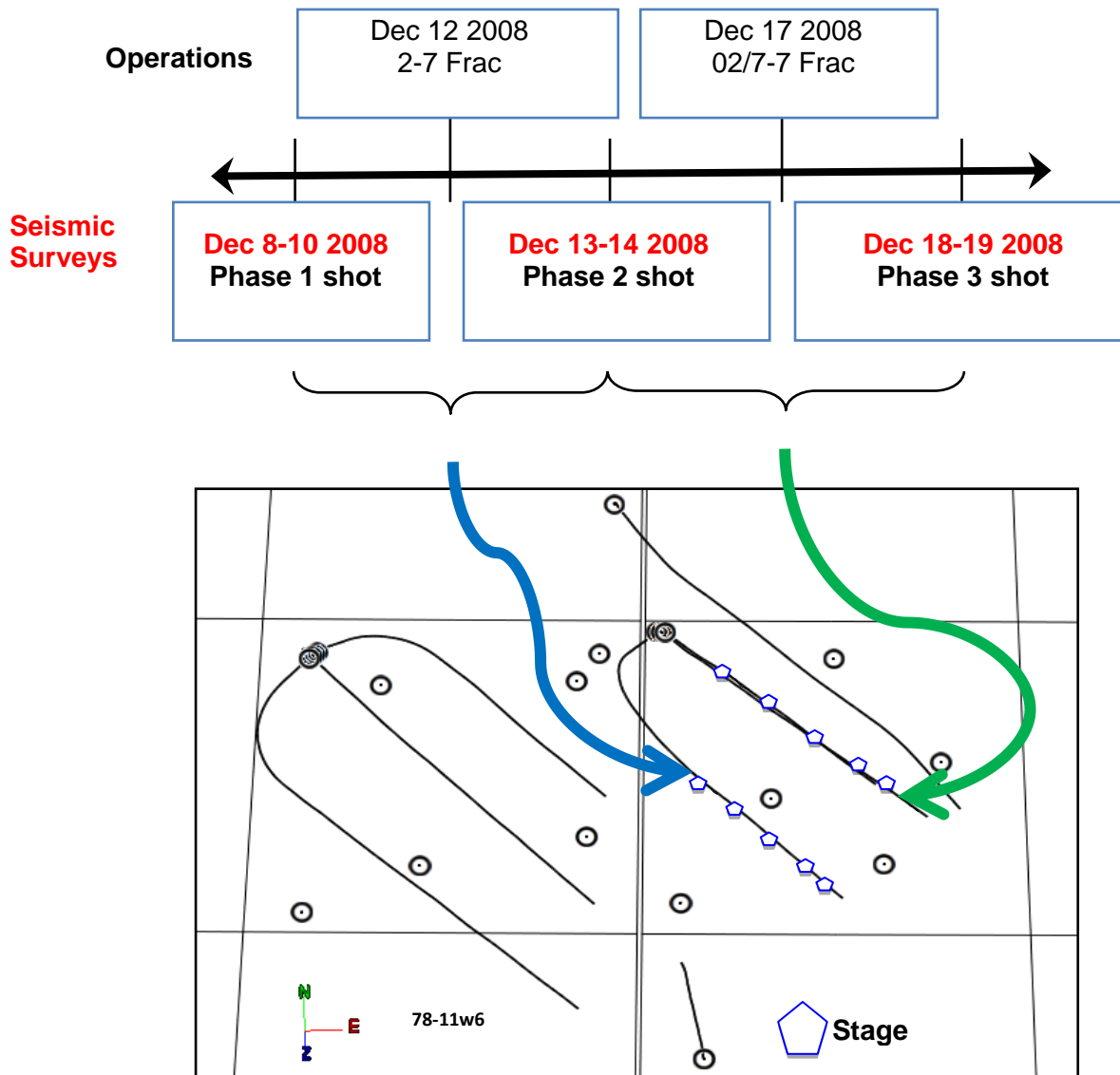


Figure 8.1 - Map view of wells and timeline for multicomponent seismic survey. The baseline survey was shot before stimulation; Monitor 1 and 2 are shot following stimulation of the 02-07 well and the 07-07 well respectively.

Table 8.1- Timeline of completions and production in the area of the seismic survey.

DATE	ITEM
February 5th, 2008	100/07-07 Minifrac
February 10th, 2008	100/07-07 Completion
December 12th, 2008	102/02-07 MNTN C Completion
December 17th, 2008	102/07-07 MNTN D Completion
Dec. 26 2008-Jan.26 2009	100/07-07 Production Report
January 9th. 2009	08-07 Completion (stages 3,4,5,6)

As stimulation occurs in the reservoir, the propagating hydraulic fracture creates stress and pressure changes, leading to failure of proximal critically-stressed fractures. Pressure variation due to dilation of the induced hydraulic fracture and shear of natural fractures will be manifested as azimuthally dependent shear strength properties; meaning shear velocities polarized parallel to fracture planes will differ from those polarized perpendicular to the fracture interface (Steinhoff 2012). Through the use of SWVA analysis, the incident shear wave can be separated into a PS1 and PS2 component, thus providing insight into the orientation and abundance of induced azimuthal anisotropy.

SWVA/SWSA analysis was conducted on all three phases of the Pouce Coupe project (Steinhoff 2012). Layer stripping was utilized to remove any shear-wave splitting effects from the overburden layers. Any shear wave energy reflected from within the zone of interest must subsequently pass through the layers above, and thus arrives at the receivers encoded with the cumulative propagation effects from the overlying layers (Steinhoff 2012).

To relate the results of the borehole scale geomechanical results with the seismic scale shear wave anisotropy results, the first step was to understand relationships at the initial reservoir conditions. As shown in Chapter 7, there are two dominant orientations of natural fractures in the reservoir, one oriented parallel to σ_{Hmax} and one perpendicular. Based on the PS1 orientations determined by the layer stripping analysis, it is observed that these two orientations vary over the length of the horizontal wellbores, as expected (Steinhoff 2012). These two orientations are apparent throughout the stimulation treatment, as seen in the Monitor 1 and Monitor 2 surveys of Figure 8.2.

The next relationship to observe was that between the Rock Quality Index (RQI) and baseline azimuthal anisotropy. Figure 8.3 shows the baseline SWVA plotted beside the modified Rock Quality Index (RQI) for the northern well (02/07-07-78-10W6), as determined by the methods outlined in Chapter 5. All subsequent comparisons with Rock Quality Index (RQI) refer to this well. A good correlation is observed between areas of high Rock Quality Index (RQI) and high azimuthal anisotropy. There are two reasons for this correlation. Firstly, as seen by the results of Chapter 6, zones of high Rock Quality Index (RQI) are not only relatively more brittle but often more heterogeneous. It is likely that the azimuthal anisotropy observed is reflective of a heightened stress state due to high internal heterogeneity, and possibly increased natural fracturing associated with more brittle rock. Secondly, the modified Rock Quality Index (RQI)

definition will be higher where the stress differential ($\sigma_v - \sigma_{hmin}$) is larger. Therefore, those areas of high Rock Quality Index (RQI) are reflective of a lower σ_{hmin} , and possibly a larger stress differential. Zones of high Rock Quality Index (RQI) would be reflected by a higher anisotropy signature.

Figure 8.2 also displays a linear anomaly (3-5%) at the toe of the southern well (02/02-07-78-10W6), associated with a wrench fault trending parallel to the present day regional σ_{Hmax} (Steinhoff 2012). The dominant orientation of SWSA anomalies at the central and heelward fracture stages have values between 4-7% and are associated with fractures oriented parallel to σ_{hmin} , providing evidence that there are more natural fractures parallel to σ_{hmin} in these areas. Given the fracture failure analysis of Chapter 7, it is expected that these areas with more abundant sub-parallel σ_{hmin} fractures will show a more complex network during stimulation.

After examining the baseline SWSA results, Monitor 1 and Monitor 2 SWVA results were correlated to the borehole scale conclusions. A lack of image logs in the Pouce Coupe Field requires borehole-scale conclusions to be inferred from the Farrell Creek analysis. In the Monitor 1 survey, which occurred following the fracture treatment of the southern well (02/02-07-78-10W6), the azimuthal anisotropy signature changes not only at the wellbore which was stimulated but also at the northern wellbore (02/07-07-78-10W6). At the time of Monitor 1 this well was unstimulated and therefore the change in azimuthal anisotropy indicates pressure perturbations are large enough from the neighboring wellbore to induce stress and/or fracture changes here.

Following the initial examination the Rock Quality Index (RQI) index in conjunction with Monitor 1 (Figure 8.4), Monitor 2 (Figure 8.5) was examined in detail. Monitor 2 occurred after the stimulation of both the northern and southern wells, and in this case an increase in the same azimuthal anisotropy signature as seen in Monitor 1 is evident. As mentioned previously, greater azimuthal anisotropy at the central and heelward portions of the southern well is associated with fractures aligned with σ_{hmin} . It is assumed that this association is consistent across the 4D study area, meaning that zones of heightened azimuthal anisotropy at the northern well are also associated with σ_{hmin} -aligned fractures. As seen in Figure 8.3, high azimuthal anisotropy generally corresponds to high Rock Quality Index (RQI). The particularly high Rock Quality

Index (RQI) at the end of the well is believed to be associated with a known fault, oriented approximately perpendicular to the wellbore (Steinhoff 2012).

High azimuthal anisotropy (and generally corresponding high RQI) shows a change with progression of the stimulation. There are two elements that account for this scenario; both fractures and stress. Firstly, according to the image log analysis at Farrell Creek, σ_{hmin} -oriented fractures are more likely to fail with induced pressure changes. Therefore, zones of initially higher azimuthal anisotropy (and corresponding higher RQI) should show a decrease in azimuthal anisotropy with the introduction of a hydraulic fracture. Because the hydraulic fracture and pre-existing natural fractures are orthogonal to one another, the presence of both in the reservoir will equalize the anisotropic signature. This equalized effect is seen in Figures 8.3, 8.4, and 8.5, where in the baseline SWVA (Figure 8.3) areas of high anisotropy (and high RQI) become less anisotropic in Monitor 1 and 2. Additionally, it appears that those areas now having higher anisotropy are coincident with more homogenous RQI portions of the reservoir.

Induced anisotropy; reflective of the activation of natural fractures and/or stress changes associated with a hydraulic fracture, is higher where reservoir homogeneity allows for easier propagation of the hydraulic fracture. As seen in the microseismic analysis from Farrell Creek, microseisms seem to be most prolific in more homogenous reservoir areas; zones in which less stress heterogeneity makes propagation of a hydraulic fracture easier and therefore proximal shear on natural fractures more likely. Homogenous zones along the 02/07-07-8-10W6 wellbore were determined by overlaying a zero-variation Rock Quality Index line (red lines in Figure 8.6) and highlighting zones with greater deviation from the straight line. Identified homogenous zones are outlined in Figure 8.4 and 8.5. It appears that the same correlation holds true here; once the hydraulic fracture commences in the homogenous area, shear failure on natural fractures is likely to occur proximal to, but not distant from the induced pressure site.

Proximal shear failure to the hydraulic fracture is not observed in all cases, which leads to the second influence, stress factors. It is apparent in Monitor 1 that there is a high azimuthal anisotropy anomaly around Stage 4 of the southern well (Figure 8.2). Stress shadowing theory states that as stimulation occurs in a reservoir, reservoir pressurization is an additive effect. Depending on the lithology and initial stresses, there is a threshold pressure at which the stress contrast generated by the propped-open fracture exceeds the in-situ stress contrast, thereby creating a localized zone of stress reversal. It is possible that at stage 4 this threshold pressure

has been reached and widespread failure of the previously defined σ_{hmin} -parallel fractures occurred. The presence of stronger azimuthal anisotropy here also indicates that proppant must be present at some level in these fractures, as they are remaining open for some time following stimulation.

Stress shadowing is also evident in the microseismic (Figure 8.7). More events are observed in the first three stages of the 07-07 stimulation, and these events are more dispersed spatially. It is likely that as observed in Farrell Creek, reservoir pressurization occurs additively beginning at stage 1, and in this case by the time stage 3 is reached hydraulic energy dissipation occurs. This energy dissipation likely corresponds to the zone of high Rock Quality Index (RQI- and inferred high brittleness/fracturing) near the stage 3 perforation.

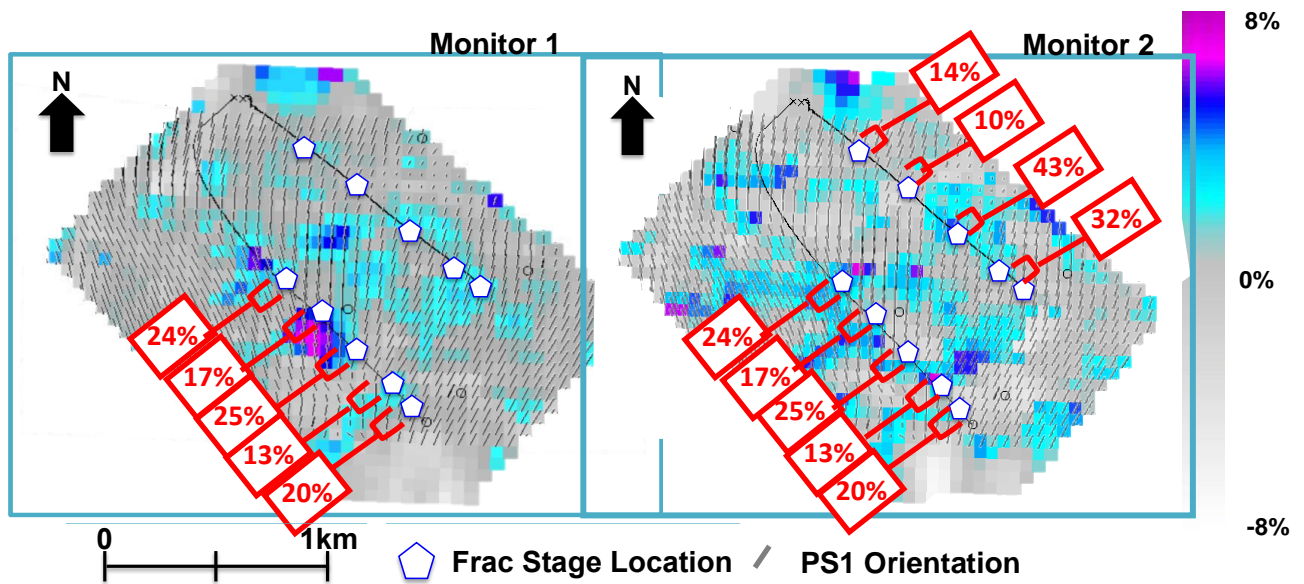


Figure 8.2 - SWVA/SWSA in Monitor 1 & 2 of the time lapse survey (Steinhoff 2012). Anisotropy is displayed on a scale from -8-8% anisotropy, and the PS1 orientation is shown by the dark grey lines. Spinner gas flow rates for each perforation are shown in percent flow for that wellbore.

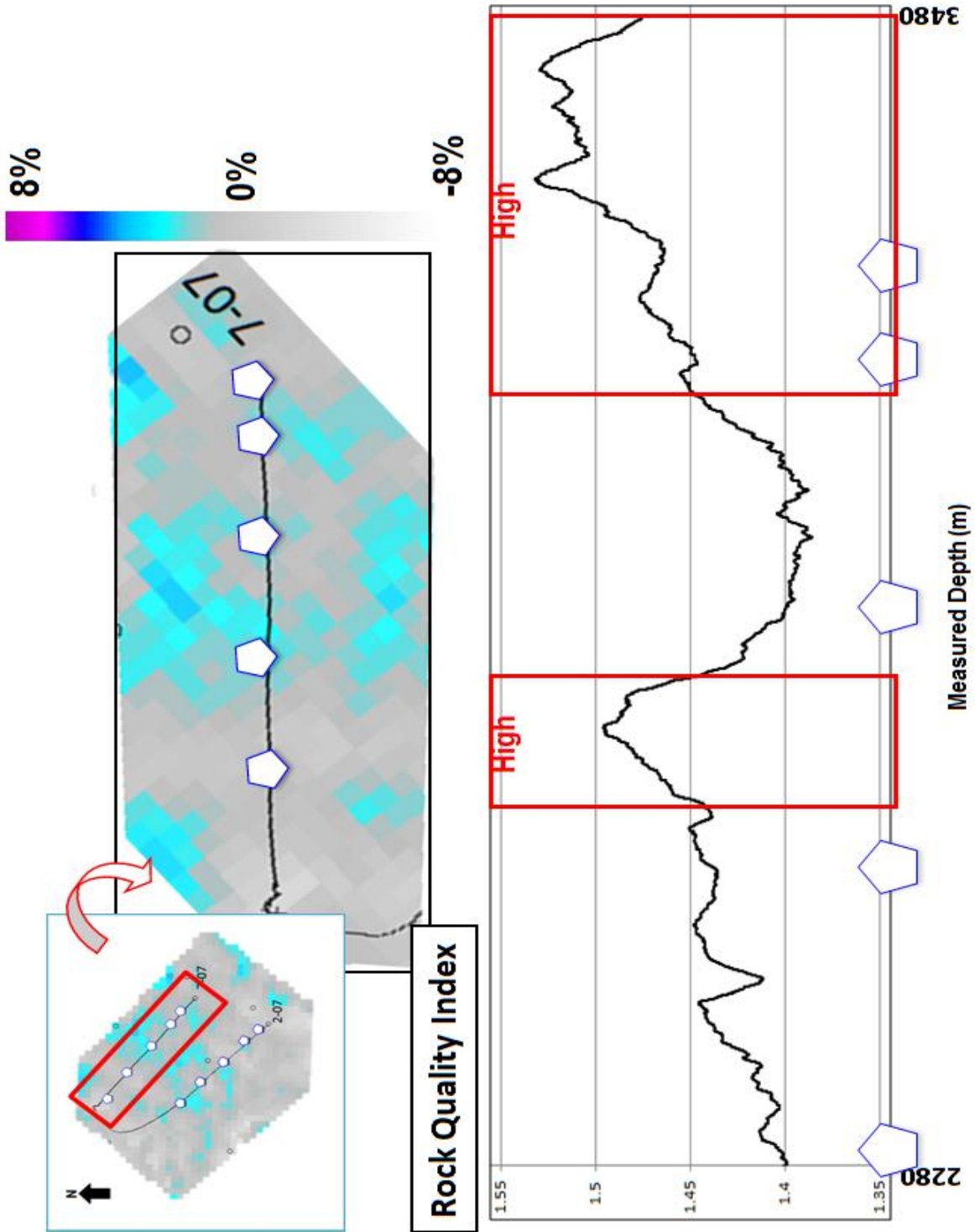


Figure 8.3 - Baseline SWVA correlated with Rock Quality Index (RQI). Initially high Rock Quality Index (RQI) corresponds to areas of elevated baseline anisotropy, indicating a correlation between initially brittle rock and a greater degree of natural fracturing on the seismic scale.

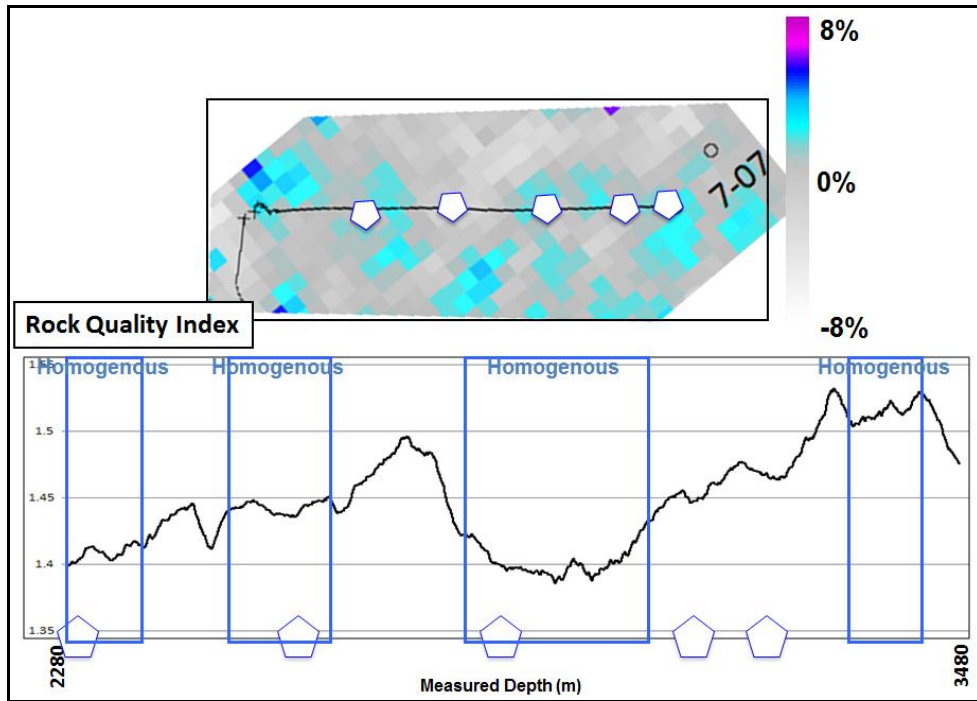


Figure 8.4 - Monitor 1- Baseline anisotropy correlated with Rock Quality Index (RQI). As hypothesized in earlier analysis, hydraulic energy will preferentially propagate to more homogenous areas of the reservoir. Monitor 1 comparison shows induced anisotropy correlating to more homogenous areas of the Rock Quality Index (RQI) curve, as expected.

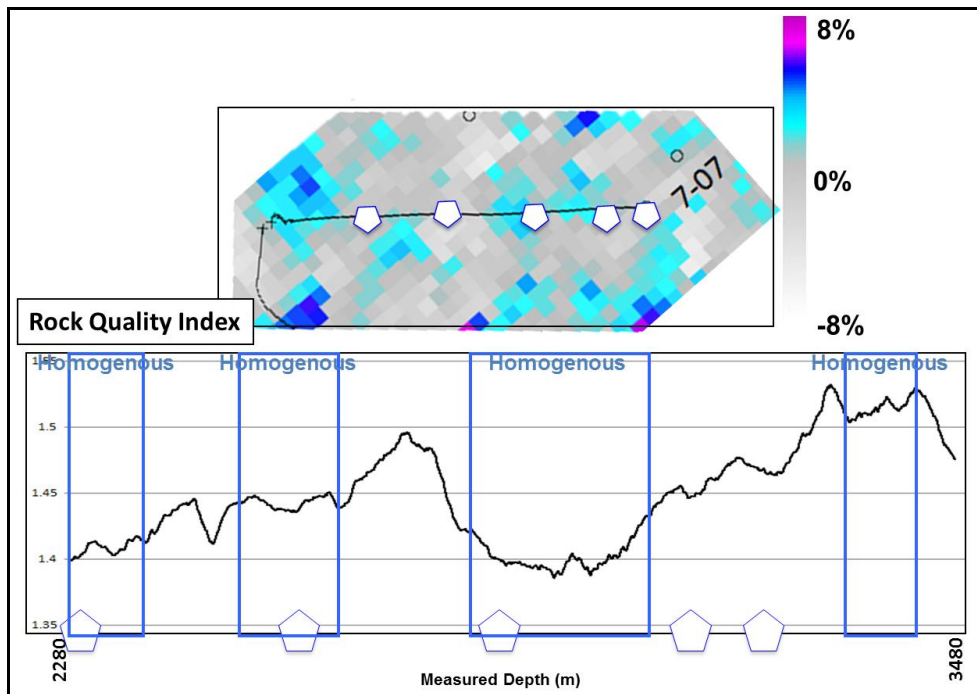


Figure 8.5 - Monitor 2- Baseline anisotropy correlated with Rock Quality Index (RQI).

Rock Quality Index

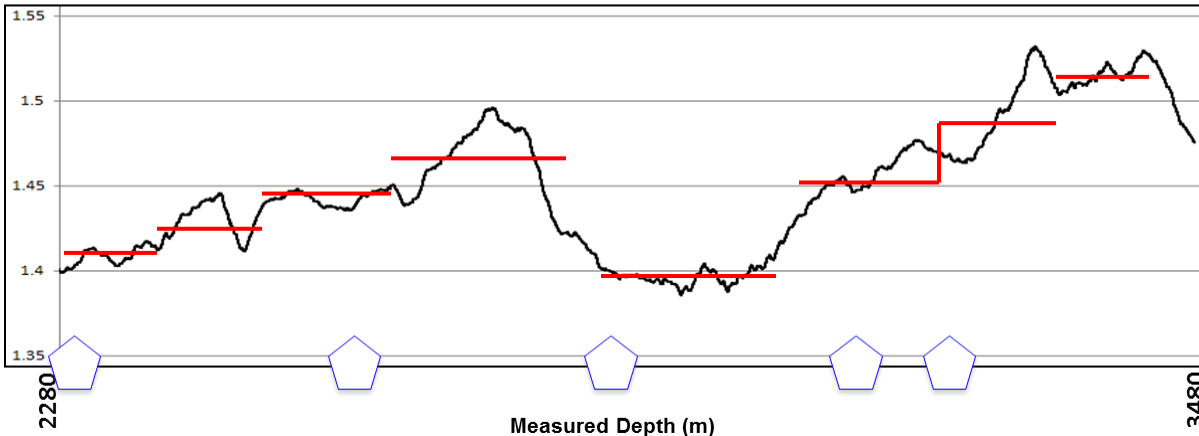


Figure 8.6 - Determination of homogenous zones, performed by overlaying a line of zero-variation Rock Quality Index and observing where the curve deviated from this straight line.

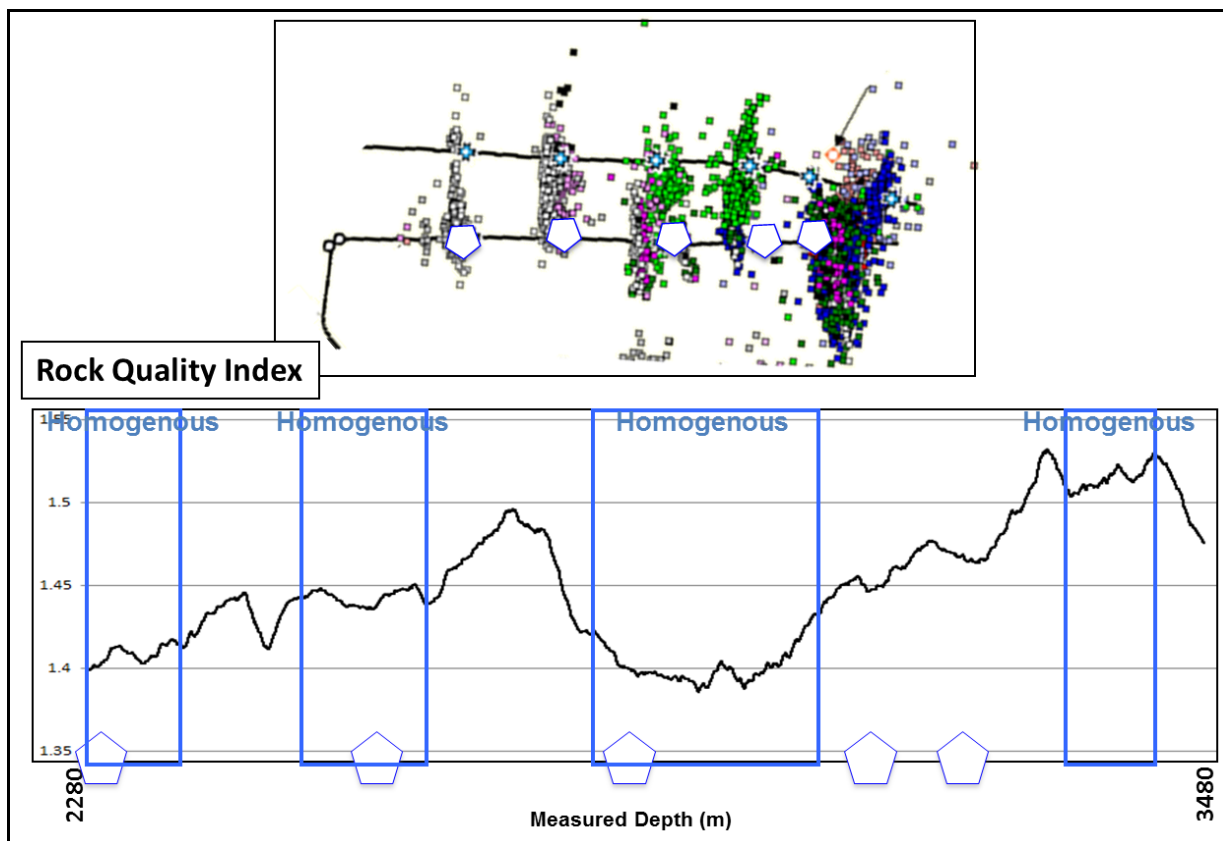


Figure 8.7 - Microseismic results correlated to Rock Quality Index (RQI). More prolific microseismic is observed in the first three stages and energy dissipation at the third stage results in a more planar geometry and fewer events in stage 4 and 5.

CHAPTER 9

INTEGRATION OF RESULTS

A final correlation between Chapters 5, 6, 7, and 8 is undertaken in Chapter 9 to understand the relationship of all results. Figure 9.1 shows the relationship between the Rock Quality Index (RQI), the mechanical stratigraphy, and the abundance of high-graded microseismic events for well C-085-I/094-B-01 in the Farrell Creek area.

It is apparent based on the microseismic event count that there is a strong control on the presence of shear events in the reservoir. This observation is consistent with the interpretation of DFIT data in section 7.6, where fracture height recession is the dominant behavior observed. Both datasets point to a predominant mechanical stratigraphic control on hydraulic fracture propagation in the reservoir. Microseismic events occur primarily in the Yellow 5A and Yellow 5 facies, and induced shear events occur very close to this zone. Induced shear events are likely to occur along fractures oriented orthogonally to the hydraulic fracture, as shown in Chapter 7, resulting in multiplet microseismicity and a further concentration of microseismicity in and around these facies (Raymer et al 2008). This hydraulic energy concentration again manifested as fracture height recession seen in the DFIT analysis. Low reservoir permeability, as well as high stresses parallel to σ_{hmin} following stimulation, aid in the microseismic activity proximal to the hydraulic fracture.

As outlined in Chapter 7, higher production is believed to result from the failure of the orthogonal natural fractures linking to the hydraulic fracture. In the microseismic data, it was observed that once a hydraulic fracture is initiated in a certain zone, activation of shear events occurs proximal to this zone, due to pressure perturbations and low permeability (Agarwal et al. 2012). According to the mechanical stratigraphy of Figure 5.1, the two zones surrounding the prolific microseismic are both relatively brittle compared to the yellow zones; being the Blue 5 and Blue 4 facies. Therefore, shear failure of natural fractures is likely probable in these zones where the induced pressure from the stimulation is highest.

To return to the special case of the Blue 5 facies, this zone is not only relatively brittle, but also relatively homogenous in terms of Rock Quality Index (RQI). On top of this, an important element which was discussed in Chapter 8 is stress shadowing effects. As fluid and

proppant is introduced through perforations, shown by the pentagons in Figure 9.2 and 9.3, reservoir pressurization occurs as an additive effect. By the time the third stage occurs, located in the Blue 5 facies (Figure 9.2), pore pressure increases may be sufficient to shift the stress state to a reverse regime. With this stress shift, the likelihood of pancake fractures is high, as discussed in section 7.6. As the overburden stress is lifted, in conjunction with the abundant laminated character of the Blue 5 facies, widespread failure along laminations and the creation of a widespread fracture network is probable.

Conceptually, then, it can be concluded that the brittle zones surrounding the zone of hydraulic fracture propagation will be the zones of prolific fracture networks. Spinner gas results are shown in Figure 9.2 and 9.3 for the well C-085-I/094-B-01. Highest production (45%) occurs from the perforation placed in the Blue 5 facies, which as discussed is a zone of high brittleness, homogenous Rock Quality Index (RQI), and a likely candidate for widespread failure due to stress shifts. This facies also acts as a barrier to further propagation upwards because of widespread energy dissipation in this layer. Moderately high production is also seen in the two perforations placed in the Yellow 8 facies. In this case, while distance from the propagating hydraulic fracture is large, the presence of abundant steeply-dipping natural fractures appears to compensate for the lesser pressure effects (Figure 9.4).

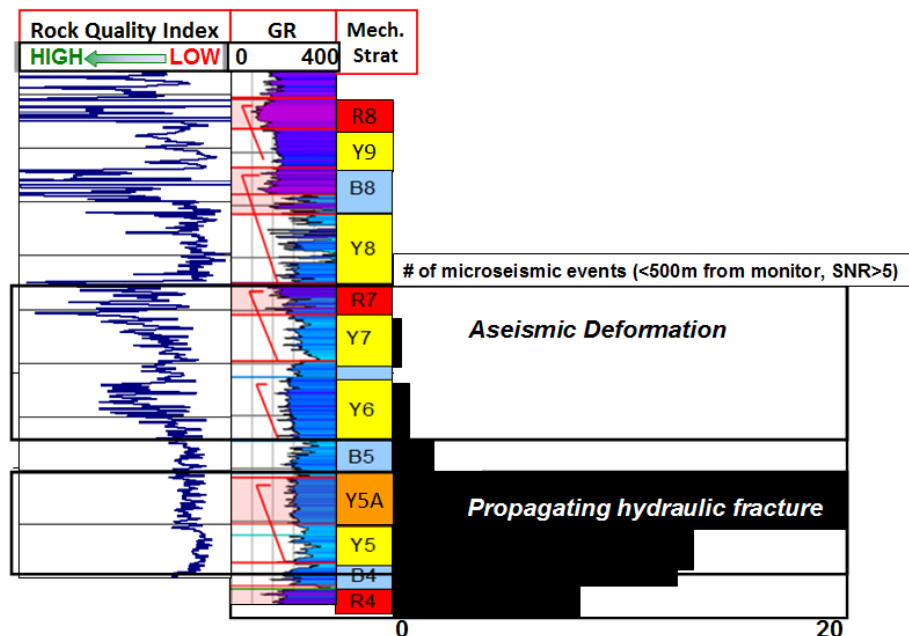


Figure 9.1 - Rock Quality Index (RQI), mechanical stratigraphy, and microseismic event abundance. In the Yellow 5A and Yellow 5 facies high event counts are observed, correlating with the lowermost homogenous zone in the Rock Quality Index (RQI) log.

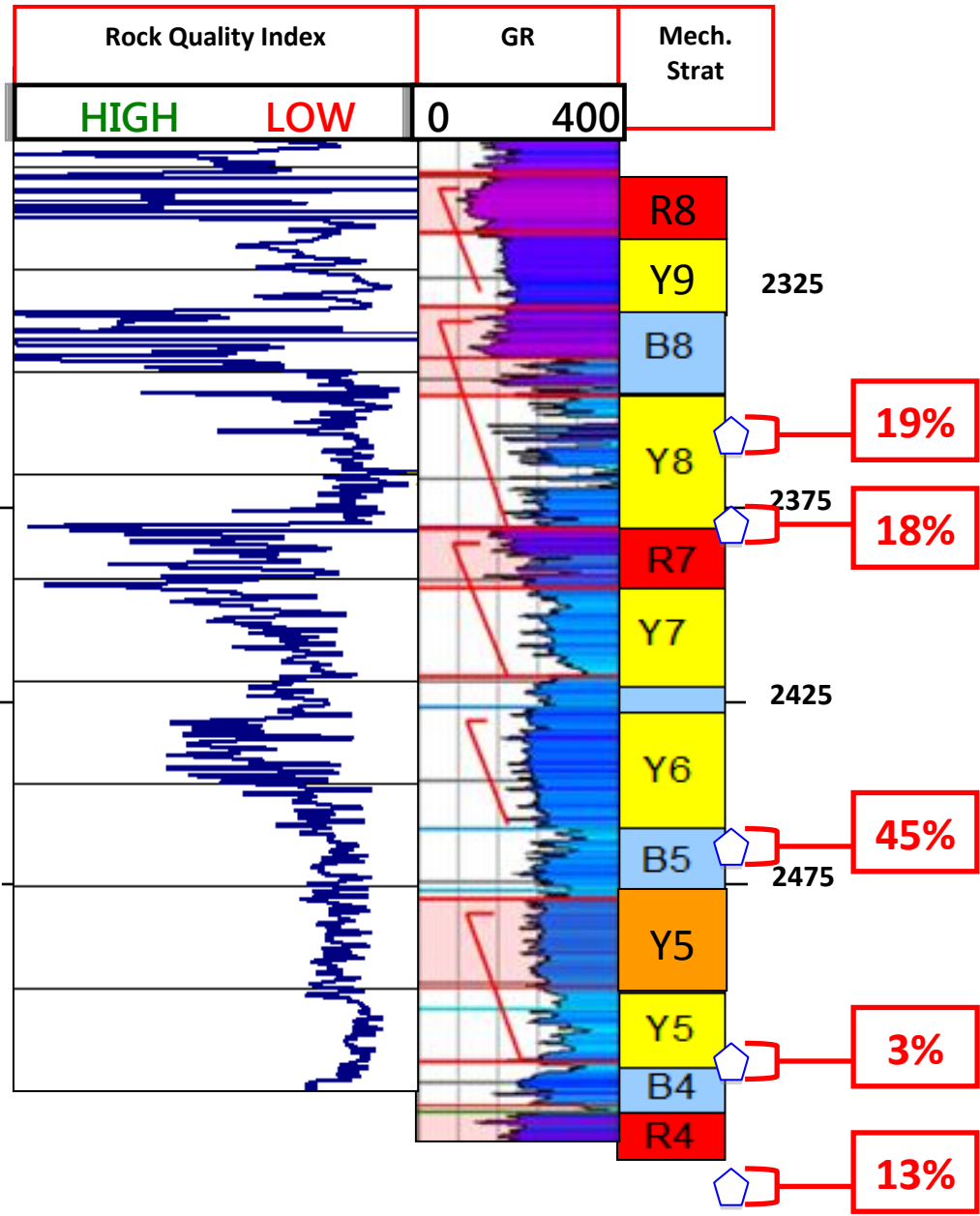


Figure 9.2- Rock Quality Index (RQI), mechanical stratigraphy, and spinner-derived gas flow. Gas flow is greatest where the zone of homogenous RQI (in terms of stress and brittleness as defined earlier) meets an interface with a highly laminated Blue facies. Homogenous Rock Quality Index (RQI) allows for growth and propagation of hydraulic energy, and this energy can then be dissipated along layers and fractures in the laminated zone, creating a large reservoir reach and higher production here.

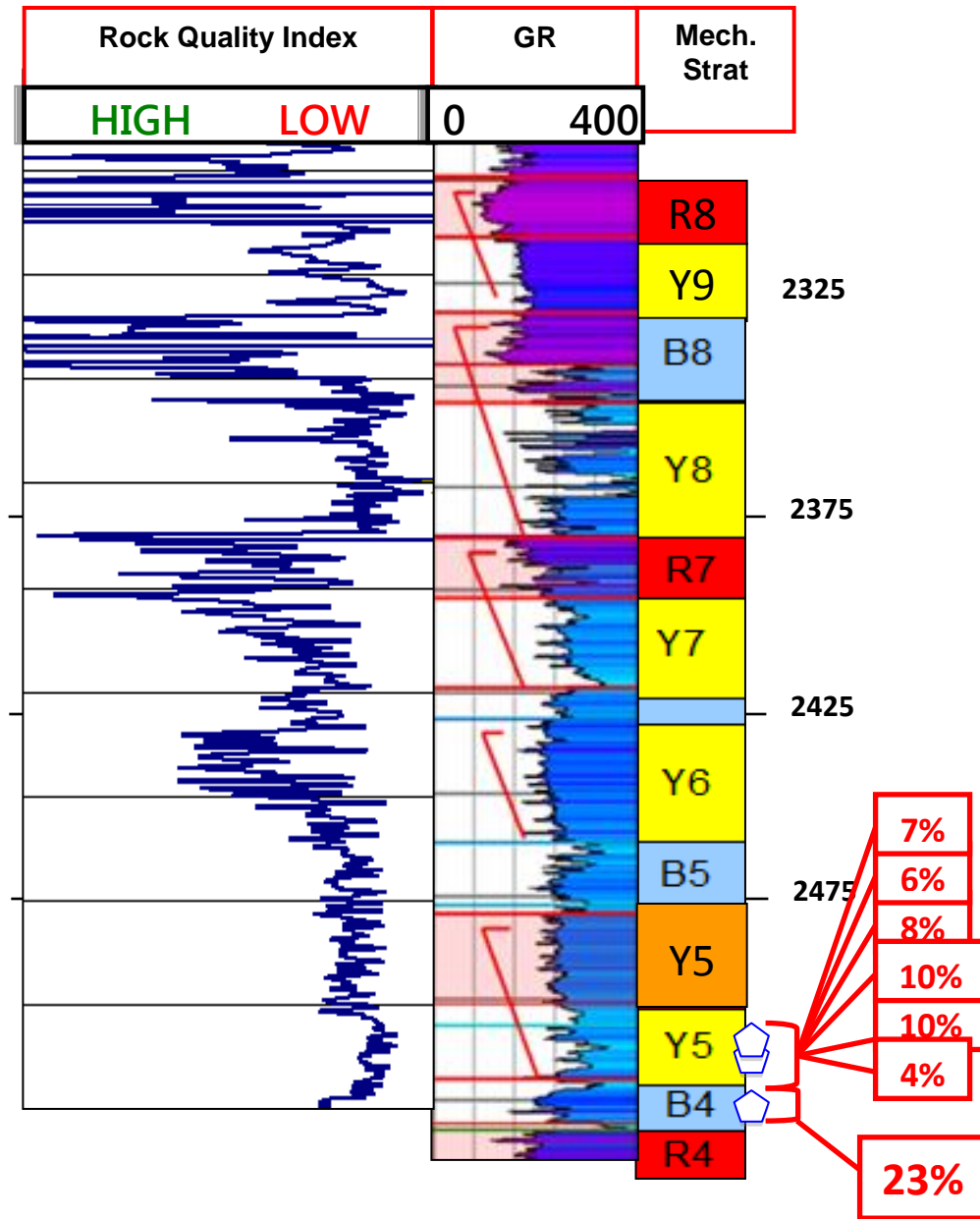


Figure 9.3 -Rock Quality Index (RQI), mechanical stratigraphy, and spinner-derived gas flow.

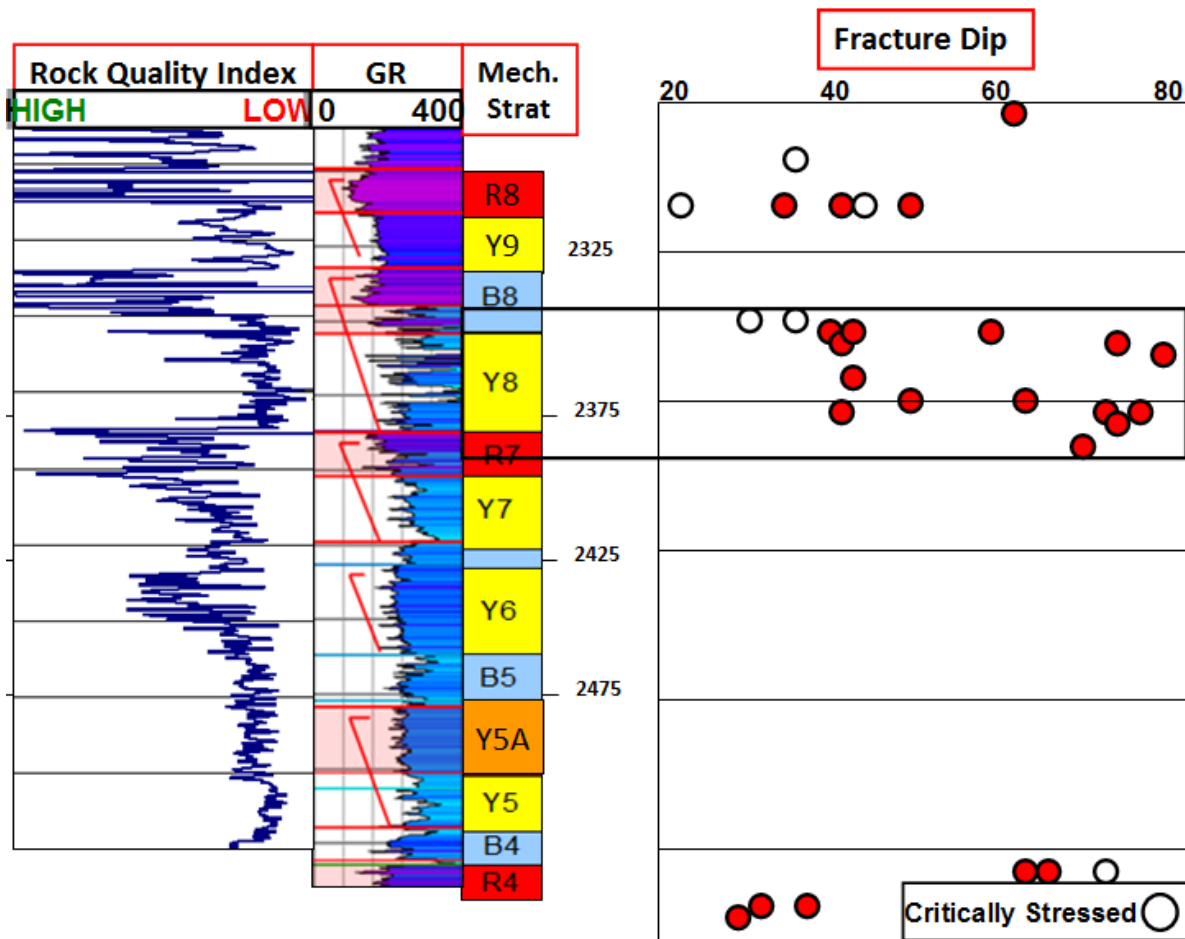


Figure 9.4 - Fracture abundance, plotted as a function of dip, correlated to the mechanical stratigraphy and Rock Quality Index (RQI). In the Yellow 8 facies distance from the propagating hydraulic fracture is large; however the presence of abundant steeply-dipping natural fractures appears to compensate for the lesser pressure effects.

Similar results are observed in the SWVA signature of the 4D time-lapse survey. Figure 8.3 shows initial baseline anisotropy, which correlates well with the Rock Quality Index (RQI). As stimulation occurs, it is observed that azimuthal anisotropy propagates to areas of the reservoir which are more homogenous, analogous to the thick homogenous zone created by the Yellow 5A and Yellow 5 facies in the vertical Farrell Creek well. The presence of an extensive homogenous zone allows uninhibited growth of the hydraulic fracture. Around these zones of pressure perturbation, shear along natural fracture faces will be highly likely. Between the third and fourth stage of the northern well (02/07-07-78-10W6), there is a zone of very high Rock

Quality Index (RQI) as outlined in Figure 8.3. Toward stages 3 and 2 there is a homogenous zone as outlined in Figure 8.4.

As concluded from the Farrell Creek vertical well analysis, this homogenous zone allows for propagation of the hydraulic energy, and as this energy reaches the neighboring brittle zone, widespread failure and energy dissipation is observed. Here a prolific fracture network would be created, and evidence that this network was created can be seen in spinner gas data, the microseismic, and the change in azimuthal anisotropy signature with time. The SWVA correlation is shown in Figure 9.5, with the analogous facies from the vertical well analysis outlined, as well as the proposed fracture barrier shown by the purple vertical line. The correlation with microseismic events and spinner gas flow in shown in Figure 9.6, where more abundant events are seen in the zone of reservoir pressurization surrounding the hydraulic stimulation, and a decrease in event count past the fracture barrier. The highest gas flow is also seen in the stage at the boundary between the propagating hydraulic fracture and proximal shear zone. These production correlations hold true in both vertical and horizontal well cases (Figure 9.7).

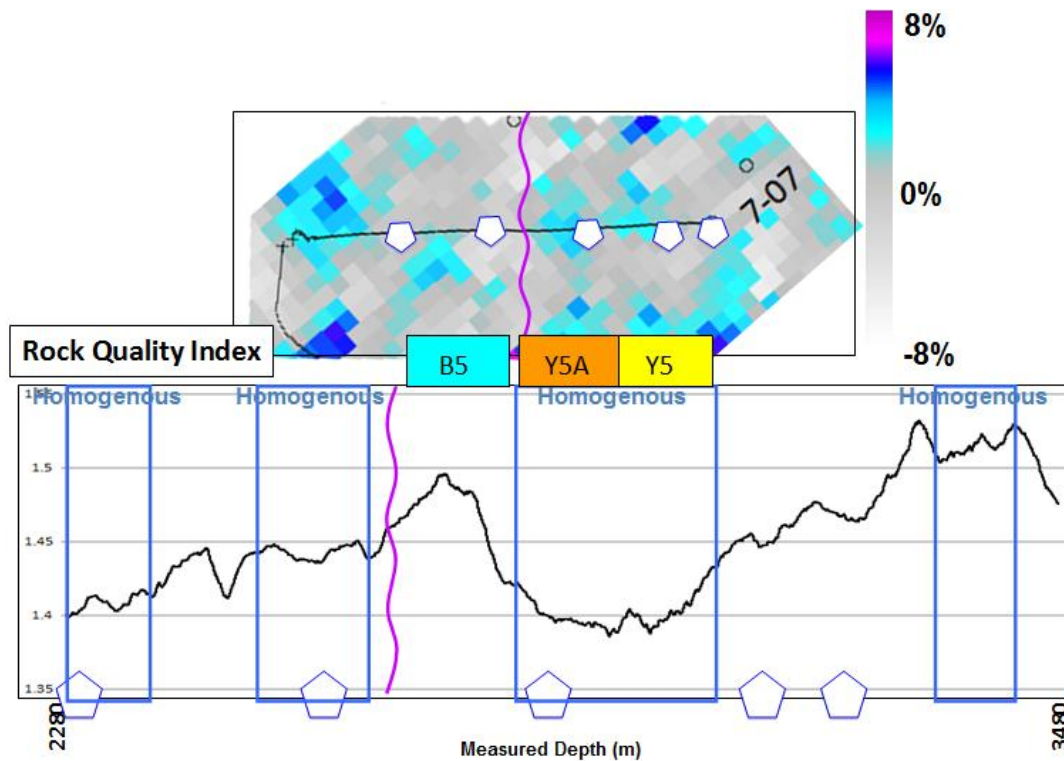


Figure 9.5 - SWVA signature in Monitor 2 with proposed homogenous zone, brittle zone, and fracture barrier outlined in purple.

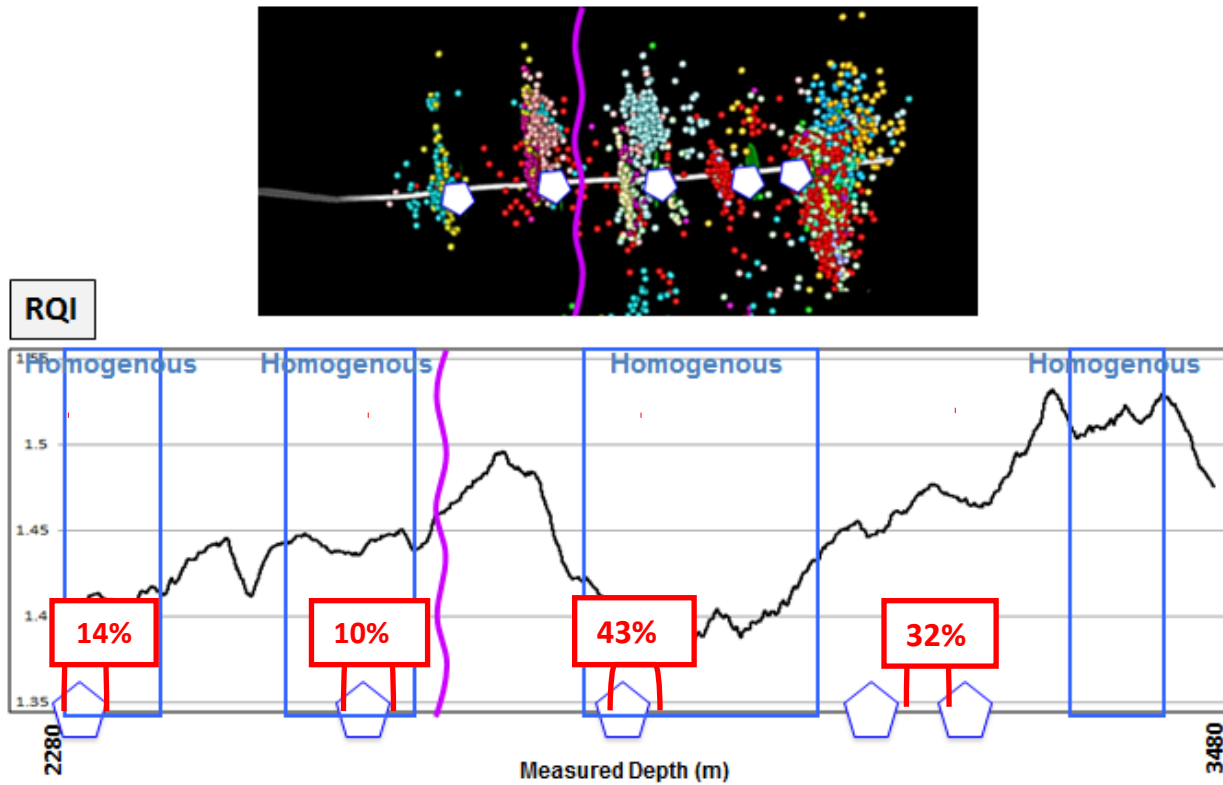


Figure 9.6 - Microseismic events correlated with spinner gas data and the Rock Quality Index (RQI). Both prolific microseismic and relatively high gas flow are observed at the intersection between a homogenous Rock Quality Index (RQI) zone and a brittle zone.

The overall conclusion is that homogeneity in the composition and texture of the formation is necessary for growth and propagation of a hydraulic stimulation. Proximal brittle and laminated zones are necessary to induce shear failure and link together a complex network of natural and hydraulic fractures. Stress shifts occurring in conjunction with pore pressure increases during the stimulation have an overarching influence on which zones will be most productive.

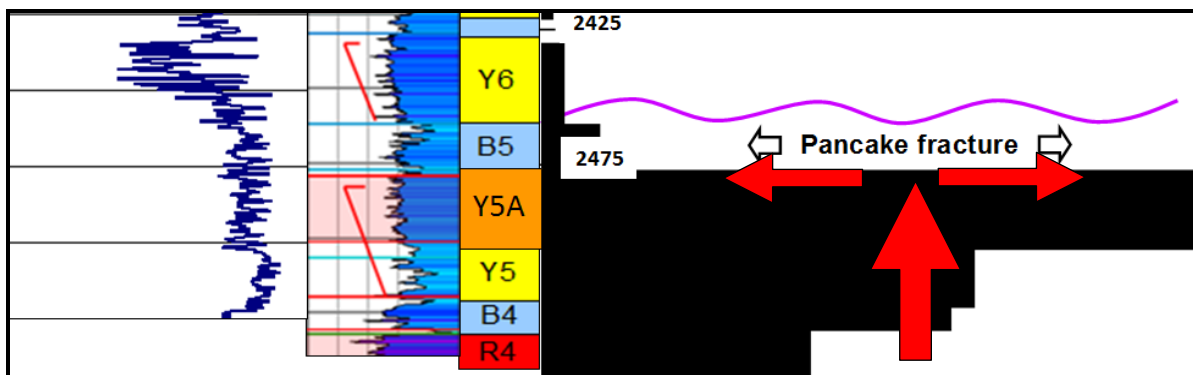
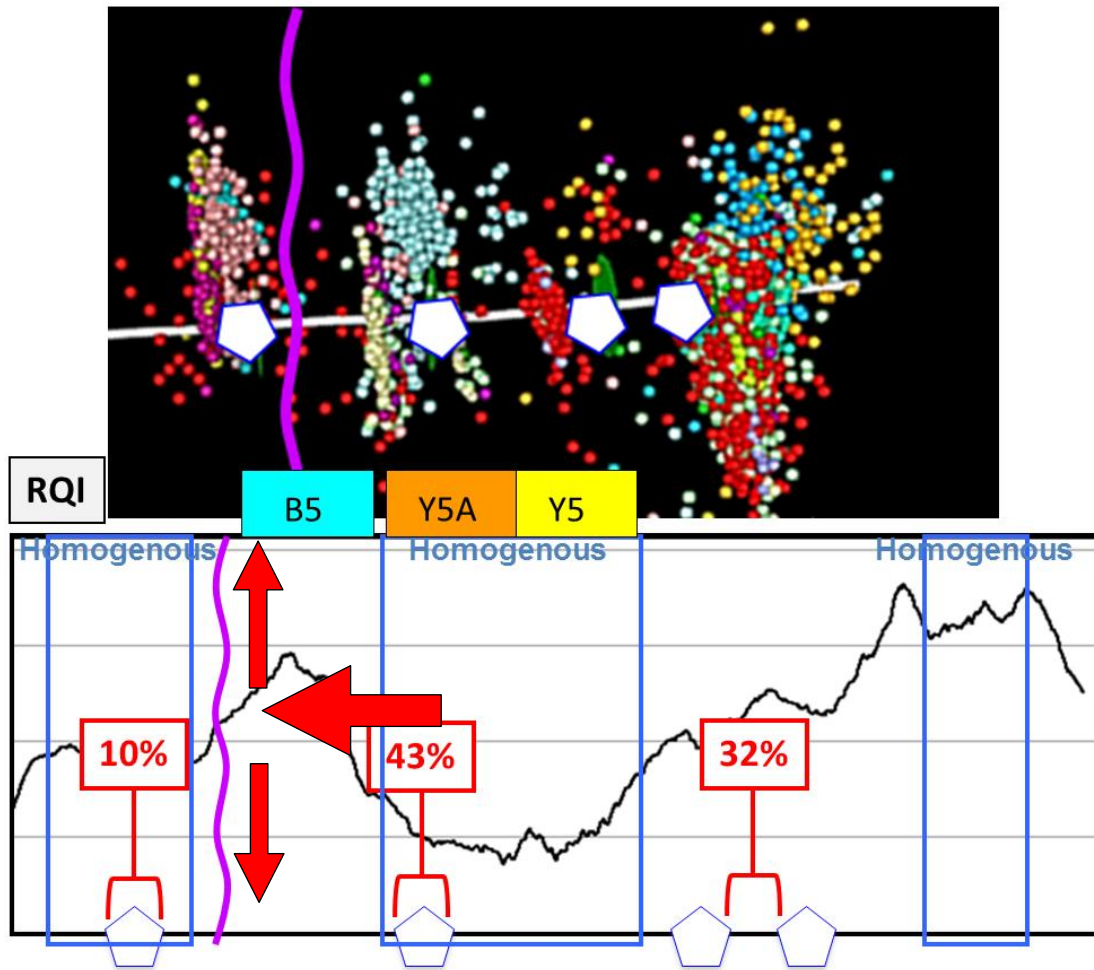


Figure 9.7 - Energy dissipation due to stress shadowing and fracture activation in both horizontal (top) and vertical (bottom) well cases.

CHAPTER 10

CONCLUSIONS

The production success of an unconventional shale reservoir is dependent on the quality of reservoir and the quality of the hydraulic stimulation treatment introduced to it. Without a successful stimulation, shales are not economically targetable; therefore accurate characterization of reservoir quality and heterogeneity is vital. I have determined a method for an integrated approach to reservoir characterization. The principal factors found to be affecting shale reservoir quality are natural fractures, the orientation and magnitude of stresses, and rock brittleness. An integrated multi-scale approach employing well logs, engineering, completions, time-lapse seismic and production data is used to relate these properties and determine methods for correctly monitoring and characterizing a hydraulic stimulation. In order for this approach to be considered useful and viable, the costs for data collection and processing must prove to be a worthwhile cost saving initiative, when compared to the cost for drilling and completion plans. The costs of logging and processing for geomechanical characterization are approximately 10% the cost of the completion of a single wellbore. The costs of the multicomponent seismic survey and the downhole microseismic are both approximately equivalent to the completion cost of a single wellbore. Therefore, when the results of the small-scale Pouce Coupe study are up-scaled to the scale of the development scheme at Farrell creek; where roughly 40 wells have been drilled to date and more are planned, this study is cost effective and of benefit to future Montney Shale development.

The overall conclusions of this geomechanical study of the Montney shale are outlined as follows:

- The mechanical stratigraphy defined for the formation provides a framework in which to compare between and within zones. This definition considers rock properties and standard log-based measurements such as density, sonic velocity, and gamma ray. Therefore, it indirectly examines both compositional and fabric-based brittleness, but excludes stress.
- The modified Rock Quality Index (RQI) incorporates both stress and brittleness elements. From this index it can be concluded that brittle zones are also zones of high internal heterogeneity.

- Through the use of diagnostic fracture injection tests (DFIT) and microseismic, it can be observed that there is a strong formation influence on the progression of hydraulic fractures. It is inferred here that this is due to the degree of heterogeneity within a zone. The Rock Quality Index (RQI) is an accurate indicator of this heterogeneity.
- In the case of the Montney reservoir, hydraulic fractures are easily initiated and grow in zones of homogeneity. When they reach the interface with a heterogeneous/brittle zone, the hydraulic energy is dissipated in the highly stressed zone. These zones often exhibit relatively higher production. Therefore, the interaction of both hydraulic fracture propagation and natural fracture failure within laminated/brittle zones is necessary for the creation of a complex fracture network and increased production.
- There is the potential for re-fracturing of wells which were previously stimulated with equal perforation spacing. The Rock Quality Index (RQI) is a viable method for designing differential spacing and fluid/proppant volumes, based on the interfaces between homogeneous and heterogeneous Rock Quality Index (RQI).
- Stress shadowing amplifies the effects of energy dissipation in brittle zones. Pressurization of the reservoir in the stages leading up to interaction with the brittle zones means the failure in these zones and energy dissipation is more prolific than if prior pressurization was not present.
- The same fracture and stress mechanisms are present in both vertical and horizontal well cases (Figure 63).

10.1 Recommendations for Future Work

The work presented in this thesis focused largely on hydraulic and natural fracture behavior within the defined mechanical stratigraphic framework. The study utilized data from several related disciplines, including geophysical (4D multicomponent seismic, microseismic), engineering (DFITs, production & completion data), and geochemical (thermal maturity). However, the exploration of these related topics was broad and further work would benefit from a more detailed examination of certain parameters.

Geochemical: Finer scale in-depth characterization of the geochemical character of the rock is warranted. Thermal maturity was accounted for in the Rock Quality Index through the TOC term in the mineralogy-based Brittleness Index. However this is a broad-scale examination of this factor, and does not account for temporal evolution and variation in the reservoir. Thermal maturity and related diagenesis will have an effect on both mineralogy and rock fabric, through the evolution of micro-fabrics and kerogen volume/porosity. These factors must be further examined.

Microseismic: Similarly, microseismic data was examined at the preliminary level, primarily as a correlation tool to other results. An in-depth study of microseismic locations, error, magnitudes, and the initial velocity model is vital for proper correlation to the established rock framework.

Moving Forward: In taking this work to other wellbores or other study areas, certain data must be initially collected to ensure full analysis can be done. The importance of having a complete dataset in at least one wellbore cannot be understated. A full waveform sonic & density log are necessary to define log-based rock properties. Core triaxial testing should be undertaken as a quality-control for the log-derived properties. Quantitative TOC and rock mineralogy measurements are necessary to define the composition-based brittleness input for the Rock Quality Index (RQI). XRD (x-ray diffraction) and SRA (source rock analysis) of core samples is the most accurate way to define TOC and mineralogy. In the absence of these datasets, QEMSCAN (Quantitative Evaluation of Minerals by SCANNing electron microscopy) can be used to determine the mineralogy, however error bars are larger. If neither core nor log-based mineralogy is available the Rock Quality Index (RQI) can be defined using the fabric-based brittleness only. This approach was found to show comparable results to the full Rock Quality Index (RQI), however results are based on only one wellbore and therefore further investigation is necessary to determine if Rock Quality Index (RQI) determination without the mineralogy component maintains accuracy in all cases.

4D multicomponent seismic has proven to be the most effective tool in confirming the hypothesized behavior of the reservoir. While this is a relatively new science, future 4D multicomponent surveys in other reservoirs will be vital for accurate reservoir characterization.

REFERENCES

- Agarwal K, Mayerhofer, M, Warpinski, N, 2012, Impact of Geomechanics on Microseismicity: paper presented at the SPE/EAGE European Unconventional Resources Conference and Exhibition in Vienna, Austria, 20-22 March.
- Akrad, O, Miskimins, J, Prasad, M, 2011, The Effects of Fracturing Fluids on Shale Rock Mechanical Properties and Proppant Embedment: paper presented at the SPE Annual Technical Conference and Exhibition, Denver, CO, 30 October- 2 November.
- Bandyopadhyay, K, 2009, Seismic Anisotropy: Geological Causes and its Implications to Reservoir Geophysics: PhD Thesis, Department of Geophysics, Stanford University.
- Barree, R & Gilbert, J, 2009, Stress and Rock Property Profiling for Unconventional Reservoir Stimulation: paper presented at the 2009 SPE Hydraulic Fracturing Technology Conference, the Woodlands, TX, USA, 19-21 January.
- Barree & Associates, 2012, Fracture Advances Presentation: Barree & Associates Consulting.
- Billingsley, R & Kuuskraa, V, 2006, Multi-site Application of the Geomechanical Approach for Natural Fracture Exploration: DOE Award No. DE-RA26-99FT40720, Advanced Resources International Inc. (In Association with Union Pacific Resources, Barrett Resources, Burlington Resources, and Colorado School of Mines).
- Bustin, M & Smith, M, 2000, Late Devonian and Early Mississippian Bakken and Exshaw Black Shale Source Rocks, Western Canada Sedimentary Basin: A Sequence Stratigraphic Interpretation: *AAPG Bulletin* vo. 84, no. 7, pp. 940-960.
- Byerlee, J, 1978, Friction of rocks. *Pure and Applied Geophysics*, vo. 116, no. 4-5. Pp. 615-626.
- Cipolla, C, Weng, X, Mack, M, Ganguly, U, Gu, H, Kresse, O, Cohe, C, 2011, Integrating Microseismic Mapping and Complex Fracture Modeling to Characterize Fracture Complexity: Paper presented at the SPE Hydraulic Fracturing Technology Conference, The Woodlands, TX, 24-25 January.
- Cipolla, C, Lewis, R, Maxwell, S, Mack, M, 2012, Appraising Unconventional Resource Plays: Separating Reservoir Quality from Completion Effectiveness: paper presented at the International Petroleum Technology Conference, Bangkok, Thailand, 7-9 February.

- Crews, J, Weimer, P, Pulham, A, Waterman, A 2000, Integrated Approach to Condensed Section Identification in Intraslope Basins, Pliocene-Pleistocene, Northern Gulf of Mexico: *AAPG Bulletin* vo. 84, no. 10, pp. 1519-1536.
- Doyen, P, Malinverno, A, Prioul, R, Hooyman, P, Noeth, S, Sayers, C, Smit, T, van Eden, C, Wervelman, R, 2004, Seismic Pore Pressure Prediction with Uncertainty Using a Probabilistic Mechanical Earth Model.
- Ehlig-Economides, C, Economides, M, 2011, Water as Proppant: paper presented at the SPE Annual Technical Conference and Exhibition held in Denver, Colorado, USA, 30 October- 2 November.
- Embry, A, Johannessen, E, Owen, D, Beauchamp, B, Gianolla, P, 2007, Sequence Stratigraphy as a “Concrete” Stratigraphic Discipline. Report of the ISSC Task Group on Sequence Stratigraphy.
- Folk, R, 1980, *Petrology of Sedimentary Rocks*. Hemphill Publishing Company, Austin, TX.
- Hart, B, 2011, Shale Gas- Production and Sequence Stratigraphy: What Makes the Best Part of the Best Plays? Paper presented at the 2011 AAPG Hedberg Conference, December 5-10, 2010, Austin, Texas.
- Hennings, P, 2009, The Geologic Occurrence and Hydraulic Significance of Fractures in Reservoirs: paper presented at the AAPG-SPE-SEG Hedberg Research Conference.
- Hill, D, 2008, Dynamic Stresses, Coulomb Failure, and Remote Triggering. *Bulletin of the Seismological Society of America*, vo. 98, no. 1, pp. 66-92.
- Hillis, R, 2000, Pore Pressure/stress coupling and its implications for seismicity: *Exploration Geophysics*, vo. 31, no. 2, pp. 448- 454.
- Holt, R, Fjaer, E, Nes, O, Alassi, H, 2011, A Shaley Look at Brittleness: paper presented at the 45th US Rock Mechanics/Geomechanics Symposium, San Francisco, CA, 26-29 June.
- Jaeger, J, Cook, N & Zimmerman, R 2007, *Fundamentals of Rock Mechanics*. Fourth edition, Blackwell Publishing.
- Jarvie, D, 1991, Total organic carbon (TOC) analysis, in R. K. Merrill, ed., *Treatise of petroleum geology: Handbook of petroleum geology, source and migration processes and evaluation techniques*: AAPG, pp. 113–118.
- Jones, J & Britt, L, 2009, *Design and Appraisal of Hydraulic Fractures*: SPE Book.
- Kale, S, 2009, *Petrophysical Characterization of Barnett Shale Play*. Master Thesis, Oklahoma University, Norman, Oklahoma.

- Kolymbas, D, 2003, *Advanced Mathematical and Computational Geomechanics*, Springer-Verlag.
- Kulhanek, O, 2005, Seminar on b-value: Presented at the Department of Geophysics, Charles University, Prague, 10-19 December.
- Lajtai, E & Alison, J, 1979, A study of residual stress effects in sandstones: *Canadian Journal of Earth Sciences*, vo. 16, pp. 1547–1557.
- Loutit, T, Hardenbol, J, Vail, P, Baum, G, 1988, Condensed sections: the key to age-dating and correlation of continental margin sequences. In: Wilgus, C, Hastings, B, Kendall, C, Posamentier, H, Ross, C, Van Wagoner, J (Eds.), *Sea Level Changes—An Integrated Approach*, SEPM Special Publication, vo. 42, pp. 183–213.
- Maxwell, S, 2009, Microseismic Location Uncertainty: CSEG Recorder Focus Article, pp. 41-46.
- Maxwell, S, 2011, Microseismic Hydraulic Fracture Imaging: The Path Toward Optimizing Shale Gas Production: *The Leading Edge* vo. 30, no. 3, pp. 340-346.
- Maxwell, S & Cipolla, C, 2011, What Does Microseismicity Tell Us About Hydraulic Fracturing?: paper presented at the SPE Annual Technical Conference and Exhibition held in Denver, Colorado, USA, 30 October- 2 November.
- Mayerhofer, M, 2012, DFIT- Diagnostic Fracture Injection Test: SWPLA Meeting, 16 May.
- Meckel, L, 2012, *Unconventional Petroleum Systems Lecture Notes*. Department of Geology & Geological Engineering, Colorado School of Mines, Golden, Colorado.
- Mishra, V, 2011, Applications of Minifrac/ Microfrac/ Stress Testing: paper presented at the Western Oil & Gas 6th International Symposium, 23-25 August.
- Mitchum, R, 1977, Seismic Stratigraphy and Global Changes of Sea Level: Part 11. Glossary of Terms used in Seismic Stratigraphy: Section 2. Application of Seismic Reflection Configuration to Stratigraphic Interpretation, Memoir 26, pp. 205 - 212.
- Momper, J, 1980, Oil Expulsion- A Consequence of Oil Generation: *AAPG Bulletin*, vo. 64, no. 8, pp. 1279.
- Moslow, T, 2000, Reservoir Architecture of a Fine-Grained Turbidite System, Lower Triassic Montney Formation, Western Canada Sedimentary Basin: *Regional Montney Formation Study*, Graham Davies Geological Consultants Ltd.
- Mullen, M & Enderlin, M 2010, Is that Frac Job Really Breaking New Rock or Just Pumping Down a Pre-Existing Plane of Weakness? The Integration of Geomechanics and Hydraulic

Fracture Diagnostics: paper presented at the 44th Annual US Rock Mechanics Symposium and 5th U.S.- Canada Rock Mechanics Symposium, Salt Lake City, Utah, 27-30 June.

- Newsham, K & Rushing, J, 2001, An Integrated Work-flow Model to Characterize Unconventional Gas Resources: Part I-Geological Assessment and Petrophysical Evaluation: paper presented at SPE Annual Technical Conference and Exhibition, New Orleans, Louisiana, 30 September – 2 October.
- Norton, M & Tushingham, K, 2011, Integrating Data Crucial in Shale Plays: *American Oil & Gas Reporter*, Special Report: Oil & Gas Shales, March.
- O’Connell, S, 2011, Hyperpycnal Flow Deposits: Examples from the Mississippian and Cretaceous of the Alberta Basin: paper presented at the 2011 CSPG CSEG CWLS Convention.
- Passey, Q, Bohacs, K, Esch, W, Klimentidis, R, Sinha, S 2010, “From Oil-Prone Source Rock to Gas Producing Shale Reservoir- Geological and Petrophysical Characterization of Unconventional Gas Reservoirs”: *Society of Petroleum Engineers*, paper presented at the International Oil and Gas Conference and Exhibition, Beijing, China, 8-10 June.
- Posamentier, H, Bhattacharya, J, 2011, Sequence Stratigraphy and Allostratigraphic Applications in the Alberta Foreland Basin: *Geological Atlas of the Western Canadian Sedimentary Basin*, Alberta Geological Survey, Chapter 25.
- Posamentier, H & Allen, G, 1999, Siliciclastic Sequence Stratigraphy: concepts and applications: *SEPM Concepts in Sedimentology and Paleontology*, no. 7, pp. 210.
- Priest, S, *Discontinuity Analysis for Rock Engineering*: Chapman & Hall, 202 and 442.
- Ratcliffe, G & Schmidt, K, 2011, Application of Inorganic Whole-Rock Geochemistry to Shale Resource Plays: an Example from the Eagle Ford Shale, Texas: presented at the Houston Geological Society, Northsiders Luncheon Meeting.
- Raymer, D, Rutledge, J, Jacques, P, 2008, Semi-automated Relative Picking of Microseismic Events, SEG Expanded Abstracts.
- Rice, J, 1992, Chapter 20- Fault Stress States, Pore Pressure Distributions and the Weakness of the San Andreas Fault: *Fault Mechanics and Transport Properties of Rock*, Academic Press Ltd., pp. 475-503.
- Rodriguez, N & Slatt, R, 2000, Comparative Sequence Stratigraphy and Organic Geochemistry of North American Unconventional Gas Shales: Commonality or Coincidence?: *AAPG Bulletin* vo. 84, no. 7, pp. 940-960.

- Ross, D & Bustin, R, 2009, The Importance of Shale Composition and Pore Structure Upon Gas Storage Potential of Shale Gas Reservoirs: *Marine and Petroleum Geology*, vo. 26, pp. 916-927.
- Rutledge, J, Phillips, W, Mayerhofer, M, 2004, Faulting Induced by Forced Fluid Injection and Fluid Flow Forced by Faulting: An Interpretation of Hydraulic-Fracture Microseismicity, Carthage Cotton Valley Gas Field, Texas: *Bulletin of the Seismological Society of America* vo. 94, no. 5, pp. 1817-1830.
- Sayers, C, 2006, An Introduction to Velocity-Based Pore-Pressure Estimation: *The Leading Edge*, vo. 25, pp. 1496-1500.
- Slatt, R, & Abousleiman, Y, 2011, Merging Sequence Stratigraphy and Geomechanics for Unconventional Gas (and Oil) Shales. *Institute of Reservoir Characterization & Poromechanics Institute, University of Oklahoma*: paper presented at the CSPG CSEG CWLS Joint Annual Convention.
- Soh, M, 2012, Australian Coal Bed Methane: Principles and Development Challenges: WA Oil & Gas Facilities Group, a co-venture between Engineers Australia and the Society of Petroleum Engineers (SPE).
- Sondhi, N, 2011, Petrophysical Characterization of the Eagle Ford Shale: Master's Thesis, Oklahoma University, Norman, Oklahoma.
- Steinhoff, C, 2012, Pouce Coupe field revisited: time-lapse multicomponent monitoring of hydraulic stimulations in an unconventional shale reservoir, Pouce Coupe, Alberta, Canada: Master's Thesis, Department of Geophysics, Colorado School of Mines, Golden, Colorado.
- Teufel, L & Clark, J, 1984, Hydraulic Fracture Propagation in Layered Rock: Experimental Studies of Fracture Containment: *SPE Journal*, vo. 24, no. 1.
- Texas Department of Transportation (TXDOT), 1999, Triaxial Compression Test for Undisturbed Soils, Construction Division, Tex-118-E.
- Tezuka, K, Namikawa, T, Tamagawa, T, 2002, Roles of the Fractures System and State of Stress for Gas Production from the Basement Reservoir in Hokkaido, Japan: paper presented at the SPE Gas Technology Symposium held in Calgary, AB, Canada, 30 April- 2 May.
- Tissot & Welte, 1984, *Petroleum Formation and Occurrence*, Springer-Verlag.
- Toro, J, 2011, *Petroleum Prospect Evaluation*. Department of Geology and Geography, West Virginia University.

- Warpinski, N, 2011, Hydraulic Fracture Height in Gas Shale Reservoirs: paper presented at the SEG Annual Meeting, 18-23 September, San Antonio, TX.
- Warpinski, N, Kramm, R, Heinze, J, 2005, Comparison of Single and Dual-Array Microseismic Mapping Techniques in the Barnett Shale: paper presented at the SPE Annual Technical Conference and Exhibition, Dallas, Texas, 9-12 October.
- Williams, K, 2012, The Permeability of Overpressure Shale Seals and of Source Rock Reservoirs is the Same: adapted from poster presentation at AAPG 2012 Annual Convention and Exhibition, Long Beach, California, 22-25 April.
- Zahm, C & Hennings, P, 2009, Complex fracture development related to stratigraphic architecture: Challenges for structural deformation prediction, Tensleep Sandstone at the Alcova anticline, Wyoming: *AAPG Bulletin*, vo. 93, no. 11, pp. 1427-1446.

SELECTED BIBLIOGRAPHY

Resources not specifically cited but related to the work presented

- Blood, R & Lash, G, 2011, Sequence Stratigraphy as Expressed by Shale Source Rock and Reservoir Characteristics- Examples from the Devonian Succession, Appalachian Basin: adapted from oral presentation at the AAPG Annual Convention and Exhibition, Houston, TX, USA.
- Canadian National Energy Board, 2011, Tight oil developments in the Western Canadian Sedimentary Basin: Energy Briefing Note.
- Chuprakov, D, Akulich, A, Siebrits, E, Thiercelin, M, 2011, Hydraulic-Fracture Propagation in a Naturally Fractured Reservoir: *SPE Production and Operations*, pp. 88-97.
- Dimitrios, K, 2003, Advanced Mathematical and Computational Geomechanics. Lecture Notes in Applied and Computational Mechanics V13, XVI, 315 pages.
- Fisher, K, Warpinski, N 2011, Hydraulic-Fracture Height Growth: Real Data: paper presented at the SPE Annual Technical Conference and Exhibition held in Denver, Colorado, USA, 30 October- 2 November.
- Goertz-Allman, B, Goertz, A, Wiemer, S 2011, Stress drop variation of induced earthquakes at the Basel geothermal site. *Geophysical Research Letters* vo. 38, pp. L09308
- Hart, B 2010, Shale-gas production and Sequence Stratigraphy: What Makes a Good Gas Shale? *Search and Discovery*, Article #90122, adapted from oral presentation at the AAPG Hedberg Conference, Austin, Texas.
- Harami-Moussavi, R 1990, Stratigraphy, petrography, and depositional environment of sandstones in the Rock Lake Shale Member of the Stanton Limestone (Missourian Stage, Upper Pennsylvanian) in southeastern Kansas. *Kansas Geological Survey, Series 5*.
- Laughrey, C, Ruble, T, Lemmens, H, Kostelnik, J, Butcher, A, Walker, G, Knowles, W, 2011, Black Shale Diagenesis: Insights from Integrated High Definition Analysis of Post-Mature Marcellus Formation Rocks, Northeastern Pennsylvania: *Search and Discovery* Article #110150; adapted from oral presentation at Session, U.S. Active and Emerging Plays- Paleozoic Basins and Cretaceous of Rockies, AAPG Annual Convention and Exhibition, Houston, TX, USA, 10-13 April.
- McCarthy, K, Niemann, M, Palmowski, D, Peters, K, Stankiewicz, A 2011, Basic Petroleum Geochemistry for Source Rock Evaluation. *Oilfield Review*, vo. 23, no. 2.

- Olson, J, Bahorich, B, Holder, J, 2012, Examining Hydraulic Fracture-Natural Fracture Interaction in Hydrostone Block Experiments: paper presented at the SPE Hydraulic Fracturing Technology Conference, Woodlands, TX, USA, 6-8 February.
- Rozhko, A 2010, Role of Seepage Forces on Seismicity Triggering. *Journal of Geophysical Research*, vo. 115, pp. B11314.
- Utah Geological Survey, in association with Golder Associates, Utah State University, Anadarko Petroleum Corporation, Wind River Resources Corporation 2012, Gas Production Forecasting from Tight Gas Reservoirs: Integrating Natural Fracture Networks and Hydraulic Fractures, 2 September 2008 to 31 October 2012.
- University of Alberta/Ichnology Research Group, Sedimentary Framework and Stratigraphic Architecture of the Montney Formation in the Foothills and Western Plains Area of Northeastern British Columbia
- Warpinski, N 2009, Microseismic Monitoring: Inside and Out. *Journal of Petroleum Technology*, vo. 61, no. 11, pp. 80-85